

Universal low-temperature fluctuation of unconventional superconductors revealed: ‘Smoking gun’ leaves proper bosonic superfluidity the last theory standing

Anthony Hegg^{1†}, Ruoshi Jiang^{1†}, Jie Wang^{1†}, Jinning Hou¹,
Tao Zeng¹, Yucel Yildirim², Wei Ku^{1,3,4*}

¹Tsung-Dao Lee Institute & School of Physics and Astronomy, Shanghai
Jiao Tong University, Shanghai, 200240, China.

²Department of Energy Systems Engineering Bilgi University, Istanbul,
34060, Turkey.

³Key Laboratory of Artificial Structures and Quantum Control Ministry
of Education, Shanghai, 200240, China.

⁴Shanghai Branch Hefei National Laboratory, Shanghai, 201315, China.

*Corresponding author(s). E-mail(s): weiku@sjtu.edu.cn;

[†]These authors contributed equally to this work.

Abstract

Low-temperature thermal fluctuations offer an essential window in characterizing the true nature of a quantum state of matter, a quintessential example being Fermi liquid theory. Here, we examine the leading thermal fluctuation of the superfluid density across numerous families ranging from relatively conventional to highly unconventional superconductors (MgB₂, bismuthates, doped buckyballs, heavy fermions, UTe₂, doped SrTiO₃, Chevrel clusters, intermetallics, organic superconductors, transition metal dichalcogenides, ruthenates, iron-pnictides, cuprates, and kagome metals). Amazingly, in all of them an unprecedented universal T^3 depletion materializes in the low-temperature superfluid density, even in the believed-to-be-conventional MgB₂. This reveals a new quantum superfluid state of matter and requires a necessary change of paradigm in describing modern superconductors. We demonstrate that such unorthodox yet generic behavior can be described by a strictly Galilean consistent theory of bosonic superfluidity hosting a long-lived ‘true condensate’.

1 Introduction

Superconductivity has remained one of the most important topics in condensed matter physics since its discovery long ago [1–4]. Although traditional ‘conventional’ superconductors seem to be well-described by the Bardeen-Cooper-Schrieffer (BCS) theory [5] as Fermi liquids with spontaneously broken U(1) symmetry, in the modern era a vast and ever-growing array of ‘unconventional’ superconductors has been discovered that display behaviors beyond the applicability of the standard lore. A satisfactory understanding of the coherent quantum state of matter behind this purely quantum phenomenon therefore remains an open question without consensus.

The most essential and experimentally accessible properties of such a *quantum* state are its thermal fluctuations at low temperature. Given that qualitatively different fluctuations arise out of distinct quantum states of matter, they offer a ‘smoking gun’ signature that quickly falsifies any theories with incorrect ground states. On the other hand, around a ground state with otherwise correct macroscopic properties, consistency of the characteristic fluctuations validates the effectiveness of a theory. This greatly contrasts with the obfuscating effects of universality in the vicinity of a phase transition, where many qualitatively different models can exhibit identical behavior. A good analogy to such a state is the 3D Fermi liquid, whose quantum nature is characterized by T^2 resistivity, T^2 one-body scattering rate, T^2 Hall angle, T -linear specific heat, $1/T$ thermal conductivity, T -independent magnetic susceptibility, and T -independent Hall coefficient [6]. These universal fluctuations provide unambiguous criteria to determine whether a material is described by a particular known quantum state of matter (e.g. Fermi liquid) or not (i.e. non-Fermi liquid).

In terms of superconductivity, the most direct characterization is naturally through *low-temperature* thermal fluctuations of the superfluid density (or correspondingly, the penetration depth). Particularly, through continuous improvement in experimental setup, an unprecedented resolution for the penetration depth at low temperature and over a wide range of carrier density has been reached (e.g. in [7]). Unfortunately, unlike studies on several other indirect quantities like resistivity, magnetic susceptibility and specific heat (e.g. [8–10]), a careful study of the low-temperature superfluid density has been largely overlooked by the community in favor of the multi-gap fitting over the entire superconducting temperature range [11–17]. As such, in absence of a careful characterization of the low-temperature properties, there is simply not enough guidance to reliably identify a compatible quantum state of matter, aside from ruling out some obvious scenarios (such as single-gap BCS).

Here, we carefully perform this essential analysis based on the available low-temperature superfluid response data from a large number of superconductor families, ranging from the conventional to the highly unconventional, including MgB₂, bismuthates, doped buckyballs, heavy fermions, UTe₂, doped SrTiO₃, Chevrel clusters, intermetallics, organic superconductors, transition metal dichalcogenides, ruthenates, iron-pnictides, cuprates, and kagome metals. Surprisingly, in all of the compounds presented below (both fully-gapped and nodal), the low-temperature superfluid density displays a universal T^3 depletion. Mysteiously, this is beyond that of the standard BCS state but more restrained than that of the traditional bosonic superfluid state. This unprecedented universal behavior therefore precludes the corresponding quantum

states in the existing theories and reveals a new quantum superfluid state of matter requiring a change of paradigm in describing modern superconductors.

To this end, we develop a strictly Galilean consistent quantum theory of superfluidity beyond the current lore. Through employment of *long-lived* fully-dressed eigen-particles of general interacting bosonic systems, we introduce a rigorous ‘true condensate’ and associated with it an exact microscopic definition of super-current. Specifically, via the rigorous analytical structure of the current fluctuation, we identify beyond the standard sound velocity the essential inertial mass velocity responsible for the net current. This addition not only enables proper Galilean frame transformation for the elementary excitations, but also straightforwardly establishes an *equivalence* between the superfluid density and the true condensation density for an arbitrary quantum state. Thermal depletion of superfluid density in such a proper microscopic superfluid theory thus follows the T^3 thermal fluctuation of the three-dimensional true condensate. To the best of our knowledge, this strictly Galilean consistent theory of bosonic superfluidity is the only remaining theory capable of describing the quantum nature of the unconventional superconductivity in these materials.

2 Results

2.1 Unorthodox universal low-temperature fluctuation

Figure 1 reveals an incredible *universal* low-temperature fluctuation in nearly all modern superconductor families. The figure displays the observed bulk 3D low-temperature superfluid density ρ_s for many materials, found earlier[11–14, 18–24] and more recently[15–17, 25–28], data-collapsed to a single function via $\rho_s(T)/\rho_s(0)$ vs rescaled temperature T/\tilde{T} using extrapolated zero-temperature superfluid density $\rho_s(0)$. The inset displays the same data, now collapsed to $1 - \rho_s(T)/\rho_s(0)$ as a function of $(T/\tilde{T})^3$ as an aid to the eye. Amazingly, *all* of them fall onto a universal T^3 power-law form at low enough temperature. Particularly, K_3C_{60} , Nb-doped $SrTiO_3$, and Sr_2RuO_4 even maintain a T^3 form over the entire superconducting phase! In fact, the same universal T^3 form is also applicable to doped $YBa_2Cu_3O_7$ (c.f. Appendix A), *independent* of doping level, where high-quality data is available [7] in the doping limit, where the superconductivity ceases to exist even as $T \rightarrow 0$. This unexpected *quantum* universality spans virtually all of the superconductor families studied over the past several decades and certainly requires an equally general theory to account for it.

2.2 Direct physical implications

However, such a power-law fluctuation, as opposed to gap-protected exponential behavior, is inconceivable for fully-gapped superconductors [29] such as MgB_2 , $B_{0.6}K_{0.4}BiO_3$, $LaMo_6Se_8$, Nb-doped $SrTiO_3$ and K_3C_{60} . Particularly, the 3D nature of the *low-temperature* superconductivity in these materials renders inapplicable the gapless phase-fluctuation scenario[30, 31], whereas from the Anderson-Higgs mechanism one expects that not only the amplitude mode but also the phase mode should

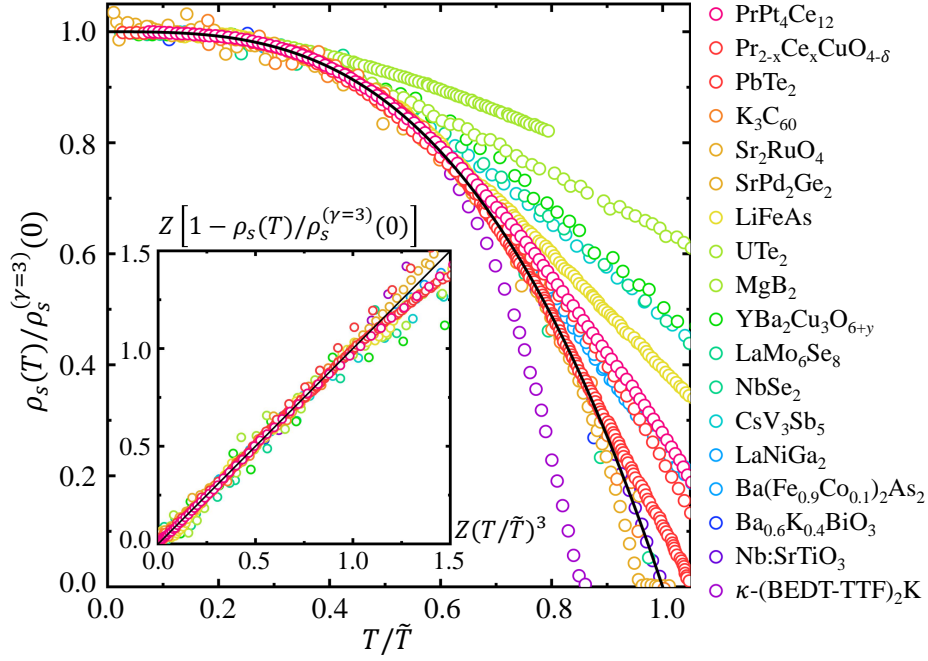


Fig. 1 Universal T^3 thermal depletion of superfluid density Experimentally observed superfluid density is analyzed via data-collapse to $\rho_s(T)/\rho_s(0)$ vs rescaled temperature T/\tilde{T} and to $1 - \rho_s(T)/\rho_s(0)$ vs $(T/\tilde{T})^3$ (inset) using extrapolated zero-temperature superfluid density $\rho_s(0)$. For easier visualization, the horizontal and vertical axes of the inset are rescaled by a material-dependent Z factor (c.f. Table 1) such that the T^3 behavior dominates below the value 1.0 in the axes. A clear cubic T^3 depletion is found at low temperature for all displayed materials. Doping value is $x = 0.131$ in $\text{Pr}_{2-x}\text{Ce}_x\text{CuO}_{4-\delta}$ and $y = 0.419$ in $\text{YBa}_2\text{Cu}_3\text{O}_{6+y}$, carrier density in Nb:SrTiO_3 is $0.33 \times 10^{20} \text{ cm}^{-3}$, and the component K is $\text{Cu}[\text{N}(\text{CN})_2]\text{Br}$ in organic superconductor $\kappa\text{-(BEDT-TTF)}_2\text{K}$.

be fully gapped. One has no choice but to conclude a lack of local $U(1)$ symmetry for the charged superflow, presumably due to screening at higher energy.

Even more puzzling is the same T^3 depletion displayed in Fig. 1 in gapless superconductors such as $\text{YBa}_2\text{Cu}_3\text{O}_{6+y}$ ($y = 0.419$), $\text{Pr}_{2-x}\text{Ce}_x\text{CuO}_{4-\delta}$ ($x = 0.131$) and $\text{Ba}(\text{Fe}_{0.9}\text{Co}_{0.1})_2\text{As}_2$. Since thermal population of gapless Bogoliubov quasi-particles is inescapable, gapless BCS theories generally would result in T -linear (line node) or T^2 (point node) depletion of the superfluid density [32], given that a Bogoliubov quasi-particle represents exciting a fermion from Cooper pairs in the superflow. It is therefore yet again inconceivable how, for example, p -wave and/or d -wave BCS theories could ever account for such results. The only remaining scenario is that, contrary to all existing pairing theories, in those gapless superconductors [33–36] the low-energy fermions were *never* part of the superflow (e.g. part of a Cooper pair) even before being excited! In turn, this unorthodox behavior validates a previous proposal [37] for a second type of superconducting quasi-particle gap, in which the Bogoliubov-like excitation removes

a bare fermion *not* from a Cooper pair, but instead from a ‘super-polaron’, a fermion coherently dressed by a bosonic superfluid.

However, for a 3D-coherent bosonic superflow absent local U(1) symmetry, the traditional hydrodynamic theory[4] exhibits T^4 depletion instead, close but not identical to the above T^3 depletion. Whereas, the T^3 fluctuation of 2D superfluidity is inapplicable here, as these materials all demonstrate 3D coherent superconductivity at temperatures lower than the coherent energy scale of the third dimension. It is therefore necessary to *meticulously* re-visit the thermal depletion of the superfluid density.

2.3 Rigorous bosonic superfluid theory and generic T^3 -depletion

To this end, we develop a ‘proper’ superfluid theory for quantum interacting bosonic systems with translational symmetry via an unorthodox employment of fully-dressed long-lived ‘eigen-particles’ [38–40], $\tilde{a}_{\mathbf{k}}^\dagger$, that carry the same inertial mass m and momentum $\hbar\mathbf{k}$ of the bare particles. This allows unprecedented *direct* access to properties of long time-scale, particularly a physical ‘true condensate’,

$$\tilde{N}_0 \equiv \tilde{a}_{\mathbf{k}_0}^\dagger \tilde{a}_{\mathbf{k}_0}, \quad (1)$$

consisting of \tilde{N}_0 eigen-particles of momentum $\hbar\mathbf{k}_0$.

Using the curl-less nature of the supercurrent as a “potential flow” [41] of *inertial mass-carrying* matter with stiffness, we identify an unprecedented rigorous *microscopic* definition for the supercurrent excitation $\tilde{\mathbf{J}}_{\mathbf{q}}^s$ of long wavelength (small wavenumber $\mathbf{q} \neq \mathbf{0}$),

$$\tilde{\mathbf{J}}_{\mathbf{q} \neq \mathbf{0}}^s = \frac{1}{\mathcal{V}} (\tilde{a}_{\mathbf{k}_0 + \mathbf{q}}^\dagger \tilde{\mathbf{v}}_{\mathbf{k}_0 + \mathbf{q}, \mathbf{k}_0} \tilde{a}_{\mathbf{k}_0} + \tilde{a}_{\mathbf{k}_0}^\dagger \tilde{\mathbf{v}}_{\mathbf{k}_0, \mathbf{k}_0 - \mathbf{q}} \tilde{a}_{\mathbf{k}_0 - \mathbf{q}}) \quad (\text{in the presence of stiffness}), \quad (2)$$

of the eigen-particles in a system of volume \mathcal{V} . This establishes that *only* fluctuations involving the eigen-particles in the true condensate contribute to the supercurrent fluctuation. Importantly, in addition to the constant sound velocity in standard treatments [4, 42], the velocity operator $\tilde{\mathbf{v}}_{\mathbf{k}, \mathbf{k}'}$ also rigorously contains the inertial mass velocity $\frac{\hbar(\mathbf{k} + \mathbf{k}')}{2m}$, crucially recovering the proper Galilean frame transformation. Consistently, the corresponding supercurrent contribution to the total current of the system,

$$\tilde{\mathbf{J}}^s = \frac{1}{\mathcal{V}} \frac{\hbar\mathbf{k}_0}{m} \tilde{a}_{\mathbf{k}_0}^\dagger \tilde{a}_{\mathbf{k}_0} \quad (\text{in the presence of stiffness}), \quad (3)$$

contains only the *sound-independent* inertial mass flow of the eigen-particles in the true condensate.

Given eigen-particles’ preservation of bare inertial mass m , this unambiguously establishes a rigorous *state-independent* quantum mechanical equivalence between the

superfluid (inertial mass) density ρ_s and the ‘true condensate’ density, \tilde{N}_0/\mathcal{V} ,

$$\rho_s = m\tilde{N}_0/\mathcal{V} \quad (\text{in the presence of stiffness}). \quad (4)$$

Trivially, such a direct equivalence between ρ_s and \tilde{N}_0 implies a similar equivalence between the normal fluid density ρ_n and the number of uncondensed particles $N - \tilde{N}_0$, such that $\rho_{\text{tot}} = \rho_s + \rho_n \propto N$ is strictly satisfied.

Finally, with this quantum mechanical equivalence, in the linear-response regime that corresponds to most of the experiments in Fig. 1, the thermal depletion of the T^3 -superfluid density then straightforwardly follows,

$$\frac{\rho_s}{\rho} = 1 - AT^3, \quad (5)$$

(with coefficient A) according to the canonical thermal statistics of \tilde{N}_0 in a superfluid with finite stiffness. This result nicely reproduces the universal (yet unorthodox) T^3 -depletion found above in Fig. 1.

2.4 Numerical verification of T^3 -depletion via quantum Monte Carlo

Concerning the superfluid density, one might be interested in the consistency between the standard numerical methods and the above analytical proof on a generic T^3 thermal depletion. In particular, such a method must account for many-body information (i.e. as in Ref. [43]) that goes *beyond* the standard sound mode-based considerations [4]. Indeed, as a generic example, for the typical Bose-Hubbard model [44] on a 3D square lattice, Fig. 2 shows that the same T^3 thermal depletion is reproduced by the standard quantum Monte Carlo calculation within a numerically reliable low-temperature range. (Results at T higher than this range suffer from a change of particle mass in this model, while results at lower temperature are affected by the discretization of energy levels in finite size systems.) Interestingly, other than the expected finite-size sensitivity near the phase transition temperature $T_c/t \sim 4$ (in unit of kinetic strength t), the T^3 dependence appears to dominate the entire superfluid phase. Presumably, this is because in this case, the low-temperature physics is dominated by a single scale protected by the superfluid stiffness, which is comparable to T_c with our choice of parameters. Furthermore, as to be published elsewhere [45], through Monte Carlo evaluation, the same T^3 -depletion of superfluid density is also found via the dynamical response that are in direct correspondence to many of the experimental probes employed in Fig. 1.

3 Discussion

Remarkably, the above generic T^3 depletion of bosonic superfluidity at low-temperature exactly reproduces the unorthodox universal fluctuation identified in Fig. 1 unaccounted for by standard theories of superconductivity. These modern superconductors therefore must be understood *not* as Cooper-paired Fermi liquids, but

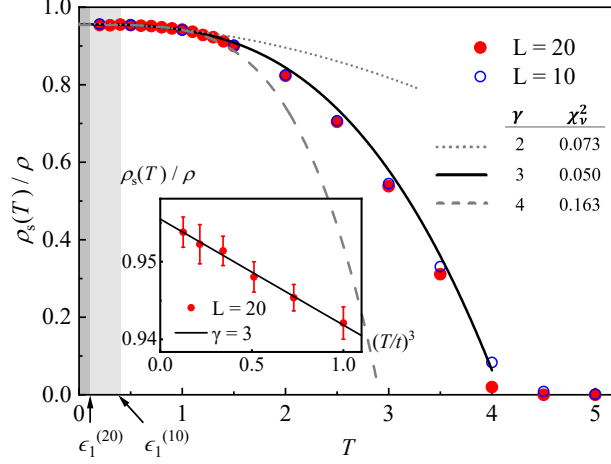


Fig. 2 Numerical verification of the generic T^3 thermal depletion of bosonic superfluidity Superfluid density fraction, $\rho_s(T)/\rho$, in the standard Bose-Hubbard model with moderate interaction strength (5/12 of the bandwidth) is obtained from the standard world-line quantum Monte Carlo calculation for $L \times L \times L$ periodic square lattices with large $L = 20$ (filled circles) and smaller $L = 10$ (open circles). Both systems display a good convergence hosting a T^3 thermal depletion in the low-temperature range in unit of the kinetic strength t . The finite- L effect is stronger only near the transition temperature, $T_c/t \sim 4$, as expected. The statistical error bars are much smaller than the size of the symbols. The grey area indicates the lowest excitation energy $\epsilon_1^{(L)}$ of the systems, below which resemblance to the thermodynamic limit is not guaranteed. Within the numerically reliable temperature range $[4\epsilon_1^{(20)}, 1]$, our fitting of the $L = 20$ data to $B - AT^\gamma$ for $\gamma = 2$ (dashed line), 3 (solid line), and 4 (dotted line) finds the lowest reduced chi-square deviation χ^2_ν (given in the legend) for the $\gamma = 3$ fit, consistent with the trend in the inset.

rather as charged superfluids of emergent bosons, *regardless* of the microscopic origin of such emergent bosonic carriers. Furthermore, recall that above the superconducting temperature many of these materials exhibit non-Fermi liquid behavior [46–72, 72, 72–74], which is trivially consistent with the fact that a Bose liquid is a non-Fermi liquid [75–77]. Altogether, our results suggest a new paradigm where the dominant quantum states of these superconducting materials are those of an emergent Bose liquid [37, 38, 75, 76, 78, 79] and their low-temperature superconducting phase is just the corresponding superfluid phase.

Furthermore, since superfluidity is known to persist in two dimensions [80], contrary to the inapplicability of BCS-meanfield treatment below 3D [81], the above strictly Galilean consistent theory of bosonic superfluidity is naturally capable of explaining pure 2D superconductivity through a finite ‘true condensate’ with stiffness. Indeed, contrary to the lack of bare condensate in 2D Bose gas [82], a finite ‘true condensate’ is expected in a 2D Bose liquid with stiffness. (In addition, the standard particle-*non*-conserving meanfield argument [83] against breaking U(1) symmetry in 2D systems does not directly apply to a particle-conserving Bose liquid.) Specifically, our strictly Galilean consistent superfluid theory gives a universal T^2 -depletion of the superfluid density in a pure-2D bosonic superfluid. It would be highly valuable to experimentally examine the low-temperature thermal depletion in pure-2D

superconducting materials, such as those discovered in the interface [84], single-layer FeSe [85–87], twisted bilayer graphenes [88–92], twisted trilayer graphenes [93–96], and few-layer transition metal dichalcogenides [97–100].

Interestingly, the above T^3 thermal depletion of 3D superfluidity differs from the current lore of T^4 depletion obtained from previous microscopic quantum calculations [42, 101]. Such qualitative difference results from three significant improvements in our derivation over the standard treatment. First, our derivation strictly enforces particle conservation. While the previous Bogoliubov meanfield treatment might be reasonable to realize spontaneous ordering, the lack of associated continuity equation surely renders transport properties highly uncontrolled. Second, our microscopic supercurrent is properly defined directly through a true condensate of long-lived eigen-particles. In contrast, the standard definition is indirectly through a bare condensate $N_0(t)$ that fluctuates in time and does not account for the full superflow [42, 101]. Third and most importantly, as discussed in detail in Section 5.2.4, the essential inertial mass velocity, $\mathbf{v}_I \equiv \frac{\hbar \mathbf{k}}{m}$, as the part of the rigorous velocity operator responsible for describing the net flow of the inertial mass, is completely *absent* in previous treatments. Without including such essential physics, not only would the description fail to properly obey Galilean frame transformation, but it also would not have the information necessary to describe the inertial flow correctly [102]. Indeed, previous careful hydrodynamic analysis [102] has shown that sound-based evaluation of normal fluid density [4, 42, 101] only account for the “entropy flow”, not the essential “mass flow”.

More crucially, 1) the additional capability of reliable number counting (for inertial mass carrying particles) offered by the long-lived eigen-particles and 2) our separating the quantum problem from the thermal statistics together reveal a *complete inadequacy of the standard thermal statistics* assumed in the traditional two-fluid description [4] involving static equilibrium with a *moving* wall. (c.f. Appendix H) As a simple illustration, consider a low-lying eigenstate of a superfluid with a significant Boltzmann weight at very low temperature shown in Fig. 3(a). In the true condensate’s rest frame, the superfluid is stationary while the environment, say the wall of a container, is moving with velocity $-\mathbf{u}$. At low temperature, a physical equilibrium with the wall would dictate that the small number of uncondensed particle (in red) must be moving along with the wall, with velocity similar to $-\mathbf{u}$. Notice a finite energy gap exists in the particle occupation in such distribution Fig. 3(a). As illustrated in Section 5.2.3, this finite energy scale is precisely what protects the system against dissipation in the wall frame. This necessary gap in the distribution, however, does not correspond to any standard thermal distribution.

Indeed, in the standard thermal statistics, even if one carefully constrains [4] the average group velocity of the sound modes to match the wall, $\langle \nabla_{\mathbf{k}} \omega_{\mathbf{k}} \rangle = -\mathbf{u}$, states with large Boltzmann weight would still have most uncondensed eigen-particles at low energy around *zero* momentum. Given the equivalence of the canonical momentum of the elementary excitations to the additional kinematic momentum of the inertial mass-carrying particles (c.f. Section 5.2.4), such a small momentum must corresponds to small inertial mass velocity for these uncondensed eigen-particles, unable to match the velocity of the wall. In other words, in such a standard statistics the normal fluid component, instead of following the wall, would follow the superfluid component

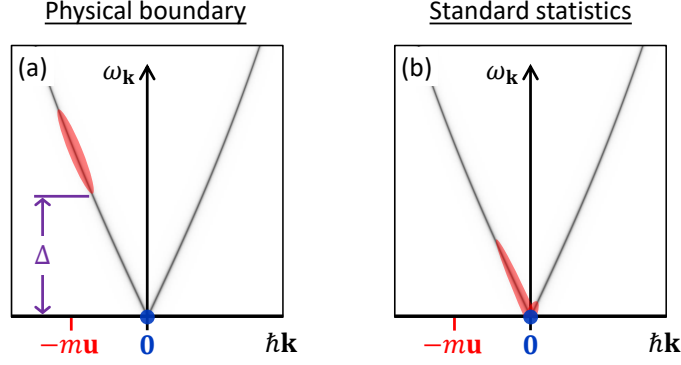


Fig. 3 Demonstration of inapplicability of standard statistics in the presence of steady superflow (a) A typical low-energy eigenstate of a superfluid with large statistical weight at low temperature, when observed in the condensate rest frame, in which the environment, e.g. the wall of the container, is moving steadily with velocity $-\mathbf{u}$. This state is shown together with the dispersion relation between the energy $\omega_{\mathbf{k}}$ and momentum $\hbar\mathbf{k}$ of the elementary excitations. (Since the true condensate is at zero momentum in this frame, $\hbar\mathbf{k}$ is also the *kinematic* momentum of the eigen-particles created from the true condensate.) This state is composed of eigen-particles mostly in the true condensate (in blue) at momentum zero and a small number of uncondensed eigen-particles (in red) with momentum around $-m\mathbf{u}$ to match the velocity of a moving wall, as required by the physical equilibrium with the wall. Correspondingly, the occupation of uncondensed particles has an energy gap, $\Delta > m\mathbf{u}^2$, that protects the system against dissipation (depleting the blue condensed particles). (b) The same for an eigenstate with large Boltzmann weight in the standard thermal statistics. Notice that even with care to ensure a perfect matching between the velocity of the wall and the average group velocity of the sound modes, the corresponding uncondensed particles (in red) are located at momenta around zero, much smaller than $-m\mathbf{u}$, as if the normal fluid component is still following the superfluid one despite the absence of friction between these two components. Such a distribution is obviously inconsistent with the physical equilibrium with the wall as shown in (a). The presence of a steadily flowing supercurrent therefore generally invalidates the standard thermal statistics.

despite the lack of friction between them. Such a standard thermal distribution is therefore *inconsistent* with the physical equilibrium with the wall.

Essentially, sound modes with linear dispersion only describe propagation of the vibration of the liquid, so its average group velocity is *completely unrelated* to the net flow of inertial mass of real matter. That is why such flow contributes only to the “entropy flow” in hydrodynamic analysis [102], instead of the more relevant mass flow on which the superfluid density is physically defined.) Consequently, upon incorrect assignment of sound modes’ average group velocity, $\langle \nabla_{\mathbf{k}} \omega_{\mathbf{k}} \rangle = -\mathbf{u}$, as the average velocity of the normal mass flow, $\mathbf{w} = \sum_{\mathbf{k} \neq \mathbf{k}_0} \frac{\hbar\mathbf{k}}{m} \hat{a}_{\mathbf{k}}^\dagger \hat{a}_{\mathbf{k}} \neq -\mathbf{u}$, evaluating the normal fluid mass density at low temperature via the kinematic momentum \mathbf{P} and volume \mathcal{V} of the system, $\frac{1}{w^2} \mathbf{w} \cdot \mathbf{P} / \mathcal{V}$, would lead to a serious *underestimation*, corresponding to a slower T^4 -thermal depletion [4] instead.

The sound modes’ insensitivity to the inertial mass flow has another serious implication on the existing experimental observation of the thermal depletion of superfluid density. In great contrast to the measurement of bare condensate density [103] and excitation spectrum [104] in liquid helium, to the best of our knowledge, nearly all observations of the superfluid density below 1K are obtained via the second sound

(temperature wave) measurement [105, 106]. However, since the propagation of the entropy-associated low-energy elementary excitations are completely overwhelmed by the sound (vibration) velocity \mathbf{v}_s instead of the inertial mass velocity \mathbf{v}_I (c.f. Section 5.2.4), it is unreasonable to expect properties of second sound to provide a sensitive measure of the inertial mass-carrying superfluid density.

Indeed, it was shown long ago [107–109] that at low temperature the propagation of the vibrational modes alone accurately describe the second sound, in the *absence* of the superfluidity. Even in solids that are not superfluid, second sound with similar temperature dependence to liquid helium has been experimentally observed [110–112]. In fact, given that \mathbf{v}_s is temperature-insensitive and the low-temperature elementary excitations are dominated by it, our more complete description would fall back to the standard theory of second sound and reproduce such experiments. Therefore, it would be highly valuable if other techniques sensitive to the real mass flow [113, 114] can be applied to low enough temperature to directly examine the thermal depletion of the superfluid density. On the other hand, if indeed most modern superconductors in Fig. 1 are simply charged superfluids of emergent bosons, the sensitive response to electromagnetic fields of these charged bosons would offer an unsurpassed advantage over charge-neutral atoms in studying low-temperature superfluid properties.

Finally, in earlier experiments, very often one finds T -linear depletion in some of the materials in Fig. 1 (e.g. in [115]). This distinct behavior is perhaps related to the presence of disorder and impurities in earlier samples. Indeed, the low-temperature superfluid density in our strictly Galilean consistent superfluid theory switches from T^3 to T -linear depletion upon introduction of disorder (c.f. Appendix E).

4 Conclusion

In conclusion, we identify from published experimental data a *universal* T^3 thermal depletion of the low-temperature 3D superfluid density in nearly all modern superconductor families. Contrary to standard lore, this unorthodox behavior persists *independent* of their (fully gapped or nodal) superconducting gap structure. Absent any known generic theory to account for this, we develop a strictly Galilean consistent microscopic quantum theory of superfluidity based on long-lived eigen-particles. With strict particle conservation and inclusion of necessary inertial mass velocity in the theory, the superfluid density is then proven rigorously equivalent to the ‘true condensation’ density for any quantum state of interacting bosonic systems, thus naturally producing the identified universal T^3 thermal fluctuation. Altogether, the revealed fluctuation inevitably leaves charged superfluid of emergent bosons the only remaining theory capable of describing the quantum nature of the unconventional superconductivity in these materials.

5 Methods

5.1 Fitting procedure for experimental data collapse

In this section we describe the procedure used to generate the data collapse plots in Figure 1 of the main text. For clarity, we illustrate the procedure for LaNiGa₂ as an

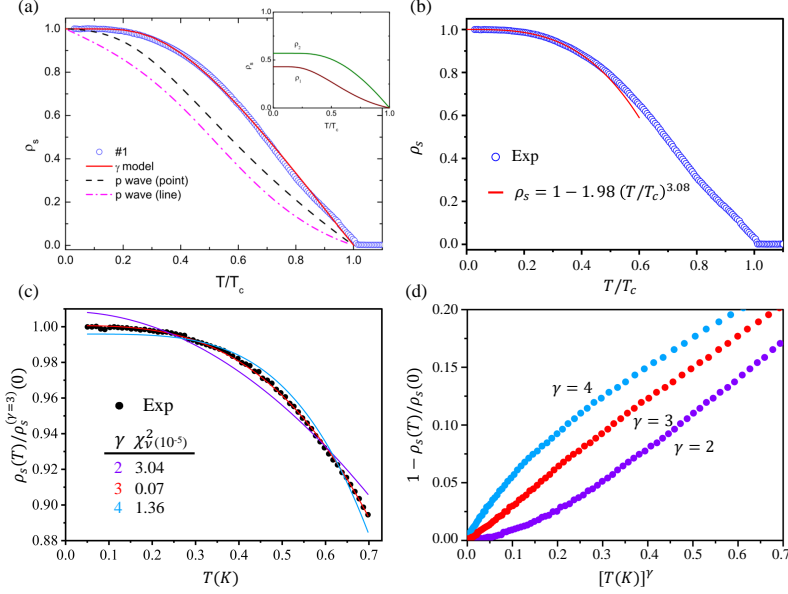


Fig. 4 Demonstration of the fitting procedure applied to (a) the superfluid density ρ_s vs reduced temperature T/T_c in a data set [15] for LaNiGa₂. (b) Extracted data (blue) from (a) with best-fit power-law line (red) fit to data below a threshold where the fit converges. (c) A simple comparison between least square fits to $\rho_s(T)/\rho_s^{(\gamma=3)}(0) = B - AT^\gamma$ with integer exponents $\gamma = 2$ (purple), 3 (red), and 4 (blue) of the data set in (b) with standard reduced chi-square deviation χ^2_ν shown in the table. Notice the very poor fit with $\gamma = 2$ and $\gamma = 4$ with opposite data clustering above and below the fit line, indicating that the best fit lies between them. (d) Plot of $1 - \rho_s$ vs T^γ clearly illustrating that only $\gamma = 3$ fits well (i.e. converges to a straight line) at low temperature.

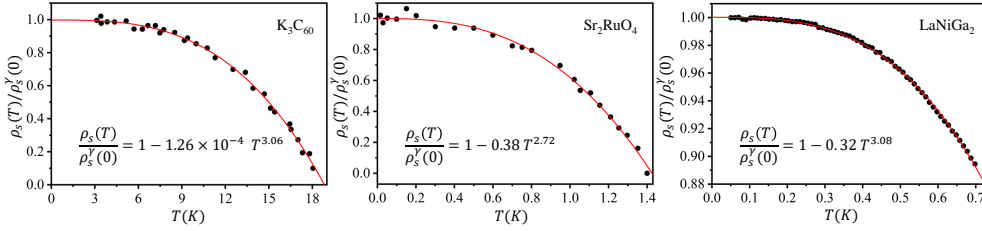


Fig. 5 Examples of $1 - AT^\gamma$ fits using non-integer γ to the experimental data [15, 19, 26] of three materials, all giving an exponent γ closest to integer 3.

example. A figure taken from [15] is displayed in Fig. 4(a). Using the Origin Digitizer, we extract the superfluid density data displayed in Fig. 4(b) and fit the extracted data to a single power-law curve of the form

$$\rho_s(T)/\rho_s(0) = B - AT^\gamma. \quad (6)$$

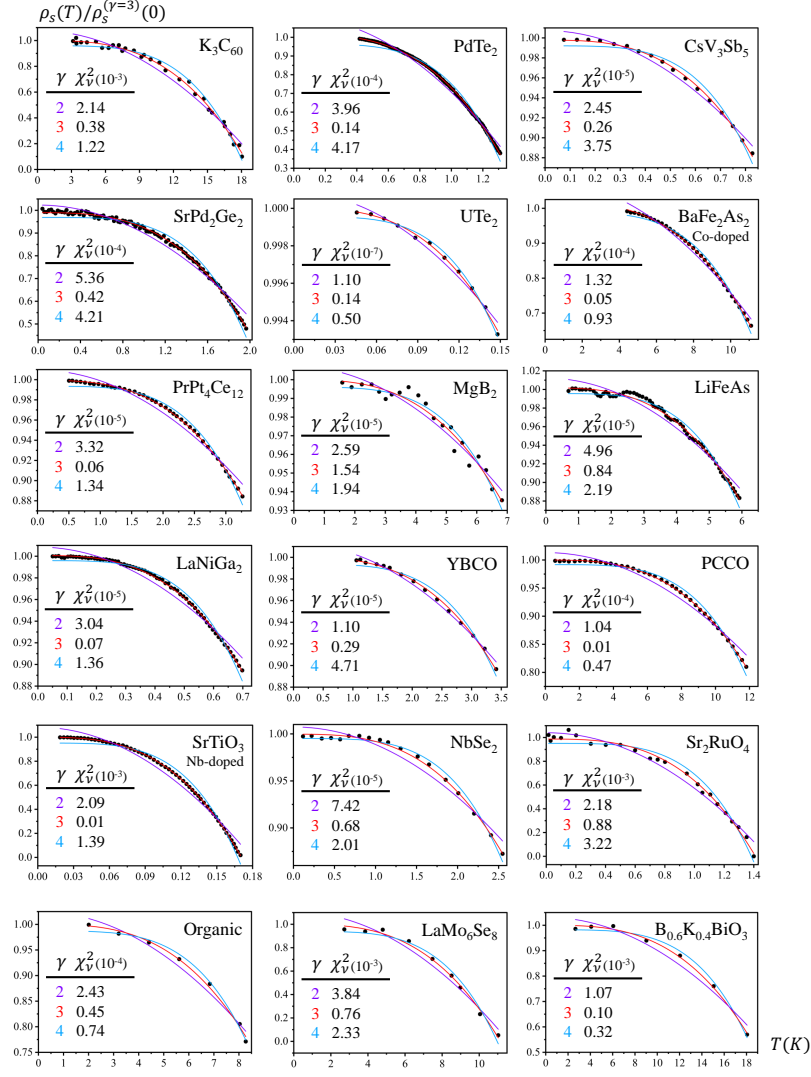


Fig. 6 Least square fits to $B - AT^\gamma$ with integer $\gamma = 2$ (puple), 3 (red), and 4 (blue) for several example data sets at low temperature, with standard reduced chi-square deviation χ^2_ν given in the table. In all cases, $\gamma = 3$ is superior to 2 and 4.

Since we are interested in the low-temperature behavior of the superfluid density in these materials, we discard data near the transition temperature systematically until we find that the fitting procedure appears to converge. The result of such a converged fitting is displayed as a red dotted line in Fig. 4(b). In fact, all of the materials presented here exhibit a resulting power-law fitting with $\gamma \sim 3$, and to illustrate this fact we present three such fittings side-by-side in Fig. 5.

We are interested in the leading order fluctuations at the lowest temperatures and far from any phase transition. A cursory attempt to fit to a (gapped) exponential indicates it is an extremely poor fit, so we search for integer power-law monomial behavior. To that end, we simply display each data set along with best fit lines for fixed integer exponents ($\gamma = 2, 3, 4$ corresponding to purple, red, and blue dotted lines respectively) in Fig. 4(c), where it is clear that $\gamma = 2$ and $\gamma = 4$ each provide very poor fits that significantly underestimate and overestimate γ respectively. To see the convergence to $\gamma = 3$ more clearly in this example, we plot $1 - \rho_s(T)/\rho_s(0)$ vs T^γ in Fig. 4(d) to show that the data converge to a straight line (red points) for $\gamma = 3$ but not for $\gamma = 2$ (purple) or $\gamma = 4$ (blue). In Fig. 6 we display the integer exponent fitting, analogous to Fig. 4(c), for each data set presented in the main text.

In order to display the results in a single data-collapse figure, especially since the onset temperature of this effect ($\sim 0.14\text{K} - 18.05\text{K}$) spans more than two orders of magnitude across all of these materials, we further rescale the temperature to absorb the coefficient

$$\tilde{T} = A^{-\frac{1}{3}}. \quad (7)$$

Finally, in the inset of Figure 1 in the main text, we illustrate the convergence of all data sets to $\gamma = 3$ via a plot analogous to the example in Fig. 4(d). For clarity, we introduce a data-set dependent ‘zoom’ factor Z , identified for each material in Table 1, such that the deviation from $\gamma = 3$ occurs at around the same point in the inset.

Table 1 The zoom factor Z used to scale the inset of Fig. 1 for easier visualization.

Material	$1/Z$
MgB ₂ [11]	0.07
CsV ₃ Sb ₅ [17]	0.15
LiFeAs [12]	0.13
NbSe ₂ [21]	0.1
LaNiGa ₂ [15]	0.25
Ba(Fe _{0.9} Co _{0.1}) ₂ As ₂ [14]	0.35
PrPt ₄ Ge ₁₂ [13]	0.18
PdTe ₂ [25]	0.6
K ₃ C ₆₀ [19]	1
SrPd ₂ Ge ₂ [23]	0.5
Pr _{2-x} Ce _x CuO _{4-δ} ($x = 0.131$) [20]	0.08
Ba _{0.6} K _{0.4} BiO ₃ [18]	0.45
LaMo ₆ Se ₈ [16]	0.45
Sr ₂ RuO ₄ [26]	0.7
UTe ₂ [27]	0.015
YBa ₂ Cu ₃ O _{6+y} [22]	0.1
Nb : SrTiO ₃ [28]	1
κ -(BEDT - TTF) ₂ Cu[N(CN) ₂]Br [24]	0.2

5.2 Rigorous theory of standard superfluidity

To circumvent the key challenge of traditional approaches, namely the lack of direct access to long time-scale properties such as Bose-Einstein condensation and superfluidity, due to quantum fluctuation, here we will employ the eigen-particle representation that absorbs *all* quantum fluctuations into the internal structure of them [40]. For the system's symmetry-protected constants of the motion, such as the total particle number, inertial mass, and kinetic momentum, these eigen-particles carry the same contribution as the underlying bare particles. They thus offer a convenient means to track the flow of these properties directly through the current of eigen-particles.

We then introduce a rigorous many-body quantity, a long-lived ‘true condensate’, and show that only these condensed eigen-particles can generate a curl-less current response, i.e. a supercurrent, with a net flow velocity described by the inertial mass velocity that has been missed in previous theories. Correspondingly, the inertial mass density of superfluid is therefore equivalent to the number density of the ‘true condensation’ density for arbitrary pure quantum states and thus any ensemble of them. Finally, in the linear response regime, where thermal equilibrium is reached before external stimuli are applied, a T^3 -depletion of the superfluid density follows that of the true condensate density.

5.2.1 Eigen-particles

Consider a general translational invariant N -particle bosonic system that hosts superfluidity described by a generic interacting Hamiltonian [116] without local $U(1)$ symmetry,

$$H = \sum_{\mathbf{k}_1} \epsilon_{\mathbf{k}_1} a_{\mathbf{k}_1}^\dagger a_{\mathbf{k}_1} + \frac{1}{2!} \sum_{\mathbf{q}, \mathbf{k}_1, \mathbf{k}_2} V_{\mathbf{q}} a_{\mathbf{k}_1+\mathbf{q}}^\dagger a_{\mathbf{k}_2-\mathbf{q}}^\dagger a_{\mathbf{k}_2} a_{\mathbf{k}_1}, \quad (8)$$

represented by second-quantized creation operators $a_{\mathbf{k}}^\dagger$ of momentum \mathbf{k} having kinetic energy $\epsilon_{\mathbf{k}} = \frac{\hbar^2}{2m} \mathbf{k} \cdot \mathbf{k}$. (For simpler counting, the momentum space is discretized by imposing a spatial periodic boundary condition of the system size.) As to be elaborated below, an essential difficulty in the existing quantum descriptions [4, 42, 101] is to identify a *long-lived* curl-less portion of the current in a *particle-conserving* system as the superfluid component. To this end, we resort to the diagonal-representation of H [38, 40] (c.f. Appendix B.1),

$$\begin{aligned} H_{\text{diag}}[\{\tilde{a}_{\mathbf{k}}^\dagger\}] &\equiv H[\{a_{\mathbf{k}}^\dagger\}] \\ &= \sum_{\mathbf{k}_1} \epsilon_{\mathbf{k}_1} \tilde{a}_{\mathbf{k}_1}^\dagger \tilde{a}_{\mathbf{k}_1} + \frac{1}{2!} \sum_{\mathbf{k}_1, \mathbf{k}_2} \epsilon_{\mathbf{k}_1, \mathbf{k}_2} \tilde{a}_{\mathbf{k}_1}^\dagger \tilde{a}_{\mathbf{k}_2}^\dagger \tilde{a}_{\mathbf{k}_2} \tilde{a}_{\mathbf{k}_1} \\ &\quad + \cdots + \frac{1}{N!} \sum_{\mathbf{k}_1 \cdots \mathbf{k}_N} \epsilon_{\mathbf{k}_1 \cdots \mathbf{k}_N} \tilde{a}_{\mathbf{k}_1}^\dagger \cdots \tilde{a}_{\mathbf{k}_N}^\dagger \tilde{a}_{\mathbf{k}_N} \cdots \tilde{a}_{\mathbf{k}_1}, \end{aligned} \quad (9)$$

using the *long-lived* fully-dressed ‘eigen-particles’, $\tilde{a}_{\mathbf{k}}^\dagger \equiv U^\dagger a_{\mathbf{k}}^\dagger U$, transformed from the ‘bare’ particle creation operators $a_{\mathbf{k}}^\dagger$ via a unitary operator U . Since U is tasked to bring

only the beyond-one-body terms in H into a diagonal form, the coefficients $\epsilon_{\mathbf{k}}$ of the *already diagonal* one-body terms in Eq.(8) are preserved in Eq.(9), independent of its precise form. The coefficients $\epsilon_{\mathbf{k}_1 \dots \mathbf{k}_M}$ of the remaining M -body terms are determined through diagonalization, $H_{\text{diag}}[\{\tilde{a}_{\mathbf{k}}^\dagger\}] = H[\{a_{\mathbf{k}}^\dagger\}] = UH[\{\tilde{a}_{\mathbf{k}}^\dagger\}]U^\dagger$, via the a unitary operator U under a *fixed* particle number N . The standard commutation, $[\tilde{a}_{\mathbf{k}}, \tilde{a}_{\mathbf{p}}^\dagger] = \delta_{\mathbf{k}\mathbf{p}}$, testifies to the bosonic nature of the eigen-particles represented by $\tilde{a}_{\mathbf{k}}^\dagger$, while the diagonal structure of H_{diag} ensures preservation of eigen-particles during time evolution as all interaction-induced quantum fluctuations (of finite time scale) are fully absorbed into $\tilde{a}_{\mathbf{k}}^\dagger$.

Extraordinarily, for long-wavelength properties the eigen-particles carry the same inertial mass m , charge, and momentum $\hbar\mathbf{k}$ of the bare particles. This is evident since the unitary transformation U must respect all constants of motions, such as total particle number N , inertial mass M , and kinematic momentum \mathbf{P} , $[U, N] = [U, M] = [U, \mathbf{P}] = 0$. One thus finds,

$$N \equiv \sum_{\mathbf{k}} a_{\mathbf{k}}^\dagger a_{\mathbf{k}} = U^\dagger N U = \sum_{\mathbf{k}} \tilde{a}_{\mathbf{k}}^\dagger \tilde{a}_{\mathbf{k}} \quad (10)$$

$$M \equiv \sum_{\mathbf{k}} m a_{\mathbf{k}}^\dagger a_{\mathbf{k}} = U^\dagger M U = \sum_{\mathbf{k}} m \tilde{a}_{\mathbf{k}}^\dagger \tilde{a}_{\mathbf{k}} \quad (11)$$

$$\mathbf{P} \equiv \sum_{\mathbf{k}} \hbar \mathbf{k} a_{\mathbf{k}}^\dagger a_{\mathbf{k}} = U^\dagger \mathbf{P} U = \sum_{\mathbf{k}} \hbar \mathbf{k} \tilde{a}_{\mathbf{k}}^\dagger \tilde{a}_{\mathbf{k}} \equiv \tilde{\mathbf{P}} . \quad (12)$$

Superior to the generally fluctuating bare particles, the eigen-particles are therefore ideal when number-counting for properties of a long time scale.

5.2.2 True condensate

A good example of such a phenomenon of long time scale is the Bose-Einstein condensation in an interacting system. The diagonal form of Eq.(9) guarantees that all N -body eigenstates of the system are simply collections of N eigen-particles in *direct product* form,

$$|\{N_{\mathbf{k}}\}\rangle \equiv \prod_{\mathbf{k}} \frac{(\tilde{a}_{\mathbf{k}}^\dagger)^{N_{\mathbf{k}}}}{\sqrt{N_{\mathbf{k}}!}} |0\rangle \Big|_{\sum_{\mathbf{k}} N_{\mathbf{k}}=N} . \quad (13)$$

For standard translational-invariant kinetic energy-dominated superfluid systems, the ground state is therefore a ‘true Bose-Einstein condensate’ $|\Omega\rangle \equiv \frac{1}{\sqrt{N!}} (\tilde{a}_{\mathbf{k}_0}^\dagger)^N |0\rangle$, containing all N eigen-particles residing at momentum $\mathbf{k}_0 = \mathbf{0}$ that has the lowest kinetic energy. Similarly, the low-lying elementary excited states are those with eigen-particles excited from the true condensate, for example $|E_{\mathbf{k}}\rangle = \frac{1}{\sqrt{(N-1)!}} \tilde{a}_{\mathbf{k}}^\dagger (\tilde{a}_{\mathbf{k}_0}^\dagger)^{N-1} |0\rangle = \frac{1}{\sqrt{N}} \tilde{a}_{\mathbf{k}}^\dagger \tilde{a}_{\mathbf{k}_0} |\Omega\rangle = \tilde{\alpha}_{\mathbf{k}}^\dagger |\Omega\rangle$, corresponding to creation of long-lived excitation, $\tilde{\alpha}_{\mathbf{k}}^\dagger \equiv \tilde{a}_{\mathbf{k}}^\dagger \tilde{a}_{\mathbf{k}_0} \tilde{N}_0^{-\frac{1}{2}}$, from the ground state.

The above unconventional definition of ‘true condensate’ makes perfect physical sense, since $\tilde{N}_0(t) \equiv \tilde{a}_{\mathbf{k}_0}^\dagger(t) \tilde{a}_{\mathbf{k}_0}(t)$ in the Heisenberg picture is a constant of motion,

$\tilde{N}_0(t) = \tilde{N}_0$ given $[\tilde{N}_0, H_{\text{diag}}] = 0$, consistent with condensation being a long-lived phenomenon. In contrast, the standard ‘bare’ condensate, $a_{\mathbf{k}_0}^\dagger(t)a_{\mathbf{k}_0}(t)$, always fluctuates on a much shorter time scale ($[a_{\mathbf{k}_0}^\dagger(t)a_{\mathbf{k}_0}(t), H] \neq 0$) and is therefore not directly applicable to any long-lived property of the system.

5.2.3 Superfluid and its stiffness in eigen-particle picture

Now, as an illuminating example, consider observing a superfluid in this many-body ground state $|\Omega\rangle$ from a lab frame with a relative velocity $-\mathbf{u}$ to the superfluid. Rather uniquely, against potential dissipation/excitations triggered by coupling to the lab environment, a superfluid would continue to flow steadily with a constant velocity \mathbf{u} far beyond the experimental time scale of the observer. Obviously, since in this case the whole system remains in the same perfectly coherent quantum state, the superfluid fraction ρ_s/ρ of such a quantum pure state is simply 1, same as the true condensation fraction \tilde{N}_0/N . This is in great contrast to the ‘bare’ condensation density $\langle\Omega|a_{\mathbf{k}_0}^\dagger a_{\mathbf{k}_0}|\Omega\rangle < N$ due to its quantum fluctuation. Below we will show that *only* eigen-particles in the true condensate contribute to the super-current, and ρ_s/ρ is in fact identical to \tilde{N}_0/N for *arbitrary* quantum states (and thus any ensemble of them.)

As well-established in the literature [117], the superfluid’s resilience against dissipation is phenomenologically associated with the emergence of stiffness (in the superflowing part of the liquid) that restricts the allowed excitations to only *long-lived* elementary excitations with a minimum group velocity $v_s\hat{\mathbf{k}}$ in the condensate frame. In the eigen-particle representation, such long-lived excitations correspond to the condensation-enhanced probability of promoting eigen-particles from the true condensate to an uncondensed momentum, $\tilde{a}_{\mathbf{k}_0+\mathbf{q}}^\dagger\tilde{a}_{\mathbf{k}_0}$, via injection of momentum $\hbar\mathbf{q}$. (In contrast, given the smooth distribution of occupation among the uncondensed momenta $\hbar\mathbf{k}$, their promotion via the same momentum, $\tilde{a}_{\mathbf{k}+\mathbf{q}}^\dagger\tilde{a}_{\mathbf{k}}$, together would give rise to short-lived fluctuation within an energy-momentum continuum.) To facilitate the discussion, Fig. 7 also shows the energy-momentum dispersion of such stiffness-associated long-lived excitations. In addition, the momentum axis in the plot is shifted by the momentum of the true condensate, $\hbar\mathbf{k}_0$, to easily access the momentum of the eigen-particles.

Let’s now extend the above example of a fully condensed ground state to an excited pure quantum state of the system containing some eigen-particles already in uncondensed momenta, equivalent to injecting multiple elementary excitations to the ground state. Figure 7(a) illustrates an example of such state in the rest frame of the condensate, with most eigen-particles condensing at momentum zero (in blue) and the rest (in red) spreading out around momentum $-m\mathbf{u}$ with similar velocity $-\mathbf{u}$ to that of the environment, for example the wall of a container. Such a quantum pure state is representative of the typical states in thermal equilibrium with the wall, in which the “normal” fluid would become stationary against the wall. As shown in panel (b), upon Galilean boosting the same quantum state in the wall frame, $(\omega'_{\mathbf{k}}, \mathbf{p}') = (\omega_{\mathbf{k}} + \mathbf{v} \cdot \mathbf{p}, \mathbf{p} + m\mathbf{u})$, one finds the condensed eigen-particles moving steadily

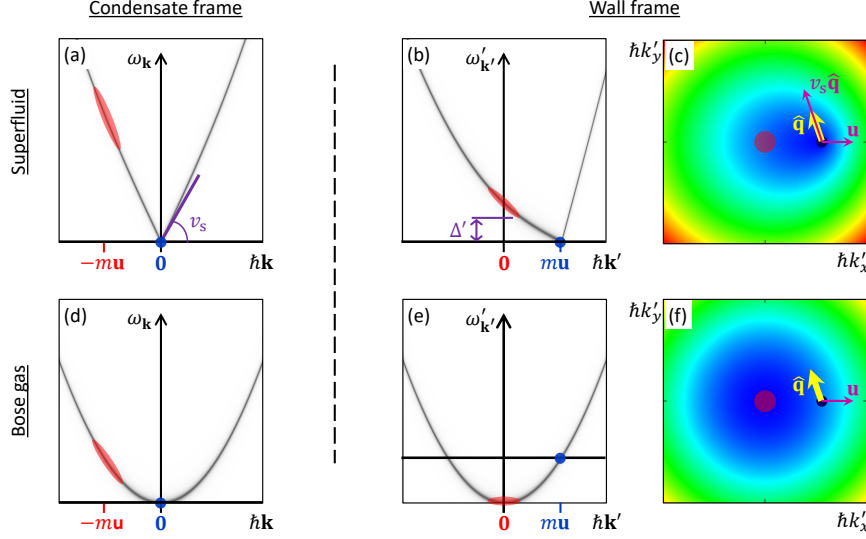


Fig. 7 Illustration of the supercurrent in a superfluid (upper panels) in comparison to a Bose gas (lower panels). (a)(d) The excitation energy $\omega_{\mathbf{k}}$ required to excite a eigen-particle from the condensate (in blue) to a different momentum $\hbar\mathbf{k}$ (in red) near momentum $-m\mathbf{u}$, having similar velocity to that of the environment, for example the wall of a pipe. (b)(e) The same quantum state observed in the wall frame, in which the condensed particles move steadily with velocity \mathbf{u} and momentum $\hbar\mathbf{k}'_0 = m\mathbf{u}$ while the uncondensed particles are nearly stationary. Here the momentum axis of the excitations' energy-momentum dispersion is shifted by the momentum of the true condensate, $\hbar\mathbf{k}'_0$, to easily access the momentum of the corresponding eigen-particles. Notice in (a) the finite velocity (slope) v_s near condensed momentum that reflects the stiffness of a superfluid. Owing to the stiffness, the momentum $m\mathbf{v}$ of the condensed eigen-particles in (b) still remains the lowest in energy and thus energetically 'protected' by Δ' against dissipation triggered by the wall. In contrast, in a Bose gas the condensed eigen-particles have no such protection in (d) and (e). (c)(f) Contour plot of the energy-momentum dispersion in the wall frame. As a result of the stiffness in the superfluid, besides the boost velocity \mathbf{u} , the condensed eigen-particles in (c) give an additional longitudinal-only contribution $v_s \hat{\mathbf{q}}$ to $\hat{\mathbf{v}}$ in the total current $\hat{\mathbf{J}}_{\mathbf{q}}$ of wavenumber \mathbf{q} [c.f. Eq.(15)]. Such a longitudinal-only contribution gives rise to the supercurrent, by definition. (f) In contrast, in a Bose gas the condensed eigen-particles give only the boost velocity \mathbf{u} but no longitudinal-only contribution associated with the supercurrent.

with velocity \mathbf{u} and momentum $\hbar\mathbf{k}'_0 = m\mathbf{u}$ and the rest of the eigen-particles nearly stationary around zero momentum. (Note that for a direct visualization of eigen-particles' momenta in Fig. 7, while $\omega'_{\mathbf{k}}$ denotes the excitation energy, \mathbf{p}' denotes the momentum of the eigen-particle $\hbar\mathbf{k}' = \hbar\mathbf{q} + \hbar\mathbf{k}'_0$, not the momentum $\hbar\mathbf{q}$ of the elementary excitations.)

Notice that the energy-momentum dispersion is different in (a) and (b) and thus *inertial frame dependent*. This unusual lack of frame invariance of the dispersion (and the corresponding low-energy effective theory) is a unique characteristic of superfluids that results from the above-mentioned finite velocity $v_s \hat{\mathbf{k}}$ of the elementary excitations. (In essence, the spontaneously broken U(1) symmetry implies the existence of a special inertial frame, the true condensate's rest frame, in which the stiffness-associated velocity is cleanly defined.) Owing to this characteristic, even in the wall frame in (b),

as long as $u < v_s$, the condensed eigen-particles still reside in the momentum with the lowest energy, and are therefore energetically ‘protected’ by Δ' against potential dissipation induced by coupling to the wall. This is in great contrast to the normal *frame invariant* dispersion of a Bose gas in panels (d) and (e), containing similar condensation. Without the above-mentioned stiffness, in the wall frame in (e) the condensed eigen-particles are no longer in the momentum with the lowest energy and thus are vulnerable to dissipation.

5.2.4 Two physical velocities of current fluctuation in a superfluid

Now, since the superflow is defined through its dissipation-less (curl-less) response to external stimuli, it can be directly detected through the off-diagonal $\tilde{\mathbf{J}}_{\mathbf{q} \neq \mathbf{0}}$ that creates an excitation by injecting to the system a spatially oscillating current of finite wavenumber \mathbf{q} . As discussed above, the superfluid component displays stiffness, so its elementary excitations are restricted to only long-lived elementary excitations that propagate with minimum velocity $v_s \hat{\mathbf{k}}$.

Before diving into this essential quantity, it is important to first realize that these elementary excitations of superfluids, in fact, consist of two physically distinct components with different velocities. On the one hand, the inertial mass in the liquid can freely flow with velocity, $\mathbf{v}_I \equiv \frac{\hbar \mathbf{k}}{m}$, according to its kinematic momentum $\hbar \mathbf{k}$. On the other, the stiffness of the superfluid component would ensure that the purely vibrational (or “sound”) modes propagate with a fixed sound velocity $v_s \hat{\mathbf{k}}$. Yet, unlike in metallic solids, where the latticed vibration (sound) and the inertial mass flow have different carriers, namely the atoms and the electrons, respectively, in a liquid both velocities share the same carriers. Consequently, as part of a particle-hole excitation in a superfluid, each particle (and hole) outside the condensate must have velocity, $\frac{\hbar \mathbf{k}}{m} + v_s \hat{\mathbf{k}}$, containing both types of physical propagation.

Figure 8 gives a simple illustration how the medium evolves over time that reflects these two components of velocity in the fluctuation. Similar to the acoustic phonon in solids, a fluctuation can be viewed as a particle-hole excitation propagating with the sound velocity \mathbf{v}_s , corresponding to the enhancement and reduction of the spatial distribution of the density, respectively. However, unlike that found in solids, the medium of the vibration in a liquid can itself flow with a inertial mass velocity, \mathbf{v}_I . This gives rise to an additional velocity \mathbf{v}_I of the enhancement (the particle) to that of the reduction (hole). Consequently, over time the peak of the enhancement would move away from the reduction, while carrying the inertial mass with it.

It is straightforward to show (c.f. Appendix G) that such a two-component velocity, $\frac{\hbar \mathbf{k}}{m} + v_s \hat{\mathbf{k}}$, is essential to ensure the equivalence between the canonical momentum of the fluctuation and the kinematic momentum of the medium. Rather intuitively, even though the $v_s \hat{\mathbf{k}}$ term appears to dominate near the condensate momentum, it only describes the energy and momentum propagation of the purely vibrational (sound) part of the current fluctuation. The more relevant net flow velocity of the inertial mass is *completely* captured by the kinematic velocity $\frac{\hbar \mathbf{k}}{m}$ term, inclusion of which is therefore *absolutely necessary*. On that note, since the standard Bogoliubov treatment [3, 118] does not retain this necessary kinematic velocity, it is not too surprising

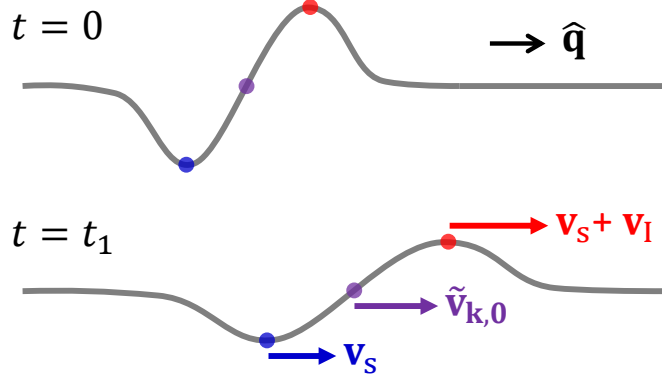


Fig. 8 Illustration of two propagation velocities of current fluctuation in a superfluid. The *longitudinal* propagation of current fluctuation contains two distinct components of velocity: 1) the inertial mass velocity $\mathbf{v}_I \equiv \frac{\hbar \mathbf{k}}{m}$, and the sound velocity $\mathbf{v}_s = v_s \hat{\mathbf{k}}$. The latter corresponds to the group velocity of the valley of fluctuation (in blue). Notice that the peak of the fluctuation (in red) has a faster velocity $\mathbf{v}_s + \mathbf{v}_I$. Consequently, over some period of time t_1 , the inertial mass associated with the peak would move away from the valley with a relative velocity \mathbf{v}_I . The node (in purple) propagates with the average velocity $\tilde{\mathbf{v}}_{\mathbf{k}_1 \mathbf{k}_0} = \mathbf{v}_s + \frac{1}{2} \mathbf{v}_I$, ($\mathbf{k}_0 = \mathbf{0}$ used here) as encoded in the current operator $\tilde{\mathbf{J}}_{\mathbf{q}=(\mathbf{k}_1 - \mathbf{k}_0)}$ in Eq.(14).

that such treatment does not uphold the essential f -sum rule in its corresponding current response [119].

Furthermore, it is important to note that this form of velocity, $\frac{\hbar \mathbf{k}}{m} + v_s \hat{\mathbf{k}}$, is already the most general form of velocity in Galilean consistent systems, as any additional contribution would necessarily violate the standard Galilean boost of velocity. Essentially, the kinematic velocity $\frac{\hbar \mathbf{k}}{m}$ ensures a proper boost of velocity across frames, allowing the momentum-independent sound velocity $v_s \hat{\mathbf{k}}$ to remain fixed across frames.

Back to the eigen-particle picture, recall that the eigen-particles contribute the same bare mass m and momentum $\hbar \mathbf{k}$ to the total mass and momentum of the system. They are therefore ideal for tracking the flow of inertial mass through total momentum of the system in various inertial frames. It is straightforward to verify (c.f. Appendix B.2) that the current operator,

$$\tilde{\mathbf{J}}_{\mathbf{q} \neq \mathbf{0}} = \frac{1}{\mathcal{V}} \sum_{\mathbf{k}} \tilde{a}_{\mathbf{k}'}^\dagger \tilde{\mathbf{v}}_{\mathbf{k}' \mathbf{k}} \tilde{a}_{\mathbf{k}} \Big|_{\mathbf{k}' = \mathbf{k} + \mathbf{q}}, \quad (14)$$

of wavenumber $\mathbf{q} \neq \mathbf{0}$, as derived from time evolution of eigen-particles' spatial distribution, not only strictly satisfies the continuity equation at length scales $2\pi/\mathbf{q}$ longer than the size of the eigen-particles. But also, the associated diagonal and hermitian velocity operator of the eigen-particles,

$$\tilde{\mathbf{v}}_{\mathbf{k}', \mathbf{k} \neq \mathbf{k}'} = \frac{1}{\hbar} \nabla_{\mathbf{k}} \left(\epsilon_{\mathbf{k}} + \sum_{\mathbf{k}_1} \epsilon_{\mathbf{k} \mathbf{k}_1} \tilde{a}_{\mathbf{k}_1}^\dagger \tilde{a}_{\mathbf{k}_1} \right)$$

$$\begin{aligned}
& + \frac{1}{2!} \sum_{\mathbf{k}_1 \mathbf{k}_2} \epsilon_{\mathbf{k} \mathbf{k}_1 \mathbf{k}_2} \tilde{a}_{\mathbf{k}_1}^\dagger \tilde{a}_{\mathbf{k}_2}^\dagger \tilde{a}_{\mathbf{k}_2} \tilde{a}_{\mathbf{k}_1} + \dots \Big|_{\underline{\mathbf{k}}=(\mathbf{k}'+\mathbf{k})/2} \\
& \equiv \frac{1}{\hbar} \nabla_{\underline{\mathbf{k}}} \left(\epsilon_{\underline{\mathbf{k}}} + \tilde{\Sigma}_{\underline{\mathbf{k}}} \right) \Big|_{\underline{\mathbf{k}}=(\mathbf{k}'+\mathbf{k})/2} \equiv \frac{1}{\hbar} \nabla_{\underline{\mathbf{k}}} \tilde{\epsilon}_{\underline{\mathbf{k}}} \Big|_{\underline{\mathbf{k}}=(\mathbf{k}'+\mathbf{k})/2} \\
& = \left(\frac{\hbar \mathbf{k}}{m} + \frac{1}{\hbar} \nabla_{\underline{\mathbf{k}}} \tilde{\Sigma}_{\underline{\mathbf{k}}} \right) \Big|_{\underline{\mathbf{k}}=(\mathbf{k}'+\mathbf{k})/2}, \tag{15}
\end{aligned}$$

indeed contains two distinct contributions corresponding to the above considerations. First, the kinematic velocity of the inertial mass, $\mathbf{v}_I \equiv \frac{\hbar \mathbf{k}}{m}$, naturally appears that describes the velocity of inertial mass flow and maintains a proper Galilean boost of velocity. In addition, there is an interaction-induced contribution to the diagonal velocity operator, $\frac{1}{\hbar} \nabla_{\underline{\mathbf{k}}} \tilde{\Sigma}_{\underline{\mathbf{k}}}$, whose expectation value, for pure states with superfluid stiffness, encapsulates the constant sound velocity, as the only remaining freedom allowed by Galilean transformable velocity.

Conveniently, the above velocity can be directly accessed through the dispersion of elementary particle-hole excitations. It is straightforward to show (c.f. Appendix B.4) that the *excitation* energy to move an eigen-particle from momentum \mathbf{k} to $\mathbf{k} + \mathbf{q}$ is simply $\tilde{\epsilon}_{\mathbf{k}+\mathbf{q}} - \tilde{\epsilon}_{\mathbf{k}}$. Thus, for a system with true condensate at momentum \mathbf{k}_0 , the energy for elementary excitations, $\tilde{\alpha}_{\mathbf{k}}^\dagger \equiv \tilde{a}_{\mathbf{k}}^\dagger \tilde{a}_{\mathbf{k}_0} \tilde{N}_0^{-\frac{1}{2}}$, is just $\omega_{\mathbf{k}} = \tilde{\epsilon}_{\mathbf{k}} - \tilde{\epsilon}_{\mathbf{k}_0}$. In turn, the expectation value of the velocity operator,

$$\langle \tilde{\mathbf{v}}_{\mathbf{k}', \mathbf{k} \neq \mathbf{k}'} \rangle = \left\langle \frac{1}{\hbar} \nabla_{\underline{\mathbf{k}}} \tilde{\epsilon}_{\underline{\mathbf{k}}} \right\rangle \Big|_{\underline{\mathbf{k}}=(\mathbf{k}'+\mathbf{k})/2} = \frac{1}{\hbar} \nabla_{\underline{\mathbf{k}}} \omega_{\underline{\mathbf{k}}} \Big|_{\underline{\mathbf{k}}=(\mathbf{k}'+\mathbf{k})/2}, \tag{16}$$

can be obtained from the gradient of the energy-momentum dispersion shown in Fig. 7.

It is important to note a distinct form of the total current of the system $\tilde{\mathbf{J}}$ (with $\mathbf{q} = \mathbf{0}$) from that of $\tilde{\mathbf{J}}_{\mathbf{q} \rightarrow \mathbf{0}}$,

$$\tilde{\mathbf{J}} = \sum_{\mathbf{k}} \frac{1}{\mathcal{V}} \tilde{a}_{\mathbf{k}}^\dagger \tilde{\mathbf{v}}_{\mathbf{k}, \mathbf{k}} \tilde{a}_{\mathbf{k}} = \frac{1}{\mathcal{V}} \sum_{\mathbf{k}} \frac{\hbar \mathbf{k}}{m} \tilde{a}_{\mathbf{k}}^\dagger \tilde{a}_{\mathbf{k}}, \tag{17}$$

in which the interaction-induced contributions, $\frac{1}{\hbar} \nabla_{\underline{\mathbf{k}}} \tilde{\Sigma}_{\underline{\mathbf{k}}}$, to $\tilde{\mathbf{v}}_{\mathbf{k}, \mathbf{k}}$ is identically zero. This is because in translational invariant systems the many-body interaction preserves the total momentum $\tilde{\mathbf{P}}$, such that

$$\tilde{\mathbf{J}} = \frac{1}{m \mathcal{V}} \tilde{\mathbf{P}} = \frac{1}{\mathcal{V}} \sum_{\mathbf{k}} \frac{\hbar \mathbf{k}}{m} \tilde{a}_{\mathbf{k}}^\dagger \tilde{a}_{\mathbf{k}} \tag{18}$$

only measures kinematic velocity of the inertial mass. (Intuitively, interaction effects, $\frac{1}{\hbar} \nabla_{\underline{\mathbf{k}}} \tilde{\Sigma}_{\underline{\mathbf{k}}}$ at best can only account for the velocity the purely vibrational motion and thus cannot contribute to the net flow of inertial mass.)

5.2.5 Supercurrent

With the above off-diagonal current fluctuation operator $\tilde{\mathbf{J}}_{\mathbf{q} \neq 0}$, one is now able to single out the supercurrent component using its curl-less nature. In the above general example, let's inspect the contribution to the long-wavelength limit, $\mathbf{q} \rightarrow \mathbf{0}$, of the dressed current $\tilde{\mathbf{J}}_{\mathbf{q}}$ in Eq.(14), $\frac{1}{\mathcal{V}} \tilde{a}_{\mathbf{k}_0+\mathbf{q}}^\dagger \tilde{\mathbf{v}}_{\mathbf{k}_0+\mathbf{q},\mathbf{k}_0} \tilde{a}_{\mathbf{k}_0}$, from the true condensate in Fig. 7(a). The linear energy-momentum dispersion associated with the superfluid phase stiffness gives $\langle \tilde{\mathbf{v}}_{\mathbf{k}_0+\mathbf{q},\mathbf{k}_0} \rangle = \frac{\hbar}{m}(\mathbf{k}_0 + \frac{\mathbf{q}}{2}) + v_s \hat{\mathbf{q}} \rightarrow v_s \hat{\mathbf{q}}$ in the condensate frame ($\mathbf{k}_0 = \mathbf{0}$). Galileo boosting the system to the wall frame by velocity \mathbf{u} would shift the condensed eigen-particles to momentum $\hbar \mathbf{k}'_0 = m\mathbf{u}$ in Fig. 7(b) and its contribution to the current becomes $\frac{1}{\mathcal{V}} \tilde{a}_{\mathbf{k}'_0+\mathbf{q}}^\dagger \tilde{\mathbf{v}}_{\mathbf{k}'_0+\mathbf{q},\mathbf{k}'_0} \tilde{a}_{\mathbf{k}'_0}$, with $\langle \tilde{\mathbf{v}}_{\mathbf{k}'_0+\mathbf{q},\mathbf{k}'_0} \rangle = \frac{\hbar}{m}(\mathbf{k}'_0 + \frac{\mathbf{q}}{2}) + v_s \hat{\mathbf{q}} \rightarrow \mathbf{u} + v_s \hat{\mathbf{q}}$. Again, one sees that the kinematic velocity term in Eq.(15) is *necessary* to maintain the proper Galilean boost here, even though it is not produced by the standard Bogoliubov approximation.

Notice that, in addition to the boost velocity associated with the choice of the inertial frame, the condensed eigen-particles' contribution to the dressed current $\tilde{\mathbf{J}}_{\mathbf{q} \rightarrow 0}$ is 'longitudinal-only' with $v_s \hat{\mathbf{q}}$ always along the direction of \mathbf{q} , regardless of the choice of the $\hat{\mathbf{q}}$ direction. Since $\mathbf{q} \times \langle \tilde{\mathbf{v}}_{\mathbf{k}'_0+\mathbf{q},\mathbf{k}'_0} \rangle = 0$ implies $\nabla \times \langle \tilde{\mathbf{v}}(\mathbf{r}) \rangle = 0$, such a spatially curl-less component of current by definition corresponds to the supercurrent component,

$$\tilde{\mathbf{J}}_{\mathbf{q} \neq 0}^s = \frac{1}{\mathcal{V}} (\tilde{a}_{\mathbf{k}_0+\mathbf{q}}^\dagger \tilde{\mathbf{v}}_{\mathbf{k}_0+\mathbf{q},\mathbf{k}_0} \tilde{a}_{\mathbf{k}_0} + \tilde{a}_{\mathbf{k}_0}^\dagger \tilde{\mathbf{v}}_{\mathbf{k}_0,\mathbf{k}_0-\mathbf{q}} \tilde{a}_{\mathbf{k}_0-\mathbf{q}}) \quad (\text{with stiffness}), \quad (19)$$

in the condensate frame. Clearly, the supercurrent is intimately tied to the response associated *only* with eigen-particles in the true condensate. In comparison, without a similar protection from the stiffness, the rest of the eigen-particles located in other momentua would not produce such a longitudinal-only contribution (of the form $v \hat{\mathbf{q}}$), and are thus part of the "normal" current,

$$\tilde{\mathbf{J}}_{\mathbf{q} \neq 0}^n = \tilde{\mathbf{J}}_{\mathbf{q} \neq 0} - \tilde{\mathbf{J}}_{\mathbf{q} \neq 0}^s \quad (\text{with stiffness}). \quad (20)$$

In great contrast, without stiffness the condensed eigen-particles in a Bose gas would not have the long-lived sound propagation, but only give $\langle \tilde{\mathbf{v}}_{\mathbf{k}_0+\mathbf{q},\mathbf{k}_0} \rangle \rightarrow 0$ in the condensate frame and correspondingly $\langle \tilde{\mathbf{v}}_{\mathbf{k}'_0+\mathbf{q},\mathbf{k}'_0} \rangle \rightarrow \mathbf{u}$ in the wall frame, both without a longitudinal-only contribution (of the form $v \hat{\mathbf{q}}$). Therefore, without stiffness a Bose gas hosts no supercurrent, $\tilde{\mathbf{J}}_{\mathbf{q} \neq 0}^s = 0$, consistent with the above energetic consideration in association with its lack of protection against dissipation.

The above tight connection between the supercurrent fluctuation and the true condensate is even more obvious from the corresponding super and normal contributions,

$$\tilde{\mathbf{J}}^s = \frac{1}{\mathcal{V}} \tilde{a}_{\mathbf{k}_0}^\dagger \tilde{\mathbf{v}}_{\mathbf{k}_0,\mathbf{k}_0} \tilde{a}_{\mathbf{k}_0} = \frac{1}{\mathcal{V}} \frac{\hbar \mathbf{k}_0}{m} \tilde{a}_{\mathbf{k}_0}^\dagger \tilde{a}_{\mathbf{k}_0} \quad (\text{with stiffness}) \quad (21)$$

$$\tilde{\mathbf{J}}^n = \sum_{\mathbf{k} \neq \mathbf{k}_0} \frac{1}{\mathcal{V}} \tilde{a}_{\mathbf{k}}^\dagger \tilde{\mathbf{v}}_{\mathbf{k},\mathbf{k}} \tilde{a}_{\mathbf{k}} = \frac{1}{\mathcal{V}} \sum_{\mathbf{k} \neq \mathbf{k}_0} \frac{\hbar \mathbf{k}}{m} \tilde{a}_{\mathbf{k}}^\dagger \tilde{a}_{\mathbf{k}} \quad (22)$$

to the total current \mathbf{J} in Eq.(17) that only measures the net flow of inertial mass and is insensitive to the vibrational motion. Such a direct mapping between eigen-particles in (or out of) the true condensate and the super (or normal) current component would naturally guarantee the conservation of inertial current density, $\rho_{\text{tot}} = \rho_s + \rho_n$, the violation of which plagued previous microscopic theory [42].

5.2.6 Equivalence of superfluid density and true condensation density

Evidently, the above one-on-one correspondence between the supercurrent and true condensate in Eq.(21) unambiguously establishes the equivalence between the true condensation density, $\tilde{N}_0/\mathcal{V} = \tilde{a}_{\mathbf{k}}^\dagger \tilde{a}_{\mathbf{k}}/\mathcal{V}$, and the superfluid density ρ_s as the inertial mass density of the superflow [4]. Still, it is illuminating to also demonstrate such *state-independent* equivalence following the standard “two-fluid” definition of superfluid density in the *wall* frame,

$$\rho_s \equiv \frac{1}{u^2} \mathbf{u} \cdot \mathbf{P}^{s'}/\mathcal{V} = \frac{1}{u^2} \mathbf{u} \cdot (\tilde{N}_0 m \mathbf{u})/\mathcal{V} = m \tilde{N}_0/\mathcal{V} \quad (\text{for } v_s > 0) \quad (23)$$

via the *kinematic* momentum of the flowing true condensate (the supercurrent). Similarly, the normal fluid density is defined as the mass density of the normal flow in the *condensate* frame,

$$\rho_n \equiv \frac{1}{w^2} \mathbf{w} \cdot \mathbf{P}^n/\mathcal{V} = \frac{1}{w^2} \mathbf{w} \cdot (\tilde{N}_n m \mathbf{w})/\mathcal{V} = m \tilde{N}_n/\mathcal{V}, \quad (24)$$

via the kinematic momentum, \mathbf{P}^n , of the normal current composed of

$$\tilde{N}_n \equiv N - \tilde{N}_0 = \sum_{\mathbf{k} \neq \mathbf{0}} \tilde{a}_{\mathbf{k}}^\dagger \tilde{a}_{\mathbf{k}} \quad (25)$$

uncondensed eigen-particles flowing with an average velocity,

$$\mathbf{w} \equiv \mathbf{P}^n (\tilde{N}_n m)^{-1}. \quad (26)$$

Note that the normal momentum component \mathbf{P}^n here can be replaced by the total momentum \mathbf{P} of the system [4], since the true condensate has zero momentum in its own rest frame. Furthermore, as long as the pure quantum states (that dominate the thermal statistics) satisfy the physical equilibrium condition with the wall, the average velocity would match that of the wall $\langle \mathbf{w} \rangle = -\mathbf{u}$. (c.f. Discussion and Appendix H) Under the same condition, $\mathbf{P}^{s'}$ in Eq.(23) can be replaced by the total momentum \mathbf{P}' of the system as well, since $\langle \mathbf{P}^{n'} \rangle = \mathbf{0}$. Being able to use the total momentum (in specially chosen inertial frames) in the two-fluid definition [4] of ρ_s and ρ_n ensures these physical quantities of long time-scale, ρ_s , ρ_n , and \tilde{N}_0/\mathcal{V} , as experimental observables.

Indeed, Eqs.(23)-(25) confirm a *rigorous* quantum mechanical equivalence of superfluid fraction ρ_s/ρ to the *true* condensation fraction \tilde{N}_0/N ,

$$\rho_s/\rho = \tilde{N}_0/N = \tilde{a}_{\mathbf{k}_0}^\dagger \tilde{a}_{\mathbf{k}_0}/N, \quad (27)$$

for *arbitrary* quantum states (and thus any ensemble of them).

Note that even though the above equivalence follows the setup of the standard two-fluid definition [4], through a finite internal relative flow resulting from the static response to a moving wall, in essence the resulting equivalence between ρ_s and \tilde{N}_0 simply originates from the fact that only the eigen-particles in the true condensate can respond to produce the dissipation-less (curl-less) supercurrent [c.f. Fig. 7 and Eq.(19)]. It is therefore straightforward to show [45] that the same conclusion can be rigorously reached as well via the dynamical current-current susceptibility that directly corresponds to many of the experimental data in Fig. 1.

5.2.7 Thermal depletion

Having finally established this *state-independent* equivalence, thermal depletion of the superfluid fraction can then be computed simply through the depletion of the true condensation fraction. Or equivalently, given the strict particle conservation in our formulation, the same can be obtained from the growth of normal fluid fraction, through the density of uncondensed eigen-particles.

Specifically in the *linear response* regime ($\mathbf{u} \rightarrow \mathbf{0}$) corresponding to most of the experimental data in Fig. 1, the thermal equilibrium is reached *before* the application of the external stimuli, when the system has no internal relative flow and satisfies the condition for canonical thermal statistics. (With finite \mathbf{u} , the standard thermal statistics is generally inapplicable to superfluid. See Appendix H.)

Therefore, given the well-established linear dispersion in the elementary excitations of a d -dimensional ($d \geq 2$) superfluid [4, 120], the standard grand canonical ensemble (c.f. Appendix D.1) gives a T^d growth of the uncondensed eigen-particle density (and thus the normal fluid density),

$$\begin{aligned} \frac{\rho_n}{m} &= \frac{\tilde{N}_n}{\mathcal{V}} = \frac{1}{\mathcal{V}} \sum_{\mathbf{k} \neq \mathbf{0}} n_B(\beta \omega_{\mathbf{k}}) = \int d\omega n_B(\beta \omega) g(\omega) \\ &\propto \frac{1}{v_s^d} \int d\omega n_B(\beta \omega) \omega^{d-1} \propto \frac{1}{(v_s \beta)^d} = \left(\frac{T}{v_s k_B} \right)^d, \end{aligned} \quad (28)$$

where $n_B(\beta \omega) = (e^{\beta \omega} - 1)^{-1}$ is the Bose-Einstein distribution function at the inverse temperature $\beta = (k_B T)^{-1}$. Here, the density of states, $g(\omega) \propto v_s^{-d} \omega^{d-1}$, is used for d -dimensional system with linear dispersion, $\omega_{\mathbf{k}} = v_s |\mathbf{k}|$, in its eigen-particle-hole excitation spectrum. (Note that at $T \rightarrow 0$ the temperature dependence of the stiffness, v_s , itself only leads to subdominant higher-order corrections to the depletion.) Correspondingly, the superfluid fraction,

$$\rho_s(T)/\rho = [N - \tilde{N}_n(T)]/N = 1 - AT^d \quad (29)$$

has a T^d -depletion (with coefficient A).

More realistically, in experiments used for Fig. 1, particle fluctuation involving the thermal bath is actually negligible. We therefore have also confirmed under the *canonical* ensemble (c.f. Appendix D.2) the same T^d growth of the normal fluid fraction and *independently* an identical depletion of the superfluid fraction as a generic property for 3D superfluidity.

5.3 Numerical confirmation via standard Monte Carlo approach

To numerically verify our analytical result of the generic T^3 -depletion of superfluid density, we compute the temperature-dependent superfluid density using the standard Bose-Hubbard model in a 3D square lattice,

$$H = -t \sum_{\langle i,j \rangle} (a_j^\dagger a_i + a_i^\dagger a_j) + \frac{V}{2} \sum_i a_i^\dagger a_i^\dagger a_i a_i, \quad (30)$$

as a generic example of interacting bosonic system, where t denotes the kinetic strength and V the onsite interaction. The superfluid density is evaluated via the standard world-line winding number, W , [43]

$$\rho_s(T) \propto T \langle W^2 \rangle, \quad (31)$$

of the world-line quantum Monte Carlo method using the well-established worm algorithm [121], while computing all observables only for configurations with the same fixed particle number to adhere to the canonical ensemble. Average values and error bars of observables are obtained via the standard binning analysis [122]. For an easier visualization, we choose $V = 5t$ (less than half of the bandwidth $12t$) and a filling factor 0.6 per lattice site, such that only a single scale dominates the physics in the superfluid phase and the leading low-temperature power-law behavior dominates over a relatively large temperature range.

Note that this standard approach accounts for many-body information *beyond* the standard sound-based considerations [4]. In addition, as to be published elsewhere [45], we have also verified the same T^3 -depletion via a new approach through dynamical current-current correlation function that are in direct correspondence to many of the experimental probes employed in Fig. 1.

5.4 Leading order effects of impurities

Upon introducing weak on-site disorder to the bosonic system described above, a perturbative calculation (c.f. Appendix E) shows that the leading low-temperature depletion of the superfluid density increases to T -linear. This result is relevant here because such a strong depletion will completely overwhelm the intrinsic T^3 behavior at low temperature. Further, many of the modern superconductor families are well-known to exhibit significant amount of impurities, which might explain the observed T -linear superfluid density in earlier measurements.

Acknowledgements. We thank P.B. Wiegmann, B. Svistunov, N. Prokof'ev, V. Grinenko, and Wei Wang for fruitful discussions on the traditional picture of superfluidity density. This work is supported by National Natural Science Foundation of China (NSFC) under Grant Nos. 12274287 and 12042507, and Innovation Program for Quantum Science and Technology No. 2021ZD0301900.

Appendix A Doping-independent universal low-temperature superfluid density depletion in YBCO

In this section we study the low-temperature superfluid density in underdoped $\text{YBa}_2\text{Cu}_3\text{O}_{6+\delta}$ measurements [22] over a range of doping. As illustrated in Fig.A1(a), this relatively high-quality sample exhibits T^3 depletion of the superfluid density $\rho_s \propto 1/\lambda^2$ via the penetration depth λ over the entire doping range of the study. In Fig.A1(b) we perform the same data collapse as in Figure 1 of the main text and described in detail in section XI of the appendix, fit to the function in Eq.(6) to clearly display the universal depletion of the superfluid density at low temperature $\rho_s(T)/\rho_s(0) = 1 - (T/\tilde{T})^3$, where \tilde{T} is defined in Eq.(7).

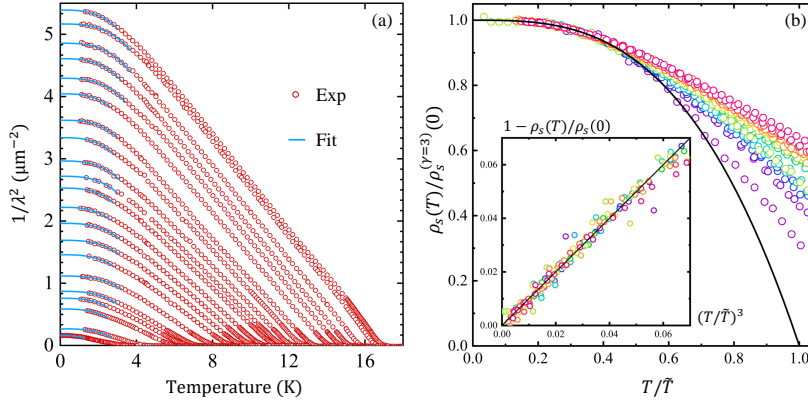


Fig. A1 (a) Superfluid density via penetration depth measurements $\rho_s \propto 1/\lambda^2$ in $\text{YBa}_2\text{Cu}_3\text{O}_{6+\delta}$ [22] showing T^3 depletion indicated in blue. (b) Collapse of the data in (a) to a single universal $1 - (T/\tilde{T})^3$ curve as a function of rescaled temperature T/\tilde{T} . The inset in (b), similar to Figure 1 in the main text, shows that T^3 remains a good fit down to the lowest temperatures of the study.

Appendix B Rigorous properties of superfluidity

B.1 Eigen-particle representation of interaction many-body problems

Consider a generic N -particle interacting bosonic system on a lattice with \mathcal{V} sites that hosts standard superfluidity, described by a Hamiltonian $H[\{a_{\mathbf{R}}^\dagger\}]$ represented by local

second-quantized creation operators $a_{\mathbf{R}}^\dagger$ with corresponding Hamiltonian

$$H = \sum_{\mathbf{R}\mathbf{R}'} t_{\mathbf{R}\mathbf{R}'} a_{\mathbf{R}}^\dagger a_{\mathbf{R}'} + \frac{1}{2} \sum_{\mathbf{R}\mathbf{R}'} V_{\mathbf{R}-\mathbf{R}'} a_{\mathbf{R}}^\dagger a_{\mathbf{R}'}^\dagger a_{\mathbf{R}'} a_{\mathbf{R}}, \quad (\text{B1})$$

where $t_{\mathbf{R}\mathbf{R}'}^* = t_{\mathbf{R}'\mathbf{R}}$ are the hopping parameters, and $V_{\mathbf{R}-\mathbf{R}'}$ is any generic translation-symmetric density-density interaction (for example, the Coulomb potential or the Hubbard interaction U). Represented via second-quantized creation operators of momentum $a_{\mathbf{k}}^\dagger$, the Hamiltonian becomes

$$H = \sum_{\mathbf{k}} \epsilon_{\mathbf{k}} a_{\mathbf{k}}^\dagger a_{\mathbf{k}} + \frac{1}{2\mathcal{V}} \sum_{\mathbf{k}\mathbf{p}\mathbf{q}} V(\mathbf{q}) a_{\mathbf{k}+\mathbf{q}}^\dagger a_{\mathbf{p}-\mathbf{q}}^\dagger a_{\mathbf{p}} a_{\mathbf{k}}, \quad (\text{B2})$$

where $V(\mathbf{q})$ can only be a function of the internal momentum \mathbf{q} .

Eq.(B2) can always be brought to a diagonal truncating form [40]

$$\begin{aligned} H_{\text{diag}}[\{\tilde{a}_{\mathbf{k}}^\dagger\}] &\equiv H[\{a_{\mathbf{k}}^\dagger\}] \\ &= \sum_{\mathbf{k}_1} \epsilon_{\mathbf{k}_1} \tilde{a}_{\mathbf{k}_1}^\dagger \tilde{a}_{\mathbf{k}_1} + \frac{1}{2!} \sum_{\mathbf{k}_1 \mathbf{k}_2} \epsilon_{\mathbf{k}_1 \mathbf{k}_2} \tilde{a}_{\mathbf{k}_1}^\dagger \tilde{a}_{\mathbf{k}_2}^\dagger \tilde{a}_{\mathbf{k}_2} \tilde{a}_{\mathbf{k}_1} \\ &+ \frac{1}{3!} \sum_{\mathbf{k}_1 \mathbf{k}_2 \mathbf{k}_3} \epsilon_{\mathbf{k}_1 \mathbf{k}_2 \mathbf{k}_3} \tilde{a}_{\mathbf{k}_1}^\dagger \tilde{a}_{\mathbf{k}_2}^\dagger \tilde{a}_{\mathbf{k}_3}^\dagger \tilde{a}_{\mathbf{k}_3} \tilde{a}_{\mathbf{k}_2} \tilde{a}_{\mathbf{k}_1} + \dots \\ &+ \frac{1}{N!} \sum_{\mathbf{k}_1 \dots \mathbf{k}_N} \epsilon_{\mathbf{k}_1 \dots \mathbf{k}_N} \tilde{a}_{\mathbf{k}_1}^\dagger \dots \tilde{a}_{\mathbf{k}_N}^\dagger \tilde{a}_{\mathbf{k}_N} \dots \tilde{a}_{\mathbf{k}_1}, \end{aligned} \quad (\text{B3})$$

using the corresponding one-body eigenoperators,

$$\tilde{a}_{\mathbf{k}}^\dagger = U^\dagger a_{\mathbf{k}}^\dagger U, \quad (\text{B4})$$

transformed from the ‘bare’ creation operators $a_{\mathbf{k}}^\dagger$ via a unitary operator U . $\epsilon_{\mathbf{k}_1}, \epsilon_{\mathbf{k}_1 \mathbf{k}_2}, \dots, \epsilon_{\mathbf{k}_1 \dots \mathbf{k}_N}$ in Eq.(B3) are the one-body, two-body, up to N -body contributions to the many-body eigen-energy.

Owing to the diagonal structure of H_{diag} and the standard bosonic commutation,

$$[\tilde{a}_{\mathbf{k}}, \tilde{a}_{\mathbf{p}}^\dagger] = \delta_{\mathbf{k}\mathbf{p}} \quad (\text{B5})$$

$$[\tilde{a}_{\mathbf{k}}, \tilde{a}_{\mathbf{p}}] = 0, \quad (\text{B6})$$

each N -body eigenstate $|\{N_{\mathbf{k}}\}\rangle$ is constructed by unique repeated application of the set of eigenoperators $\{\tilde{a}_{\mathbf{k}}^\dagger\}$ to the zero particle vacuum $|0\rangle$. These states form a complete orthonormal N -body basis and take the form of direct products,

$$|\{N_{\mathbf{k}}\}\rangle \equiv \prod_{\mathbf{k}} \frac{(\tilde{a}_{\mathbf{k}}^\dagger)^{N_{\mathbf{k}}}}{\sqrt{N_{\mathbf{k}}!}} |0\rangle \Big|_{\sum_{\mathbf{k}} N_{\mathbf{k}} = N}, \quad (\text{B7})$$

as all many-body quantum fluctuations are fully absorbed in $\tilde{a}_{\mathbf{k}}^\dagger$.

For systems where the kinetic energy dominates over the interaction V , such as those of interest in this study, the ground state is simply

$$|\Omega\rangle \equiv \frac{(\tilde{a}_{\mathbf{k}_0}^\dagger)^N}{\sqrt{N!}} |0\rangle, \quad (\text{B8})$$

with all N particles having lowest kinetic energy at zero momentum. Correspondingly, the ground state is a ‘true’ Bose-Einstein condensate containing all N particles

$$\langle\Omega| \tilde{N}_0 |\Omega\rangle \equiv \langle\Omega| \tilde{a}_{\mathbf{k}_0}^\dagger \tilde{a}_{\mathbf{k}_0} |\Omega\rangle = N. \quad (\text{B9})$$

B.2 Dressed current

Given that the eigen-particles carry the same inertial mass m and momentum $\hbar\mathbf{k}$ of the bare particles, these long-lived particles provide a convenient means to keep track of the mass flow of the system at long length and time scales.

To that end, we define the current operator $\tilde{\mathbf{J}}$ for the eigen-particles in the Heisenberg picture through the time derivative of the corresponding dressed polarization operator $\tilde{\Pi}$,

$$\tilde{\Pi} = \sum_{\mathbf{R}} \mathbf{R} \tilde{a}_{\mathbf{R}}^\dagger \tilde{a}_{\mathbf{R}} \quad (\text{B10})$$

$$\Rightarrow \tilde{\mathbf{J}} = \frac{d\tilde{\Pi}}{dt} = \frac{1}{i\hbar} [\tilde{\Pi}, H], \quad (\text{B11})$$

Notice that the diagonal representation of Eq.(B3) can be additively separated into λ -body parts

$$\begin{aligned} H = \sum_{\lambda=1}^N H^{(\lambda)} &= \sum_{\mathbf{k}_1} \epsilon_{\mathbf{k}_1} \tilde{a}_{\mathbf{k}_1}^\dagger \tilde{a}_{\mathbf{k}_1} + \frac{1}{2} \sum_{\mathbf{k}_1 \mathbf{k}_2} \epsilon_{\mathbf{k}_1 \mathbf{k}_2} \tilde{a}_{\mathbf{k}_1}^\dagger \tilde{a}_{\mathbf{k}_2}^\dagger \tilde{a}_{\mathbf{k}_2} \tilde{a}_{\mathbf{k}_1} + \dots \\ &+ \frac{1}{N!} \sum_{\mathbf{k}_1 \dots \mathbf{k}_N} \epsilon_{\mathbf{k}_1 \dots \mathbf{k}_N} \tilde{a}_{\mathbf{k}_1}^\dagger \dots \tilde{a}_{\mathbf{k}_N}^\dagger \tilde{a}_{\mathbf{k}_N} \dots \tilde{a}_{\mathbf{k}_1}, \end{aligned} \quad (\text{B12})$$

and that this separation can be carried over into the definition of the current operator

$$\tilde{\mathbf{J}} = \sum_{\lambda=1}^N \tilde{\mathbf{J}}^{(\lambda)} = \frac{1}{i\hbar} \sum_{\lambda=1}^N [\tilde{\Pi}, H^{(\lambda)}], \quad (\text{B13})$$

where we have used the fact that each eigen-particle shares its real-space center \mathbf{R} with the corresponding local bare particle due to the one-to-one mapping between real space operators,

$$\tilde{a}_{\mathbf{R}}^\dagger = U^\dagger a_{\mathbf{R}}^\dagger U, \quad (\text{B14})$$

consistent with Eq.(B4).

The definition of the dressed current $\tilde{\mathbf{J}}$ in Eq.(B11) properly encodes the hopping of each particle's center as well. For example, the one-body $\lambda = 1$ part of the dressed current is simply

$$\begin{aligned}
\tilde{\mathbf{J}}^{(1)} &= \frac{1}{i\hbar} \left[\sum_{\mathbf{R}} \mathbf{R} \tilde{a}_{\mathbf{R}}^{\dagger} \tilde{a}_{\mathbf{R}}, \sum_{\mathbf{k}_1} \epsilon_{\mathbf{k}_1} \tilde{a}_{\mathbf{k}_1}^{\dagger} \tilde{a}_{\mathbf{k}_1} \right] \\
&= \frac{1}{i\hbar} \left[\sum_{\mathbf{R}} \mathbf{R} \tilde{a}_{\mathbf{R}}^{\dagger} \tilde{a}_{\mathbf{R}}, \sum_{\mathbf{R}_1 \mathbf{R}'_1} \tilde{a}_{\mathbf{R}_1}^{\dagger} \left(\sum_{\mathbf{k}_1} \langle \mathbf{R}_1 | \mathbf{k}_1 \rangle \epsilon_{\mathbf{k}_1} \langle \mathbf{k}_1 | \mathbf{R}'_1 \rangle \right) \tilde{a}_{\mathbf{R}'_1} \right] \\
&\equiv \frac{1}{i\hbar} \sum_{\mathbf{R}_1 \mathbf{R}'_1} (\mathbf{R}_1 - \mathbf{R}'_1) \epsilon_{\mathbf{R}_1 \mathbf{R}'_1} \tilde{a}_{\mathbf{R}_1}^{\dagger} \tilde{a}_{\mathbf{R}'_1} \\
&\equiv \sum_{\mathbf{R}_1 \mathbf{R}'_1} \mathbf{J}_{\mathbf{R}_1 \mathbf{R}'_1} \tilde{a}_{\mathbf{R}_1}^{\dagger} \tilde{a}_{\mathbf{R}'_1}, \tag{B15}
\end{aligned}$$

where $\mathbf{J}_{\mathbf{R}_1 \mathbf{R}'_1} \tilde{a}_{\mathbf{R}_1}^{\dagger} \tilde{a}_{\mathbf{R}'_1}$ represents the dressed one-body current from site \mathbf{R}'_1 to site \mathbf{R}_1 located at $(\mathbf{R}_1 + \mathbf{R}'_1)/2$, and $\epsilon_{\mathbf{R}_1 \mathbf{R}'_1} = \sum_{\mathbf{k}_1} \langle \mathbf{R}_1 | \mathbf{k}_1 \rangle \epsilon_{\mathbf{k}_1} \langle \mathbf{k}_1 | \mathbf{R}'_1 \rangle$. Transforming to momentum space for wavevectors $\mathbf{q} \neq \mathbf{0}$, we find the following formula

$$\tilde{\mathbf{J}}_{\mathbf{q} \neq \mathbf{0}}^{(1)} \equiv \frac{1}{\mathcal{V}} \sum_{\mathbf{R}_1 \mathbf{R}'_1} e^{i\mathbf{q} \cdot (\mathbf{R}_1 + \mathbf{R}'_1)/2} \mathbf{J}_{\mathbf{R}_1 \mathbf{R}'_1} \tilde{a}_{\mathbf{R}_1}^{\dagger} \tilde{a}_{\mathbf{R}'_1} \tag{B16}$$

$$= \frac{1}{\hbar \mathcal{V}} \sum_{\mathbf{k}} \tilde{a}_{\mathbf{k}'}^{\dagger} (\nabla_{\mathbf{k}} \epsilon_{\mathbf{k}}) \tilde{a}_{\mathbf{k}} \Big|_{\mathbf{k}' = \mathbf{k} + \mathbf{q}, \mathbf{k} = (\mathbf{k}' + \mathbf{k})/2}. \tag{B17}$$

The general λ -body contribution $\tilde{\mathbf{J}}_{\mathbf{q}}^{(\lambda)}$ is

$$\tilde{\mathbf{J}}_{\mathbf{q} \neq \mathbf{0}}^{(\lambda)} = \frac{\lambda}{\lambda!} \frac{1}{\hbar \mathcal{V}} \sum_{\mathbf{k} \mathbf{k}_1 \dots \mathbf{k}_{\lambda-1}} \tilde{a}_{\mathbf{k}'}^{\dagger} \left[(\nabla_{\mathbf{k}} \epsilon_{\mathbf{k} \mathbf{k}_1 \dots \mathbf{k}_{\lambda-1}}) \tilde{a}_{\mathbf{k}_1}^{\dagger} \dots \tilde{a}_{\mathbf{k}_{\lambda-1}}^{\dagger} \tilde{a}_{\mathbf{k}_{\lambda-1}} \dots \tilde{a}_{\mathbf{k}_1} \right] \tilde{a}_{\mathbf{k}} \Big|_{\mathbf{k}' = \mathbf{k} + \mathbf{q}, \mathbf{k} = (\mathbf{k}' + \mathbf{k})/2}, \tag{B18}$$

and therefore the total \mathbf{q} -component of the dressed current operator is finally

$$\tilde{\mathbf{J}}_{\mathbf{q} \neq \mathbf{0}} = \frac{1}{\mathcal{V}} \sum_{\mathbf{k}} \tilde{a}_{\mathbf{k}'}^{\dagger} \tilde{\mathbf{v}}_{\mathbf{k}' \mathbf{k}} \tilde{a}_{\mathbf{k}} \Big|_{\mathbf{k}' = \mathbf{k} + \mathbf{q}} \tag{B19}$$

$$\begin{aligned}
\tilde{\mathbf{v}}_{\mathbf{k}', \mathbf{k} \neq \mathbf{k}'} &\equiv \frac{1}{\hbar} \nabla_{\mathbf{k}} \left(\epsilon_{\mathbf{k}} + \sum_{\mathbf{k}_1} \epsilon_{\mathbf{k} \mathbf{k}_1} \tilde{a}_{\mathbf{k}_1}^{\dagger} \tilde{a}_{\mathbf{k}_1} + \frac{1}{2!} \sum_{\mathbf{k}_1 \mathbf{k}_2} \epsilon_{\mathbf{k} \mathbf{k}_1 \mathbf{k}_2} \tilde{a}_{\mathbf{k}_1}^{\dagger} \tilde{a}_{\mathbf{k}_2}^{\dagger} \tilde{a}_{\mathbf{k}_2} \tilde{a}_{\mathbf{k}_1} + \dots \right. \\
&\quad \left. + \frac{1}{(N-1)!} \sum_{\mathbf{k}_1 \dots \mathbf{k}_{N-1}} \epsilon_{\mathbf{k} \mathbf{k}_1 \dots \mathbf{k}_{N-1}} \tilde{a}_{\mathbf{k}_1}^{\dagger} \dots \tilde{a}_{\mathbf{k}_{N-1}}^{\dagger} \tilde{a}_{\mathbf{k}_{N-1}} \dots \tilde{a}_{\mathbf{k}_1} \right) \Big|_{\mathbf{k} = (\mathbf{k}' + \mathbf{k})/2}
\end{aligned}$$

$$\equiv \frac{1}{\hbar} \nabla_{\mathbf{k}} \left(\epsilon_{\mathbf{k}} + \tilde{\Sigma}_{\mathbf{k}} \right) \Big|_{\mathbf{k}=(\mathbf{k}'+\mathbf{k})/2} \equiv \frac{1}{\hbar} \nabla_{\mathbf{k}} \tilde{\epsilon}_{\mathbf{k}} \Big|_{\mathbf{k}=(\mathbf{k}'+\mathbf{k})/2} \quad (\text{B20})$$

$$= \left(\frac{\hbar \mathbf{k}}{m} + \frac{1}{\hbar} \nabla_{\mathbf{k}} \tilde{\Sigma}_{\mathbf{k}} \right) \Big|_{\mathbf{k}=(\mathbf{k}'+\mathbf{k})/2}, \quad (\text{B21})$$

where $\tilde{\mathbf{v}}_{\mathbf{k}'\mathbf{k}}$ is the velocity operator of the eigen-particles. Note that the gradient in Eq.(B21) is taken with respect to the removal energy of an eigen-particle of momentum \mathbf{k} from the N particle system, $\tilde{\epsilon}_{\mathbf{k}}$, consisting of the kinetic energy $\epsilon_{\mathbf{k}}$ and the *diagonal* interaction energy $\tilde{\Sigma}_{\mathbf{k}}$ operators between the removed eigen-particle and the rest of the $N - 1$ eigen-particles.

The total current of the system $\tilde{\mathbf{J}}$ (with $\mathbf{q} = \mathbf{0}$) has a distinct form from that of $\tilde{\mathbf{J}}_{\mathbf{q} \rightarrow \mathbf{0}}$,

$$\tilde{\mathbf{J}} = \sum_{\mathbf{k}} \frac{1}{\mathcal{V}} \tilde{a}_{\mathbf{k}}^{\dagger} \tilde{\mathbf{v}}_{\mathbf{k},\mathbf{k}} \tilde{a}_{\mathbf{k}} = \frac{1}{\mathcal{V}} \sum_{\mathbf{k}} \frac{\hbar \mathbf{k}}{m} \tilde{a}_{\mathbf{k}}^{\dagger} \tilde{a}_{\mathbf{k}}, \quad (\text{B22})$$

in which the interaction-induced contributions, $\frac{1}{\hbar} \nabla_{\mathbf{k}} \tilde{\Sigma}_{\mathbf{k}}$, to $\tilde{\mathbf{v}}_{\mathbf{k},\mathbf{k}}$ is identically zero. This is because in translational invariant systems the many-body interaction preserves the total momentum $\tilde{\mathbf{P}}$, such that

$$\tilde{\mathbf{J}} = \frac{1}{m\mathcal{V}} \tilde{\mathbf{P}} = \frac{1}{\mathcal{V}} \sum_{\mathbf{k}} \frac{\hbar \mathbf{k}}{m} \tilde{a}_{\mathbf{k}}^{\dagger} \tilde{a}_{\mathbf{k}} \quad (\text{B23})$$

only measures kinematic velocity of the inertial mass.

B.3 Strict particle conservation and continuity equation

The dressed current as defined above obeys the familiar equation of continuity in the long-wavelength limit. Similar to the dressed current operator of Eq.(B13) in the previous section, by using Eq.(B12) we can separate the Heisenberg equation of motion for the density operator into λ -body parts

$$\frac{d\tilde{n}_{\mathbf{R}}}{dt} = \frac{1}{i\hbar} [\tilde{n}_{\mathbf{R}}, H] = \frac{1}{i\hbar} \sum_{\lambda=1}^N [\tilde{n}_{\mathbf{R}}, H^{(\lambda)}], \quad (\text{B24})$$

due to the associativity of the commutator. We can therefore examine an arbitrary λ -body term to determine the form of the continuity equation. For example, from Eq.(B24)

$$\begin{aligned} \frac{d\tilde{n}_{\mathbf{R}}^{(\lambda)}}{dt} &= \frac{1}{i\hbar} [\tilde{n}_{\mathbf{R}}, H^{(\lambda)}] \\ &= \frac{1}{i\hbar\lambda!} \left[\tilde{a}_{\mathbf{R}}^{\dagger} \tilde{a}_{\mathbf{R}}, \sum_{\mathbf{k}_1, \dots, \mathbf{k}_{\lambda}} \epsilon_{\mathbf{k}_1, \dots, \mathbf{k}_{\lambda}} \tilde{a}_{\mathbf{k}_1}^{\dagger} \cdots \tilde{a}_{\mathbf{k}_{\lambda}}^{\dagger} \tilde{a}_{\mathbf{k}_{\lambda}} \cdots \tilde{a}_{\mathbf{k}_1} \right] \end{aligned}$$

$$\begin{aligned}
&= \frac{1}{i\hbar} \sum_{\mathbf{R}'} \left(\tilde{a}_{\mathbf{R}}^\dagger F_{\mathbf{R}\mathbf{R}'}^{(\lambda)} \tilde{a}_{\mathbf{R}'} - \tilde{a}_{\mathbf{R}'}^\dagger F_{\mathbf{R}'\mathbf{R}}^{(\lambda)} \tilde{a}_{\mathbf{R}} \right), \text{ with} \\
F_{\mathbf{R}\mathbf{R}'}^{(\lambda>1)} &= \frac{1}{(\lambda-1)!} \sum_{\mathbf{k}_2 \dots \mathbf{k}_\lambda} \epsilon_{\mathbf{R}\mathbf{R}'\mathbf{k}_2 \dots \mathbf{k}_\lambda} \tilde{a}_{\mathbf{k}_2}^\dagger \dots \tilde{a}_{\mathbf{k}_\lambda}^\dagger \tilde{a}_{\mathbf{k}_\lambda} \dots \tilde{a}_{\mathbf{k}_2},
\end{aligned} \tag{B25}$$

where $F_{\mathbf{R}\mathbf{R}'}^{(1)} = \epsilon_{\mathbf{R}\mathbf{R}'}$ and $\epsilon_{\mathbf{R}\mathbf{R}'\mathbf{k}_2 \dots \mathbf{k}_\lambda} = \sum_{\mathbf{k}_1} \langle \mathbf{R} | \mathbf{k}_1 \rangle \epsilon_{\mathbf{k}_1 \mathbf{k}_2 \dots \mathbf{k}_\lambda} \langle \mathbf{k}_1 | \mathbf{R}' \rangle$.

Similarly, from Eq.(B13) the current operator becomes

$$\tilde{\mathbf{J}} = \sum_{\lambda=1}^N \frac{1}{i\hbar} \sum_{\mathbf{R}\mathbf{R}'} \tilde{a}_{\mathbf{R}}^\dagger F_{\mathbf{R}\mathbf{R}'}^{(\lambda)} \tilde{a}_{\mathbf{R}'}.$$
 \tag{B26}

Combining contributions to the same pair of locations as the current *passing through* a ‘boundary’ at $(\mathbf{R} + \mathbf{R}')/2$,

$$\tilde{\mathbf{J}}_{\mathbf{R}\mathbf{R}'} + \tilde{\mathbf{J}}_{\mathbf{R}'\mathbf{R}} = \frac{1}{i\hbar} \sum_{\lambda=1}^N \delta_{\mathbf{R}\mathbf{R}'} \left(\tilde{a}_{\mathbf{R}}^\dagger F_{\mathbf{R}\mathbf{R}'}^{(\lambda)} \tilde{a}_{\mathbf{R}'} - \tilde{a}_{\mathbf{R}'}^\dagger F_{\mathbf{R}'\mathbf{R}}^{(\lambda)} \tilde{a}_{\mathbf{R}} \right),$$
 \tag{B27}

and comparing with Eq. (B25), one finds the familiar continuity equation,

$$\frac{d\tilde{n}_{\mathbf{R}}}{dt} + \sum_{\mathbf{R}'} \frac{\delta_{\mathbf{R}'\mathbf{R}}}{|\delta_{\mathbf{R}'\mathbf{R}}|^2} \cdot \left(\tilde{\mathbf{J}}_{\mathbf{R}\mathbf{R}'} + \tilde{\mathbf{J}}_{\mathbf{R}'\mathbf{R}} \right) = 0,$$
 \tag{B28}

for the eigen-particle density and its associated dressed current. In the long-wavelength limit, $\mathbf{q} \rightarrow 0$, this reduces to the familiar momentum representation,

$$\frac{d\tilde{n}_{\mathbf{q}}}{dt} - i\mathbf{q} \cdot \tilde{\mathbf{J}}_{\mathbf{q}} = 0.$$
 \tag{B29}

B.4 Excitation energy of eigen-particle-hole pairs

We now show that the energies of eigen-particle-hole excitations in an interacting system, such as those encountered in the dynamical current-current response, have a simple diagonal form. In the Heisenberg picture, the time-dependent eigen-annihilation operator is,

$$\tilde{a}_{\mathbf{k}}(t) = e^{iHt} \tilde{a}_{\mathbf{k}} e^{-iHt}.$$
 \tag{B30}

Using the Baker-Campbell-Hausdorff theorem,

$$e^A C e^{-A} = C + [A, C] + \frac{1}{2!} [A, [A, C]] + \frac{1}{3!} [A, [A, [A, C]]] + \dots$$
 \tag{B31}

and the commutation with the Hamiltonian

$$\begin{aligned}
[H, \tilde{a}_{\mathbf{k}}] &= \sum_{\mathbf{k}_1} \epsilon_{\mathbf{k}_1} [\tilde{a}_{\mathbf{k}_1}^\dagger \tilde{a}_{\mathbf{k}_1}, \tilde{a}_{\mathbf{k}}] + \frac{1}{2!} \sum_{\mathbf{k}_1 \mathbf{k}_2} \epsilon_{\mathbf{k}_1 \mathbf{k}_2} [\tilde{a}_{\mathbf{k}_1}^\dagger \tilde{a}_{\mathbf{k}_2}^\dagger \tilde{a}_{\mathbf{k}_2} \tilde{a}_{\mathbf{k}_1}, \tilde{a}_{\mathbf{k}}] \\
&+ \dots + \frac{1}{N!} \sum_{\mathbf{k}_1 \dots \mathbf{k}_N} \epsilon_{\mathbf{k}_1 \dots \mathbf{k}_N} [\tilde{a}_{\mathbf{k}_1}^\dagger \dots \tilde{a}_{\mathbf{k}_N}^\dagger \tilde{a}_{\mathbf{k}_N} \dots \tilde{a}_{\mathbf{k}_1}, \tilde{a}_{\mathbf{k}}] \\
&= -(\epsilon_{\mathbf{k}} \tilde{a}_{\mathbf{k}} + \sum_{\mathbf{k}_2} \epsilon_{\mathbf{k} \mathbf{k}_2} \tilde{a}_{\mathbf{k}_2}^\dagger \tilde{a}_{\mathbf{k}_2} \tilde{a}_{\mathbf{k}} + \frac{1}{2!} \sum_{\mathbf{k}_2 \mathbf{k}_3} \epsilon_{\mathbf{k} \mathbf{k}_2 \mathbf{k}_3} \tilde{a}_{\mathbf{k}_2}^\dagger \tilde{a}_{\mathbf{k}_3}^\dagger \tilde{a}_{\mathbf{k}_3} \tilde{a}_{\mathbf{k}_2} \tilde{a}_{\mathbf{k}} \\
&+ \dots + \frac{1}{(N-1)!} \sum_{\mathbf{k}_2 \dots \mathbf{k}_N} \epsilon_{\mathbf{k} \mathbf{k}_2 \dots \mathbf{k}_N} \tilde{a}_{\mathbf{k}_2}^\dagger \dots \tilde{a}_{\mathbf{k}_N}^\dagger \tilde{a}_{\mathbf{k}_N} \dots \tilde{a}_{\mathbf{k}_2} \tilde{a}_{\mathbf{k}}) \\
&= -\tilde{\epsilon}_{\mathbf{k}} \tilde{a}_{\mathbf{k}}, \tag{B32}
\end{aligned}$$

one finds the explicit time dependence of the eigen-particle annihilation operator:

$$\begin{aligned}
\tilde{a}_{\mathbf{k}}(t) &= \tilde{a}_{\mathbf{k}} + (it)[H, \tilde{a}_{\mathbf{k}}] + \frac{(it)^2}{2!} [H, [H, \tilde{a}_{\mathbf{k}}]] + \dots \\
&= \tilde{a}_{\mathbf{k}} + (-it\tilde{\epsilon}_{\mathbf{k}})\tilde{a}_{\mathbf{k}} + \frac{(-it\tilde{\epsilon}_{\mathbf{k}})^2}{2!} \tilde{a}_{\mathbf{k}} + \dots \\
&= e^{-it\tilde{\epsilon}_{\mathbf{k}}} \tilde{a}_{\mathbf{k}}. \tag{B33}
\end{aligned}$$

Note that $[H, \tilde{\epsilon}_{\mathbf{k}}] = 0$, since both operators are diagonal in the eigen-representation. Similarly, by taking the Hermitian conjugate,

$$\tilde{a}_{\mathbf{k}}^\dagger(t) = \tilde{a}_{\mathbf{k}}^\dagger e^{it\tilde{\epsilon}_{\mathbf{k}}}, \tag{B34}$$

Now we turn to the retarded response function of the susceptibility for the current operator from the standard Kubo formula. In a system with time-translation symmetry, $\tilde{\chi}_{\mathbf{q}}$ should only depend on the time difference $t - t'$:

$$\begin{aligned}
\tilde{\chi}_{\mathbf{q}}^{\alpha\beta}(t, t') &= \tilde{\chi}_{\mathbf{q}}^{\alpha\beta}(t - t') \\
&= \frac{i\mathcal{V}}{\hbar} \theta(t - t') [\tilde{J}_{\mathbf{q}}^{\alpha\dagger}(t - t'), \tilde{J}_{\mathbf{q}}^{\beta}(0)] \\
&= \frac{i}{\mathcal{V}\hbar} \theta(t - t') \sum_{\mathbf{k}\mathbf{k}'} [\tilde{a}_{\mathbf{k}}^\dagger(t - t') \tilde{v}_{\mathbf{k}, \mathbf{k}+\mathbf{q}}^{\alpha\dagger} \tilde{a}_{\mathbf{k}+\mathbf{q}}(t - t'), \tilde{a}_{\mathbf{k}'+\mathbf{q}}^\dagger(0) \tilde{v}_{\mathbf{k}'+\mathbf{q}, \mathbf{k}'}^{\beta} \tilde{a}_{\mathbf{k}'}(0)], \tag{B35}
\end{aligned}$$

where the current operator for the eigen-particles is defined in Eq.(E50). Substituting the time-dependent creation and annihilation operators into the retarded current-current response function, and noting that $\tilde{v}_{\mathbf{k}, \mathbf{k}+\mathbf{q}}$ commutes with $\tilde{\epsilon}_{\mathbf{k}}$ (both diagonal), we find

$$\tilde{\chi}_{\mathbf{q}}^{\alpha\beta}(t - t') = \frac{i}{\mathcal{V}\hbar} \theta(t - t') \sum_{\mathbf{k}\mathbf{k}'} [\tilde{a}_{\mathbf{k}}^\dagger \tilde{v}_{\mathbf{k}, \mathbf{k}+\mathbf{q}}^{\alpha\dagger} e^{-i(\tilde{\epsilon}_{\mathbf{k}+\mathbf{q}} - \tilde{\epsilon}_{\mathbf{k}})(t-t')/\hbar} \tilde{a}_{\mathbf{k}+\mathbf{q}}, \tilde{a}_{\mathbf{k}'+\mathbf{q}}^\dagger \tilde{v}_{\mathbf{k}'+\mathbf{q}, \mathbf{k}'}^{\beta} \tilde{a}_{\mathbf{k}'}], \tag{B36}$$

with corresponding frequency Fourier transform $\tilde{\chi}_{\mathbf{q}}^{\alpha\beta}(\omega) = \int_{-\infty}^{\infty} \tilde{\chi}_{\mathbf{q}}^{\alpha\beta}(t-t')e^{i\omega(t-t')}d(t-t')$,

$$\tilde{\chi}_{\mathbf{q}}^{\alpha\beta}(\omega) = \frac{1}{\mathcal{V}\hbar} \sum_{\mathbf{k}\mathbf{k}'} \left[\tilde{a}_{\mathbf{k}}^{\dagger} \tilde{v}_{\mathbf{k},\mathbf{k}+\mathbf{q}}^{\alpha\beta} (\omega - (\tilde{\epsilon}_{\mathbf{k}+\mathbf{q}} - \tilde{\epsilon}_{\mathbf{k}})/\hbar + i\eta)^{-1} \tilde{a}_{\mathbf{k}+\mathbf{q}} \cdot \tilde{a}_{\mathbf{k}'+\mathbf{q}}^{\dagger} \tilde{v}_{\mathbf{k}'+\mathbf{q},\mathbf{k}}^{\beta} \tilde{a}_{\mathbf{k}'} \right]. \quad (\text{B37})$$

Eq.(B37) identifies the energy of eigen-particle-hole excitation through the dressed current-current response as the familiar difference in one-particle removal energies $\tilde{\epsilon}_{\mathbf{k}+\mathbf{q}} - \tilde{\epsilon}_{\mathbf{k}}$ from the N -particle system. Furthermore, it is straightforward to extend the above derivation to excitations involving multiple eigen-particle-hole pairs to access all possible excitation energies.

Appendix C Demonstration of the linear dispersion of ‘sound’ modes as particle-hole excitations

In this section we identify the linear dispersion of ‘sound’ (i.e. quanta of longitudinal waves)[120] and its equivalent description as particle-hole excitations via a demonstration of the eigensolution for the low-energy Hamiltonian in an approximation that preserves particle number. In particular we show the resulting linear dispersion and the form of the particle-hole excitations, which provide a leading order approximation to the particle-hole excitations of the true diagonalized Hamiltonian.

We begin by representing the low-energy Hamiltonian, in the presence of macroscopic occupation in the lowest one-body state of the non-interacting eigenbasis $\langle N_0 \rangle \equiv a_{\mathbf{k}_0}^{\dagger} a_{\mathbf{k}_0} \gg 1$, by bare particle-hole excitation operators that preserve particle number

$$\alpha_{\mathbf{k}}^{\dagger} \equiv a_{\mathbf{k}}^{\dagger} a_{\mathbf{k}_0} N_0^{-\frac{1}{2}} \quad \forall \mathbf{k} \neq \mathbf{k}_0 \quad (\text{C38})$$

$$\alpha_{\mathbf{k}} \equiv N_0^{-\frac{1}{2}} a_{\mathbf{k}_0}^{\dagger} a_{\mathbf{k}} \quad \forall \mathbf{k} \neq \mathbf{k}_0. \quad (\text{C39})$$

Notice the particle-hole excitation nature of the operators in Eqs.(C38,C39) and their close analogy to the excitation operators in linear spin wave theory[123].

We can now represent H using the real-particle conserving operators defined in Eqs.(C38,C39). Separating the total number operator N into a bare condensate part and the rest,

$$N = \sum_{\mathbf{k}} a_{\mathbf{k}}^{\dagger} a_{\mathbf{k}} = a_{\mathbf{k}_0}^{\dagger} a_{\mathbf{k}_0} + \sum_{\mathbf{k} \neq \mathbf{k}_0} a_{\mathbf{k}}^{\dagger} a_{\mathbf{k}}, \quad (\text{C40})$$

we can rewrite the kinetic energy in Eq.(B2),

$$\sum_{\mathbf{k}} \epsilon_{\mathbf{k}} a_{\mathbf{k}}^{\dagger} a_{\mathbf{k}} = \sum_{\mathbf{k} \neq \mathbf{k}_0} (\epsilon_{\mathbf{k}} - \epsilon_{\mathbf{k}_0}) \alpha_{\mathbf{k}}^{\dagger} \alpha_{\mathbf{k}} + \epsilon_{\mathbf{k}_0} N + O(1/N), \quad (\text{C41})$$

into a particle-hole excitation form up to a term $\epsilon_0 N$ that commutes with H .

Continuing to the interaction terms in Eq.(B2), we study an example that is \mathbf{q} -independent $V(\mathbf{q}) = V$. Starting similarly to the standard approach by using the large condensate $\langle N_0 \rangle \gg 1$ to include only those terms up to bilinear in $\mathbf{k} \neq \mathbf{k}_0$,

$$\begin{aligned} & \frac{V}{\mathcal{V}} \sum_{\mathbf{k}\mathbf{p}\mathbf{q}} a_{\mathbf{k}+\mathbf{q}}^\dagger a_{\mathbf{p}-\mathbf{q}}^\dagger a_{\mathbf{p}} a_{\mathbf{k}} \\ &= \frac{V}{\mathcal{V}} a_{\mathbf{k}_0}^\dagger a_{\mathbf{k}_0}^\dagger a_{\mathbf{k}_0} a_{\mathbf{k}_0} + \frac{V}{2\mathcal{V}} \sum_{\mathbf{k} \neq \mathbf{k}_0} (4a_{\mathbf{k}}^\dagger a_{\mathbf{k}_0}^\dagger a_{\mathbf{k}_0} a_{\mathbf{k}} + a_{\mathbf{k}}^\dagger a_{-\mathbf{k}}^\dagger a_{\mathbf{k}_0} a_{\mathbf{k}_0} + a_{\mathbf{k}_0}^\dagger a_{\mathbf{k}_0}^\dagger a_{\mathbf{k}} a_{-\mathbf{k}}) + H_{\text{fluc}} \\ &\approx V n_0 (N_0 - 1) + \frac{V}{2} \sum_{\mathbf{k} \neq \mathbf{k}_0} (4\alpha_{\mathbf{k}}^\dagger n_0 \alpha_{\mathbf{k}} + \alpha_{\mathbf{k}}^\dagger n_0 \alpha_{-\mathbf{k}}^\dagger + \alpha_{\mathbf{k}} n_0 \alpha_{-\mathbf{k}}), \end{aligned} \quad (\text{C42})$$

where H_{fluc} are the remaining neglected terms from the bare interaction, $n_0 = N_0/\mathcal{V}$ is the bare condensate density operator, and we have dropped terms of order $\mathcal{O}(\mathcal{V}^{-1})$ in commuting $\sqrt{n_0}$ into the center of $\alpha_{\mathbf{k}}^\dagger \sqrt{n_0} \alpha_{-\mathbf{k}}^\dagger \sqrt{n_0}$ and $\sqrt{n_0} \alpha_{\mathbf{k}} \sqrt{n_0} \alpha_{-\mathbf{k}}$. Contrary to the standard approach (see e.g. [4]) that results in general violation of particle conservation through terms like $a_{\mathbf{k}}^\dagger a_{-\mathbf{k}}^\dagger$ in the interaction, all of our interaction terms in Eq.(C42) are inherently particle-conserving and ensure that every many-body state remains strictly in the N -particle sector.

Combining Eqs.(C41,C42) the Hamiltonian becomes

$$H = \Xi_0 + H_{\text{ex}} + H_{\text{fluc}} \quad (\text{C43})$$

$$H_{\text{ex}} \equiv \sum_{\mathbf{k} \neq \mathbf{k}_0} \left(\alpha_{\mathbf{k}}^\dagger (\epsilon_{\mathbf{k}} - \epsilon_{\mathbf{k}_0} + 2V n_0) \alpha_{\mathbf{k}} + (\alpha_{\mathbf{k}}^\dagger \frac{V n_0}{2} \alpha_{-\mathbf{k}}^\dagger + \alpha_{\mathbf{k}} \frac{V n_0}{2} \alpha_{-\mathbf{k}}) \right), \quad (\text{C44})$$

where Ξ_0 is the N -body ground state energy.

After diagonalization, the resulting solution is

$$H_{\text{ex}} \equiv \sum_{\mathbf{k} \neq \mathbf{k}_0} \tilde{\alpha}_{\mathbf{k}}^\dagger \omega_{\mathbf{k}} \tilde{\alpha}_{\mathbf{k}} \quad (\text{C45})$$

$$\omega_{\mathbf{k}} \approx \sqrt{\xi_{\mathbf{k}} (2V \tilde{n}_0 + \xi_{\mathbf{k}})} \quad (\text{C46})$$

$$\tilde{\alpha}_{\mathbf{k}}^\dagger \approx c_{\mathbf{k}} \alpha_{\mathbf{k}}^\dagger + d_{\mathbf{k}} \alpha_{-\mathbf{k}} \quad (\text{C47})$$

$$c_{\mathbf{k}} \equiv \sqrt{\frac{\xi_{\mathbf{k}} + V \tilde{n}_0 + \omega_{\mathbf{k}}}{2\omega_{\mathbf{k}}}} \quad (\text{C48})$$

$$d_{\mathbf{k}} \equiv \sqrt{\frac{\xi_{\mathbf{k}} + V \tilde{n}_0 - \omega_{\mathbf{k}}}{2\omega_{\mathbf{k}}}}, \quad (\text{C49})$$

where $\xi_{\mathbf{k}} \equiv \epsilon_{\mathbf{k}} - \epsilon_{\mathbf{k}_0}$, and, as required by the diagonal form of the solution, the diagonal true condensation density $\tilde{n}_0 \sim n_0$ has replaced the non-diagonal bare condensate n_0 .

Importantly, we can see that these particle-hole excitations $\tilde{\alpha}_{\mathbf{k}}^\dagger$ follow a linear dispersion when $\xi \ll 2V \tilde{n}_0$ in Eq.(C46), and that the excitations generated by $\alpha_{\mathbf{k}}^\dagger$ are not conserved in Eq.(C44) even though the underlying particles are conserved. As

suggested by the solution notation, these results support the interpretation of these ‘sound’ modes $\tilde{\alpha}_{\mathbf{k}}^\dagger$ as the leading order contribution to the eigen-particle-hole excitation operator, $\tilde{\alpha}_{\mathbf{k}}^\dagger = U^\dagger \alpha_{\mathbf{k}}^\dagger U = \tilde{a}_{\mathbf{k}}^\dagger \tilde{a}_{\mathbf{k}_0} \tilde{N}_0^{-\frac{1}{2}}$, defined via the eigen-particles in Eq.(B4) and indicate that the dispersion for the eigen-particle-hole operators is linear at low energy.

It is important to note that this demonstration, similar to the standard particle-non-conserving Bogoliubov treatment, does not capture the sub-leading $\frac{\hbar^2}{m} \mathbf{k} \cdot \mathbf{k}$ contribution in $\omega_{\mathbf{k}}$, as required by the rigorous structure of the canonical transformation to reach Eq.(9). This sub-leading contribution is essential, since it is the one that describes the flow of the inertial mass. See Appendix G for a detailed discussion on this important issue.

Appendix D Thermal fluctuation of superfluid density

Having established the equivalence between the superfluid density and the true condensate density, $\rho_s/\rho = \tilde{a}_{\mathbf{k}_0}^\dagger \tilde{a}_{\mathbf{k}_0}/N$, it is straightforward to evaluate the temperature dependence of the former from that of the latter. Specifically in the *linear response* ($\mathbf{u} \rightarrow \mathbf{0}$) regime corresponding to most of the experimental data in Fig. 1, the thermal equilibrium is reached *before* the application of the external stimuli. So, the thermal equilibrium corresponds to a canonical system without relative internal flow. (It is important to note that with finite \mathbf{u} , the standard thermal statistics is generally inapplicable to superfluidity. See Appendix H.)

D.1 Estimate in the grand canonical ensemble

Let’s first consider the case with grand canonical ensemble (GCE). The condensate cannot be studied directly in the GCE, where thermally there is no particle conservation, so the total excited particle statistics are computed instead

$$\tilde{N}_n \equiv \sum_{\mathbf{k} \neq \mathbf{k}_0} n_{\mathbf{B}}(\beta \omega_{\mathbf{k}}) \rightarrow \frac{\mathcal{V}}{(2\pi)^d} \int d^d \mathbf{k} n_{\mathbf{B}}(\beta \omega_{\mathbf{k}}), \quad (\text{D50})$$

at large system size, where $n_{\mathbf{B}}(\beta \omega) = (e^{\beta \omega} - 1)^{-1}$ denotes the Bose-Einstein distribution function at the inverse temperature $\beta = 1/k_{\text{B}}T$. Here an *ad hoc* assumption is made to subtract the result from an assumed well-defined average particle number N

$$\tilde{N}_0 = N - \tilde{N}_n. \quad (\text{D51})$$

It is a standard exercise to compute the temperature dependence of the condensate in a d-dimensional system of bosons via the leading-order linear dispersion $\omega_{\mathbf{k}} = v_s |\mathbf{k} - \mathbf{k}_0|$ found at low temperature, which gives

$$\tilde{N}_0/N = 1 - \frac{\mathcal{V} S_d}{N (2\pi v_s)^d} \int_0^\infty d\omega \omega^{d-1} n_{\mathbf{B}}(\beta \omega) \quad (\text{D52})$$

$$= 1 - \frac{\mathcal{V}S_d}{N(2\pi v_s\beta)^d} \int_0^\infty d\nu \nu^{d-1} n_B(\nu) \quad (\text{D53})$$

$$= 1 - \frac{\mathcal{V}S_d\zeta(d)k_B^d}{N(2\pi v_s)^d} T^d, \quad (\text{D54})$$

where $\nu = \beta\omega$, S_d is the surface area of a d -dimensional hypersphere, and $\zeta(d)$ is the Reimann zeta function. Eq.(D54) identifies the depletion of the true condensate in 3D to be $\propto T^3$ for the low energy theory developed above.

Note that although the depletion of the condensate with temperature generally reduces the superfluid stiffness $v_s = v_s(T)$ with temperature as well, this additional depletion is a higher-order effect. This can be seen by simply inserting the condensate depletion explicitly into the dispersion of Eq.(C46) via $\omega_{\mathbf{k}} \approx \sqrt{2V\xi_{\mathbf{k}}\tilde{n}_0(T)}$, expanding this depletion to leading order in the depletion $\tilde{n}_0 \approx n - aT^\gamma$, and inserting into Eq.(D52). The leading order constant total density n results in the self-consistent solution $\gamma = d$ and the reducing stiffness only results in $\mathcal{O}(T^{2d})$ corrections. Therefore, the depletion of the superfluid density is generally $\propto T^d$ at low temperature.

D.2 Derivation in the canonical ensemble

Having maintained particle-conservation in the quantum problem at low energy, we can (and should) introduce the effects of finite temperature via an appropriately particle-conserving statistical ensemble such as the canonical ensemble (CE). The CE incorporates the highly relevant scale of total particle number N at low energy that is fundamentally absent in the GCE. Furthermore, it is well-known[124] that the CE and the GCE can produce different macroscopic properties in the presence of a condensate. Therefore, the GCE result should be considered no more than an estimate unless it is shown to converge to the CE result in the macroscopic limit.

Specifically, since our system is solved strictly in the N -particle sector, *every* many-body state satisfies the one-body constraint

$$N = \tilde{N}_0 + \tilde{N}_\epsilon \quad (\text{D55})$$

$$\tilde{N}_\epsilon \equiv \sum_{\mathbf{k} \neq \mathbf{k}_0} \tilde{a}_{\mathbf{k}}^\dagger \tilde{a}_{\mathbf{k}}, \quad (\text{D56})$$

where \tilde{N}_ϵ is the sum over excitations above the condensate. Therefore, once the condensate and the excitations are taken together, computing thermal statistics under the constraint in Eq.(D55) requires the canonical ensemble.

As shown by Fujiwara et al[125], the complications of the restricted sum in the partition function of the canonical ensemble

$$Z = \sum_{n_s} \prod_s e^{-\beta\omega_s n_s}, \quad (\text{D57})$$

can be overcome by introducing a constraint parameter t to the partition function

$$Z = \frac{1}{2\pi i} \int dt e^{-Nt} \sum_s \left(\sum_{n_s} e^{n_s(t - \beta\omega_s)} \right). \quad (\text{D58})$$

Choosing the sum over occupation statistics n_s to run from 0 to N results in a closed form for the partition function

$$Z = \frac{1}{2\pi i} \int dt \prod_s \left(\frac{1 - e^{-Dz_s}}{1 - e^{-z_s}} \right) \quad (\text{D59})$$

$$D = N + 1 \quad (\text{D60})$$

$$z_s = \beta\omega_s - t, \quad (\text{D61})$$

that is extremely well-behaved (i.e. smooth, finite, and with an infinite radius of convergence!). Therefore, steepest descent methods are reliable and result in unique saddle-point values for t in the large system limit, in great contrast to grand canonical ensemble formulations for bosons.

The saddle-point equation resulting from the above treatment

$$N = \sum_s n_B(z_s) - D n_B(Dz_s) \equiv \sum_s n_G(z_s, N), \quad (\text{D62})$$

simply applies the constraint of total particle number N on the occupation statistics resulting in the ‘Gentile-ter Haar-Wergeland’ distribution function n_G , which is itself a simple function of the Bose-Einstein distribution function n_B . Although Eq.(D62) may appear superficially similar to the equation in the grand canonical ensemble used to identify the chemical potential, here the occupation of the lowest energy state is explicitly included even in the presence of Bose-Einstein condensation (BEC).

Before studying the statistics required for our fluid responses, it is necessary to recall[125] the relevant saddle-point behavior of t . For temperatures much larger than the condensation temperature, the saddle-point is below the lowest energy state $t < \beta\omega_0$. It reaches the lowest energy $t = \beta\omega_0$ precisely when the condensate at ω_0 contains half of the total N particles $\tilde{N}_0 = n_G(-t, N) = N/2$, where \tilde{N}_0 is the occupation of the true condensate defined in Appendix B.1. As the temperature is lowered further, the saddle-point increases, but it is bounded from above $\beta\omega_0 < t < \beta\omega_1$, where ω_1 is the lowest excitation energy. However, as studied previously[125], the saddle-point t only approaches its limiting value for extremely low temperatures, namely when the temperature scale is of the same order as the energy level spacing between ω_0 and ω_1 . Our system has a gapless single-particle spectrum given by Eq.(C46), so we are interested in temperatures where the condensate is large ($t > 0$) but the temperature scale is much larger than the spacing between low-lying energy levels ($\beta \ll \omega_1 - \omega_0$). In this regime $\beta\omega_0 < t \ll \beta\omega_1$ the saddle-point at any fixed temperature T is small $t \ll 1$.

In our system the dispersion is $\omega_{\mathbf{k}} \equiv v_s |\mathbf{k} - \mathbf{k}_0|$, so the lowest energy state is zero ($\omega_{\mathbf{k}_0} = 0$). Simplifying the occupation function $n_G(z_s)$ for small positive t

$$\tilde{N}_0 = n_G(-t) \approx N - n_B(t) \approx N - \frac{1}{t} \quad (\text{D63})$$

$$n_G(\beta\omega_k - t) \approx n_B(-\beta\omega_k + t), \quad (\text{D64})$$

we use the saddle-point constraint in Eq.(D62) and find in 3D

$$t \approx \left(\frac{\mathcal{V}\zeta(3)}{\pi^2 v_s^3 \beta^3} \right)^{-1}. \quad (\text{D65})$$

In our canonical ensemble formulation, the condensate temperature dependence is simply

$$\frac{\rho_s(T)}{\rho} = \frac{\tilde{N}_0(T)}{N} = 1 - AT^3 + \mathcal{O}(T^4) \quad (\text{D66})$$

$$A = \frac{\mathcal{V}\zeta(3)k_B^3}{N\pi^2 v_s^3}. \quad (\text{D67})$$

Applying the results in Eqs.(D63-D65) to the excitations, the leading order normal fluid contribution becomes

$$\frac{\rho_n}{\rho}(T) \approx \int d^3p \, n_G(\omega_p) \approx AT^3 + \mathcal{O}(T^4), \quad (\text{D68})$$

where A is *identical* to that defined in the superfluid depletion of Eq.(D67). Therefore, Eqs.(D66,D68) are consistent with the sum rule

$$\frac{\rho_s}{\rho} + \frac{\rho_n}{\rho} = [1 - AT^3 - \mathcal{O}(T^4)] + [AT^3 + \mathcal{O}(T^4)], \quad (\text{D69})$$

which is not surprising given the strict confinement to the N -particle sector.

Appendix E Effects of weak impurities at low temperature

Here we briefly outline the dominant low-temperature effect of local impurities on the superfluid density. For simplicity, we introduce local impurities via a local random on-site potential

$$H_{\text{dis}} = \sum_{\mathbf{x}} \delta(\mathbf{x}) a_{\mathbf{x}}^\dagger a_{\mathbf{x}} \quad (\text{E70})$$

$$\delta \in \frac{1}{\sqrt{2\pi\Delta}} e^{-\frac{y^2}{2\Delta}} \quad y \in \{-\infty, \infty\}, \quad (\text{E71})$$

where $\delta(\mathbf{x})$ instances a Gaussian random variable taken from the probability density function δ at each point \mathbf{x} . Without loss of generality, we have fixed the average to vanish, leaving the variance Δ as the only remaining disorder scale

$$\bar{\delta} = 0 \quad (\text{E72})$$

$$\overline{\delta^2} \equiv \Delta \ll 1, \quad (\text{E73})$$

and therefore we perform a perturbative expansion in weak disorder $\Delta \ll 1$ to identify the qualitative effects of impurities on superfluidity.

Throughout the rest of this section, we study the large-system limit where the effects of finite-size sampling of δ are negligible. This is particularly easy to see for the low-energy, long-wavelength states relevant to this low-temperature study of superfluid and normal fluid responses. For example, the average effect of disorder on long-wavelength states $|\mathbf{k} - \mathbf{k}_0| \ll 1$ in the large system limit identifies with the population average of δ

$$\lim_{V \rightarrow \infty} \frac{1}{V} \sum_{\mathbf{x}} \delta(\mathbf{x}) e^{i\mathbf{k} \cdot \mathbf{x}} = \bar{\delta} = 0, \quad (\text{E74})$$

which vanishes. Given a system of length L and volume $V = L^d$, one way to show this is by coarse-graining the system into $M \propto L^{d-1}$ arbitrarily large regions of volume $m \propto L$, where $(mM) \propto V$ correctly scales with the system volume. In the large-system limit and for a sufficiently slow-varying phase mode (e.g. $|\mathbf{k} - \mathbf{k}_0| \propto L^{-\alpha}$ and $1/2 < \alpha < 1$) we find

$$\begin{aligned} \lim_{V \rightarrow \infty} \frac{1}{V} \sum_{\mathbf{x}} \delta(\mathbf{x}) e^{i\mathbf{k} \cdot \mathbf{x}} &= \lim_{V \rightarrow \infty} \frac{1}{M} \sum_{\mathbf{x}} e^{i\mathbf{k} \cdot \mathbf{x}} \left\{ \frac{1}{m} \sum_{\mathbf{x}'} \delta(\mathbf{x}') e^{i\mathbf{k} \cdot \mathbf{x}'} \right\} \\ &= \lim_{V \rightarrow \infty} \frac{1}{M} \sum_{\mathbf{x}} e^{i\mathbf{k} \cdot \mathbf{x}} \left\{ \frac{1}{m} \sum_{\mathbf{x}'} \delta(\mathbf{x}') \left(1 + i\mathbf{k} \cdot \mathbf{x}' + \dots \right) \right\} \\ &\leq \lim_{V \rightarrow \infty} \frac{1}{M} \sum_{\mathbf{x}} e^{i\mathbf{k} \cdot \mathbf{x}} \left\{ \frac{1}{m} \sum_{\mathbf{x}'} \delta(\mathbf{x}') \left(1 + im|\mathbf{k}| + \dots \right) \right\} \\ &= \lim_{V \rightarrow \infty} \frac{1}{M} \sum_{\mathbf{x}} e^{i\mathbf{k} \cdot \mathbf{x}} \left\{ \frac{1}{M} \sum_{\mathbf{x}} \delta(\mathbf{x}) \left(1 + \mathcal{O}[L^{1-\alpha}] \right) \right\} \\ &= \lim_{V \rightarrow \infty} \bar{\delta} \left(\frac{1}{M} \sum_{\mathbf{x}} e^{i\mathbf{k} \cdot \mathbf{x}} \right) \rightarrow 0, \end{aligned} \quad (\text{E75})$$

where our choice of exponent α implies the required $1 - \alpha > 0$ and ensures that $(\mathbf{k} - \mathbf{k}_0) \cdot \mathbf{x} \ll 2\pi$ in order to safely truncate the Taylor expansion of the phase factor. The above statistics in Eqs.(E74) help identify the leading-order relevant effects of the perturbation. The first order correction to the energy vanishes

$$E_{\mathbf{k}}^{(1)} = \left\langle \psi_{\mathbf{k}}^{(0)} \left| H_{\text{dis}} \right| \psi_{\mathbf{k}}^{(0)} \right\rangle = \frac{1}{V} \sum_{\mathbf{x}} \delta(\mathbf{x}) \rightarrow 0, \quad (\text{E76})$$

where we have used the fact that $a_{\mathbf{x}}^\dagger a_{\mathbf{x}} \equiv n_{\mathbf{x}} = 1/V$ for all states in the clean system (due to translation invariance).

We note that the second-order correction to the energy $E_{\mathbf{k}}^{(2)}$, although non-vanishing, does not contribute to the low-energy superfluid or normal fluid response in this system. This is because the low-energy spectrum of the clean system ($\omega_{\mathbf{k}} = v_s |\mathbf{k} - \mathbf{k}_0|$) is linear and therefore the density of states is linear in 3D. The second-order correction to the energy merely reshuffles the density of states in a small energy window $\Delta\omega$ around each energy ω in proportion to the local density of states in that window. But since the density of states is linear in this region this reshuffling affects each energy in exactly the same way, resulting in no net effect.

It turns out that the first-order perturbative correction to the states *does* affect the superfluid and normal fluid densities, which are now clearly the dominant effect of weak impurities on the superfluid and normal fluid responses since neither the first- nor the second-order corrections to the energy affect these quantities.

The first order corrections to the states can be identified by computing the modification of the excitation operators $\tilde{a}_{\mathbf{k}}$ in Eq.(C45) while leaving their corresponding commutators unchanged. (Generally, a truncated perturbation expansion applies a non-unitary transformation and will not preserve the commutation relations, but the resulting error is controlled by the smallness of the perturbation parameter. In this case the small variance $\Delta \ll 1$ as well as the long-wavelength $|\mathbf{k} - \mathbf{k}_0| \ll 1$ assumption make this error negligible.) Since the unperturbed system in Eq.(C45) is diagonal in $\tilde{a}_{\mathbf{k}}$, the first order perturbative corrections to the state

$$c_{\mathbf{k}\mathbf{k}'}^{(1)} = \frac{\langle \psi_{\mathbf{k}'} | H_{\text{dis}} | \psi_{\mathbf{k}} \rangle}{E_{\mathbf{k}}^{(0)} - E_{\mathbf{k}'}^{(0)}} \quad (\text{E77})$$

can be represented by the corresponding corrections to the one-body operators $\tilde{a}_{\mathbf{k}}$ and $\tilde{a}_{\mathbf{k}_0}$. To leading order (in \tilde{n}_0), these terms are given by

$$\tilde{a}_{\mathbf{k}_0} \rightarrow \tilde{a}_{\mathbf{k}_0} - \sum_{\mathbf{k} \neq \mathbf{k}_0} \frac{\delta_{\mathbf{k}, \mathbf{k}_0}}{\omega_{\mathbf{k}}} \left(c_{\mathbf{k}} \tilde{a}_{\mathbf{k}} - d_{\mathbf{k}} \tilde{a}_{-\mathbf{k}}^\dagger \right) \quad (\text{E78})$$

$$\tilde{a}_{\mathbf{k}_0}^\dagger \rightarrow \tilde{a}_{\mathbf{k}_0}^\dagger + \sum_{\mathbf{k} \neq \mathbf{k}_0} \frac{\delta_{\mathbf{k}, \mathbf{k}_0}}{\omega_{\mathbf{k}}} \left(c_{\mathbf{k}} \tilde{a}_{\mathbf{k}}^\dagger - d_{\mathbf{k}} \tilde{a}_{-\mathbf{k}} \right) \quad (\text{E79})$$

$$\tilde{a}_{\mathbf{k}} \rightarrow \tilde{a}_{\mathbf{k}} + \frac{\delta_{\mathbf{k}, \mathbf{k}_0}}{\omega_{\mathbf{k}}} \left(c_{\mathbf{k}} \tilde{a}_{\mathbf{k}} - d_{\mathbf{k}} \tilde{a}_{-\mathbf{k}}^\dagger \right) \quad (\text{E80})$$

$$\tilde{a}_{\mathbf{k}}^\dagger \rightarrow \tilde{a}_{\mathbf{k}}^\dagger - \frac{\delta_{\mathbf{k}, \mathbf{k}_0}}{\omega_{\mathbf{k}}} \left(c_{\mathbf{k}} \tilde{a}_{\mathbf{k}}^\dagger - d_{\mathbf{k}} \tilde{a}_{-\mathbf{k}} \right), \quad (\text{E81})$$

where $\delta_{\mathbf{k}, \mathbf{k}_0}$ is an off-diagonal component of the disorder $\delta(\mathbf{x})$ generated by transforming Eq.(E70) to momentum space. Since the current operator is independent of any local density term in the Hamiltonian, including the weak impurity term in Eq.(E70), the formal derivation of the superfluid and normal fluid densities remains unaffected by the introduction of the weak impurity term. Applying the perturbation identified in Eqs.(E78-E81) to these fluid response equations in the long-wavelength regime (via

canonical ensemble at finite temperature, see Appendix D.2) we find

$$\rho_s = m(\tilde{n}_0 - n^{(1)}) \quad (\text{E82})$$

$$\rho_n = m(n - \tilde{n}_0 + n^{(1)}) \quad (\text{E83})$$

$$n^{(1)} \equiv \frac{1}{m} \sum_{\mathbf{k} \neq \mathbf{k}_0} \frac{\delta_{\mathbf{k}, \mathbf{k}_0}^2}{\omega_{\mathbf{k}}^2} \langle \tilde{\alpha}_{\mathbf{k}}^\dagger \tilde{\alpha}_{\mathbf{k}} \rangle \sim \left(\frac{\Delta k_B}{2\pi^2 m v_s^3} \log(t) \right) T \quad (\text{E84})$$

results in a dominant low-temperature T -linear reduction in the superfluid density and corresponding growth of the normal fluid density as per the sum rule.

The above result shows that the leading order effect of weak impurities with temperature is to reduce the superfluid density linearly $\propto T$, which is a much stronger reduction than the $\propto T^3$ reduction found for the clean case in Appendix D.1, as expected. Further, the result of this leading order perturbation is consistent the sum rule, since the normal fluid density also increases linearly $\propto T$ and exactly matches the reduction of the superfluid density.

Appendix F No-go theorem forbidding phonons from representing the normal fluid

On one hand, the phenomenon of superfluidity generally occurs as dissipationless flow in the presence of dissipative flow, and the latter is required to come to rest (*locally* in position space) with a boundary, in order to establish equilibrium. On the other hand, traditional superfluid theory constructions assume that the non-superfluid part of the system is a so-called ‘gas of phonons,’ in other words an ensemble of waves each of well-defined wavenumber \mathbf{k} . Such waves could only satisfy a local boundary condition via construction of appropriately localized ‘wave packets’ requiring the superposition of many such waves. As we prove below, this necessary construction is impossible.

In this section, we prove two theorems and then use them to prove a corollary establishing a no-go theorem that renders *any* ensemble formed from “quanta of longitudinal waves”[41] incapable of satisfying the boundary conditions required to describe normal fluid flow as described above. Note that *all* of the assumptions utilized in this section come from prominent established literature[118, 120].

Theorem 1 *A generic state $\psi(\mathbf{r})$, composed of a sum over quanta of longitudinal waves that satisfy a system exhibiting translational symmetry, always satisfies the condition of potential flow $\nabla \times \mathbf{v} = 0$.*

Theorem 2 *The only such state that satisfies both $\nabla \times \mathbf{v} = 0$ and the boundary condition for a viscous liquid[120] $\mathbf{v}_{\text{bdry}} = \mathbf{v}_{\text{wall}}$ is a single trivial plane wave $\psi(\mathbf{r}) = e^{-i\mathbf{k} \cdot \mathbf{r}}$.*

Corollary 1 *The (excitation) waves used to generate the state in Theorem 1 do not satisfy Theorem 2 in an arbitrary inertial frame.*

To prove Theorem 1, we first define a generic state composed of a sum over quanta of longitudinal waves[118]

$$\psi(\mathbf{r}) \equiv \sum_{\mathbf{k}} \left(\alpha_{\mathbf{k}} e^{i\mathbf{k} \cdot \mathbf{r}} + \beta_{\mathbf{k}} e^{-i\mathbf{k} \cdot \mathbf{r}} \right), \quad (\text{F85})$$

where real inversion-symmetric coefficients $\alpha_{-\mathbf{k}} = \alpha_{\mathbf{k}}$ and $\beta_{-\mathbf{k}} = \beta_{\mathbf{k}}$ can be chosen for a translationally invariant liquid with linear or quadratic dispersion at low energy. This state includes those generated via excitations out of a mean-field condensate, for example.

Our goal is to compute the flow \mathbf{v} of this quantum state

$$\mathbf{v} \equiv \frac{\hbar}{2mi} \left(\psi^* \nabla \psi - \psi \nabla \psi^* \right), \quad (\text{F86})$$

where m is the so-called inertial mass of the state ψ , followed by the curl of Eq.(F86). To this end, it is straightforward to first identify the general conditions on the state itself after applying both

$$\nabla \times \mathbf{v} = \frac{\hbar}{2mi} \nabla \times \left(\psi^* \nabla \psi - \psi \nabla \psi^* \right) \quad (\text{F87})$$

$$\Rightarrow \left(\nabla \times \mathbf{v} \right)_k = \frac{\hbar}{mi} \epsilon_{ijk} \left((\nabla \psi^*)_i (\nabla \psi)_j - (\nabla \psi)_i (\nabla \psi^*)_j \right). \quad (\text{F88})$$

However, the state $\psi(\mathbf{r})$ in Eq.(F85) satisfies

$$(\nabla \psi^*(\mathbf{r}))_i (\nabla \psi(\mathbf{r}))_j - (\nabla \psi(\mathbf{r}))_i (\nabla \psi^*(\mathbf{r}))_j \quad (\text{F89})$$

$$= \sum_{\mathbf{k}\mathbf{k}'} k_i k'_j \left\{ \left(-\alpha_{\mathbf{k}} e^{-i\mathbf{k} \cdot \mathbf{r}} + \beta_{\mathbf{k}} e^{i\mathbf{k} \cdot \mathbf{r}} \right) \left(\alpha_{\mathbf{k}'} e^{i\mathbf{k}' \cdot \mathbf{r}} - \beta_{\mathbf{k}'} e^{-i\mathbf{k}' \cdot \mathbf{r}} \right) \right. \\ \left. - \left(\alpha_{\mathbf{k}} e^{i\mathbf{k} \cdot \mathbf{r}} - \beta_{\mathbf{k}} e^{-i\mathbf{k} \cdot \mathbf{r}} \right) \left(-\alpha_{\mathbf{k}'} e^{-i\mathbf{k}' \cdot \mathbf{r}} + \beta_{\mathbf{k}'} e^{i\mathbf{k}' \cdot \mathbf{r}} \right) \right\} \quad (\text{F90})$$

$$= \sum_{\mathbf{k}\mathbf{k}'} k_i k'_j \left\{ \left(\alpha_{\mathbf{k}} e^{i\mathbf{k} \cdot \mathbf{r}} - \beta_{\mathbf{k}} e^{-i\mathbf{k} \cdot \mathbf{r}} \right) \left(-\alpha_{\mathbf{k}'} e^{-i\mathbf{k}' \cdot \mathbf{r}} + \beta_{\mathbf{k}'} e^{i\mathbf{k}' \cdot \mathbf{r}} \right) \right. \\ \left. - \left(-\alpha_{\mathbf{k}} e^{-i\mathbf{k} \cdot \mathbf{r}} + \beta_{\mathbf{k}} e^{i\mathbf{k} \cdot \mathbf{r}} \right) \left(\alpha_{\mathbf{k}'} e^{i\mathbf{k}' \cdot \mathbf{r}} - \beta_{\mathbf{k}'} e^{-i\mathbf{k}' \cdot \mathbf{r}} \right) \right\} \quad (\text{F91})$$

$$= -(\nabla \psi^*(\mathbf{r}))_i (\nabla \psi(\mathbf{r}))_j - (\nabla \psi(\mathbf{r}))_i (\nabla \psi^*(\mathbf{r}))_j \quad (\text{F92})$$

$$\Rightarrow (\nabla \psi^*(\mathbf{r}))_i (\nabla \psi(\mathbf{r}))_j - (\nabla \psi(\mathbf{r}))_i (\nabla \psi^*(\mathbf{r}))_j = 0, \quad (\text{F93})$$

where the inversion symmetric coefficients $\alpha_{-\mathbf{k}} = \alpha_{\mathbf{k}}$ and $\beta_{-\mathbf{k}} = \beta_{\mathbf{k}}$ were used to go from the second line to the third. The curl of the flow vanishes upon inserting the wave property of Eq.(F89) into the irrotational condition in Eq.(F88), proving that $\psi(\mathbf{r})$ satisfies the condition of potential flow $\nabla \times \mathbf{v} = 0$. Note that this proof simply verifies, under general conditions, the well-known fact[41] that longitudinal waves, quantized or otherwise, always satisfy the condition of potential flow.

To prove Theorem 2, it is sufficient to study the flow in a region where the boundary runs parallel to the flow direction and encloses the cross-section of the flow. In this

case, the boundary condition for viscous flow, in the long-time regime where the flow is allowed to approach equilibrium with the boundary, simply becomes

$$\mathbf{v}_{\text{bdry}}(\mathbf{r}_{\text{wall}}) = \mathbf{v}_{\text{wall}}(\mathbf{r}_{\text{wall}}) = \mathbf{w}, \quad (\text{F94})$$

where \mathbf{v}_{bdry} is the flow at the boundary, \mathbf{v}_{wall} is the (inertial) motion of the boundary itself located at positions \mathbf{r}_{wall} , and \mathbf{w} is a constant independent of position along the boundary since the boundary is assumed to come from an inertial rigid body.

Irrotational flow $\nabla \times \mathbf{v} = 0$ restricts the flow function $\mathbf{v}(\mathbf{r})$ for this region to be only a function of the longitudinal direction

$$\mathbf{v}(\mathbf{r}) = \mathbf{v}(r_{\parallel}), \quad (\text{F95})$$

where the position vector has been separated into components parallel and perpendicular to the flow respectively $\mathbf{r} = \mathbf{r}_{\parallel} + \mathbf{r}_{\perp}$. On the other hand, the boundary condition in Eq.(F94), coming from a rigid inertial body, further restricts the flow to a constant, independent of the longitudinal direction as well

$$\mathbf{v}(\mathbf{r}) = \mathbf{w}. \quad (\text{F96})$$

Since Eq.(F86) directly relates this uniform flow $\mathbf{v} = \mathbf{w}$ to the state $\psi(\mathbf{r})$, the restriction in Eq.(F96) restricts the state itself. In particular, only a plane wave $\psi(\mathbf{r}) \equiv e^{-i\mathbf{k}\cdot\mathbf{r}}$ results in a uniform flow $\hbar\mathbf{k}/m$.

The requirement of a plane wave state $\psi(\mathbf{r}) \equiv e^{-i\mathbf{k}\cdot\mathbf{r}}$ in Theorem 2, requires all modes to vanish except one at $\hbar\mathbf{k}/m = \mathbf{w}$ for the state $\psi(\mathbf{r})$ in Eq.(F85). However, the remaining mode can only satisfy this condition in a single inertial frame, since it transforms (for new frame of relative velocity change \mathbf{u} written with prime notation) $\mathbf{k}' = \mathbf{k}$ trivially as a wave, whereas the boundary transforms as a mass M rigid body $\mathbf{w}' = \mathbf{w} - \mathbf{u}$. Therefore, we have also proven Corollary 1 in that the state defined in Theorem 1 cannot satisfy the conditions in Theorem 2 for an arbitrary inertial frame. Since the conditions in Theorem 2 are required for a state such as $\psi(\mathbf{r})$ to represent the normal fluid, this proves that any such state cannot contribute to the normal fluid response.

Appendix G Inertial mass velocity embedded in the group velocity of elementary excitations: necessity for beyond-linear dispersion

Unlike the sound modes in solids that only propagate energy of the vibration, the same in liquid is also accompanied by flow of inertial mass-carrying matter. Here, we demonstrate how the latter is embedded in the group velocity of the elementary excitations, and why the standard Bogoliubov treatment fails to properly describe the current of the inertial mass.

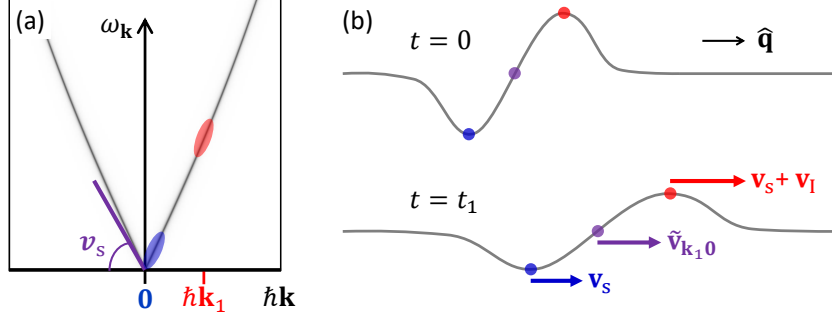


Fig. G2 inertial mass velocity in a superfluid (a) In the rest frame of a superfluid, a physical current fluctuation as particle-hole excitation with locality in both position and momentum around $\hbar\mathbf{k}_1$ is composed of a wave packet of particle of similar momentum (in red) and that of the hole around the true condensate of nearly zero momentum (in blue). While the group velocity of both the particle and hole wave packets contains the sound velocity, $\mathbf{v}_s = v_s \hat{\mathbf{k}}$, this velocity only describes propagation of the vibrational part of the fluctuation. (b) The more relevant inertial mass of the matter, on the other hand, corresponds to the relative velocity between the particle and hole wave packets, $\mathbf{v}_I = (v_s \hat{\mathbf{k}}_1 + \frac{\hbar\mathbf{k}_1}{m}) - (v_s \hat{\mathbf{k}}_1 + \frac{\hbar\mathbf{k}_0}{m}) = \frac{\hbar\mathbf{k}_1}{m}$, corresponding to an additional $m\mathbf{v}_I$ to the system's total kinematic momentum identical to the canonical momentum $\hbar\mathbf{k}_1$ of the sound mode. The center of the particle-hole pair (in purple) propagates with their average velocity $\tilde{\mathbf{v}}_{\mathbf{k}_1\mathbf{k}_0} = \mathbf{v}_s + \frac{1}{2}\mathbf{v}_I$, as encoded in the current operator $\tilde{\mathbf{J}}_{\mathbf{q}=(\mathbf{k}_1-\mathbf{k}_0)}$ in Eq.(14)

Figure G2 illustrates the elementary particle-hole excitation spectrum of a superfluid in its rest frame. According to Eq.(9), the spectrum is dominated by a linear dispersion, $v_s|\mathbf{k}|$, with velocity (slope) $v_s\hat{\mathbf{k}}$ at low energy, accompanied by the kinetic energy of the inertial mass $\frac{\hbar^2}{2m}\mathbf{k} \cdot \mathbf{k}$. Now, according to Section 5.2.2 the elementary excitations of the system rigorously correspond to creation of eigen-particle-hole pairs, $\tilde{\alpha}_{\mathbf{k}}^\dagger \equiv \tilde{a}_{\mathbf{k}}^\dagger \tilde{a}_{\mathbf{k}_0} \tilde{N}_0^{-\frac{1}{2}}$. Therefore, a physical current fluctuation with well-defined locality in both space and momentum, say around $\hbar\mathbf{k}_1$, would consist of a wave packet of eigen-particles (in red) around $\hbar\mathbf{k}_1$, and a wave packet of holes around $\hbar\mathbf{k}_0 = \mathbf{0}$, with group velocities $v_s\hat{\mathbf{k}}_1 + \frac{\hbar\mathbf{k}_1}{m}$ and $v_s\hat{\mathbf{k}}_1 + \frac{\hbar\mathbf{k}_0}{m}$, respectively, according to Eq.(15). Upon obtaining the flow of inertial mass through the relative velocity of the particle with respect to the hole, $\mathbf{v}_I = (v_s\hat{\mathbf{k}}_1 + \frac{\hbar\mathbf{k}_1}{m}) - (v_s\hat{\mathbf{k}}_1 + \frac{\hbar\mathbf{k}_0}{m}) = \frac{\hbar\mathbf{k}_1}{m}$, one finds that the additional kinematic momentum $m\mathbf{v}_I$ of the system is identical to the canonical momentum $\hbar\mathbf{k}_1$ of the sound mode excitation, as required by a proper quantum description.

Essentially, while both wave packets propagate via velocity $v_s\hat{\mathbf{k}}$ as part of the vibration that transports energy. The net flow of inertial mass is *completely* described by the kinematic $\frac{\hbar\mathbf{k}}{m}$ term of the group velocity. This is why sound modes in solids are described by a purely linear dispersion without such a kinematic contribution, since the atoms in solids only vibrate but do not flow.

Therefore, to have a proper account for the current of inertial mass, for example to obtain the superfluid density ρ_s , it is *absolutely necessary* to include the kinematic $\mathbf{v}_I \equiv \frac{\hbar\mathbf{k}}{m}$ contribution in the consideration. Note, however, this term is not captured by the standard Bogoliubov approximation, making it nearly impossible to recover the necessary f -moment sum rule in the current response [42]. Similarly, in the standard

two-fluid derivation of ρ_s [4], the thermal equilibrium is described without taking into account this essential contribution. It is therefore unclear how one is able to adhere to the physical equilibrium that the normal flow of the inertial mass moves together with the wall.

Appendix H General inapplicability of the standard statistics to steady superflow against a stationary wall

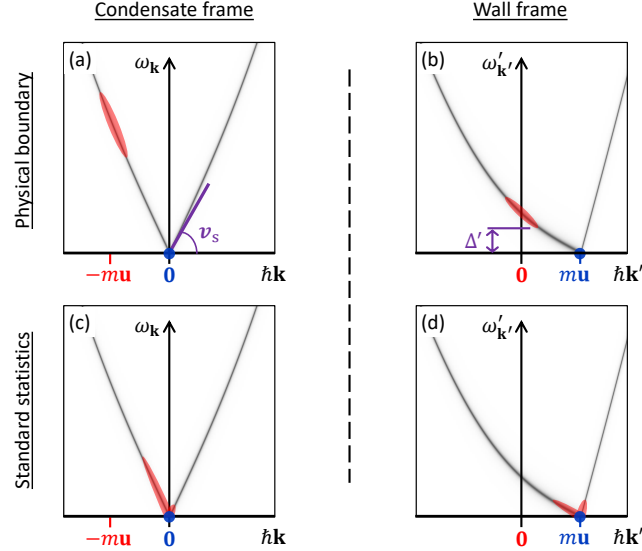


Fig. H3 Demonstration of inapplicability of standard statistics in the presence of steady superflow. (a)-(d) illustrate the energy ω_q and momentum $\hbar q$ dispersion of elementary excitations, equivalent to creating particle-hole pairs from the true condensate at $\hbar k_0$ to a finite momentum $\hbar k = \hbar q + \hbar k_0$. For easier visualization of the eigen-particles' kinematic momentum, the excitation momenta is shifted by the momentum of the hole in the true condensate $\hbar k_0$. (b) Under physical equilibrium with the wall, the excited eigen-particles (in red) should appear nearly stationary in the wall frame, and only those in the true condensate (in blue) are moving with a steady velocity u . Notice the energy gap in the occupation, $\Delta' > 0$, that protects the system against dissipation. (a) Consistently, in the rest frame of the superfluid, the excited eigen-particles (in red) would move along with the wall with velocity around $-u$. (d) In contrast, standard thermal statistics would only populate the low-energy sound modes in the wall frame, ensuring zero average group velocity of the sound modes. However, instead of adhering to the wall as required by physical equilibrium with the wall, the excited particles all have velocity around that of the superflow. (c) Corresponding, in the condensate frame, the average velocity of the excited particles are much smaller than that of the wall, $-u$. Due to presence of a steadily flowing supercurrent, the standard thermal statistics is inapplicable for the corresponding gas of sound modes.

Even though our eigen-particle description of the superfluid density presented in the main text basically follows the hydrodynamical description in the standard literature [4], our conclusion qualitatively differs from the standard lore, owing to our careful *separation* of the thermal statistics from the quantum mechanical problem. This section demonstrates the physical inconsistency in the standard treatment. Correspondingly, it only brushes the surface of a deep conceptual issue concerning the general inapplicability of the standard statistics to superfluidity. That is, the standard statistics can *only* be safely applied to a superfluid when there is no internal relative velocity between the superflow and the normal flow (e.g. as employed in our estimation of T^3 -depletion of superfluid density.)

Consider a system with superfluidity flowing steadily with relative velocity \mathbf{u} along the wall of a pipe or a container. Let's first prepare the system in its ground state [c.f. Eq.(5) of the main text] in the rest frame of the superflow, with all N particles condensing to $\tilde{a}_{\mathbf{k}_0}^\dagger$, as indicated by the blue dot in Fig. H3(a). Trivially, evaluation of the normal fluid density via total momentum \mathbf{P} of the system in the rest frame, $\rho_n = P/(u\mathcal{V}) = 0$, gives the correct zero result. Consistently in the wall frame shown in Fig. H3(b), all N particles are moving with the same velocity \mathbf{u} as part of the true condensate. Evaluation of superfluid density via $\rho_s = P'/(u\mathcal{V}) = mN/\mathcal{V} = m\tilde{N}_0/\mathcal{V}$ also produces the correct superfluid density corresponding to the true condensation density (equal to total density in this case.)

Now, let's slowly raise the temperature to a finite value T and allow the system to slowly reach thermal equilibrium *with* the wall. While the coupling to the wall does not affect the superfluid component owing to superflow's dissipation-less nature, it does impact the thermally-activated normal fluid component $\tilde{a}_{\mathbf{k}}^\dagger$ of various momentum \mathbf{k} , such that, after a long time scale, on average the normal fluid component becomes *stationary* against the wall, as illustrated by the red ellipsoid in Fig. H3(a) and (b). Consistent with the typical scenario found in the literature[4, 121], a thermally accessible quantum pure state containing such normal fluid component is thus equivalent to a quantum gas state of elementary excitation modes, $\tilde{\alpha}_{\mathbf{k}}^\dagger \equiv \tilde{a}_{\mathbf{k}}^\dagger \tilde{a}_{\mathbf{k}_0} \tilde{N}_0^{-\frac{1}{2}}$, upon interpreting the N -particle ground state as the vacuum. However, in a significant departure from the aforementioned literature, note that the above *stationary* boundary condition with the wall requires that in the wall frame the total momentum of the normal fluid component in such a pure state cannot be too far from zero, $\mathbf{P}'_n \equiv \sum_{\mathbf{k}' \neq 0} \hbar \mathbf{k}' \tilde{a}_{\mathbf{k}'}^\dagger \tilde{a}_{\mathbf{k}'} \sim 0$, where $\hbar \mathbf{k}'_0 = m\mathbf{u}$ denotes the momentum of (blue) eigen-particles in the true condensate. Therefore, evaluation of the superfluid density via $\rho_s = P'/(u\mathcal{V}) = m\tilde{N}_0/\mathcal{V}$ produces a superfluid density equivalent to the true condensation density \tilde{N}_0 . Consistently, in the superfluid rest frame the total momentum of the normal fluid component, $\mathbf{P}_n = \mathbf{P}'_n + (1 - \tilde{N}_0)m\mathbf{u} = (1 - \tilde{N}_0)m\mathbf{u}$, so again the normal fluid density is $\rho_n = P/(u\mathcal{V}) = m(1 - \tilde{N}_0)/\mathcal{V}$ as expected from mass conservation.

Up to this point, all the above considerations straightforwardly apply to arbitrary quantum many-body eigenstates (and thus any ensemble of them) and are thus conceptually rigorous in nature. One should, however, immediately realize the *inapplicability of the standard application of thermal statistics* to such an equilibrium. Specifically, given the steady relatively internal flows between the super and normal component in such physical equilibrium, one would need to find an inertial frame in which the

total energy contains *only* the (Galilean invariant) potential energy. Therefore, even in the wall frame, the total energy of the system cannot be used as the *frame-invariant* probability-determining *internal energy* [126]. Correspondingly, the standard Boltzmann distribution $e^{-\beta H}$ would not provide the correct physical probability in such equilibrium.

Indeed, notice that the occupation distribution in Fig. H3(a) and (b) has a gap at low energy and thus clearly cannot possibly correspond to the standard Bose-Einstein distribution. The physical origin of such finite energy requirement is associated with the finite velocity of the wall in the superflow's rest frame. During the slow increase of temperature from zero, consider a newly thermally enabled low-energy excited pure state corresponding to promoting one eigen-particle from the true condensate to one with tiny momentum. Coupling to the wall would attempt to drag this eigen-particle along the wall, which in turn would slow down the wall to conserve the total momentum of the system. To maintain the assigned fixed velocity of the wall, external supply of additional energy and momentum to the system is thus necessary, until the excited eigen-particle finally catches up with the wall and reaches the physical thermal equilibrium. In the superflow rest frame, the total energy and momentum injected into the system is, of course, exactly those required to accelerate the excited particle from nearly stationary up to the constant velocity of the wall.

The above non-standard thermal statistics, therefore, qualitatively differs from that employed in the traditional hydrodynamic two-fluid picture. As illustrated in Fig. H3(d), the excitations are traditionally assumed to be thermally populated sound modes, $\tilde{a}_{\mathbf{k}} = \tilde{a}_{\mathbf{k}}^\dagger \tilde{a}_{\mathbf{k}_0} \tilde{N}_0^{-\frac{1}{2}}$, following the canonical Boltzmann distribution and to have zero average *group velocity of the sound modes* in the wall frame [4, 118]. Correspondingly, in the superflow rest frame shown in Fig. H3(c), the Bose-Einstein distribution function takes the form [4] $n_B(\omega_{\mathbf{k}} + \hbar \mathbf{k} \cdot \mathbf{u})$ according to the boosted excitation energy $\omega_{\mathbf{k}}$ and eigen-particle momentum \mathbf{k} . Note, however, that at low temperature such distribution would give the excited eigen-particles an average velocity $\hbar \mathbf{k}/m$ only slightly deviating from that of the superflow. In other words, against the physical equilibrium to stick to the wall, in such a canonical equilibrium the eigen-particles would still *unphysically* follow the superflow, even though there is no friction between the normal and superfluid components.

Microscopically, this physical inconsistency results from broken U(1) symmetry of the system, which renders the low-energy excitation (and the low-energy effective theory) *no longer* frame-invariant. Particularly, even though, like states of a gas, the many-body eigenstates are pure states composed of momentum-persisting eigen-particles, these eigen-particles are heavily dressed by the superfluid component. Consequently, in the wall frame their energy-momentum dispersion is highly unusual as shown in Fig. H3(d) with minimum energy located next to the momentum of the condensed eigen-particles, completely different from a typical gas shown in Fig. 7. Again, from the consideration of thermal dynamics, this inconsistency is associated with the inadequacy of regarding the total energy of systems with internal steady flow as the probability-determining internal energy.

Naturally, in such a physically inconsistent thermal distribution, estimation of the normal fluid density via total momentum \mathbf{P} in the superfluid rest frame, *while*

incorrectly assuming the wall velocity $-\mathbf{u}$ (the average group velocity of the sound modes) as the average velocity of the uncondensed eigen-particles, $\rho_n = P/(u\mathcal{V}) \ll m(1 - \tilde{N}_0)/\mathcal{V}$, would result in a significantly smaller normal fluid density, since as illustrated in Fig. H3(d) the total kinematic momentum of the system is much smaller than $mv(1 - \tilde{N}_0)$. Similarly, a much larger superfluid density would result from $\rho_s = P'/(u\mathcal{V}) \gg m\tilde{N}_0/\mathcal{V}$, since the total momentum \mathbf{P}' of the system in the wall frame shown in Fig. H3(d) incorrectly includes dissipative normal contributions from the excited particles (in red) as well. Consequently, this leads to a slower T^4 -depletion of the superfluid density.

Our separation of the thermal statistics from the quantum mechanical problem circumvents the complications of non-standard statistics associated with the presence of steady relative flows within the system. Upon first establishing the rigorous quantum equivalence between the superfluid density and the true condensation density, thermal fluctuations of the former can be straightforwardly evaluated through the canonical thermal occupation of the latter. This is possible since, in the linear response regime, thermal equilibrium is reached without any internal relative flow and therefore bypasses the above issue of non-standard statistics. Our resulting T^3 thermal depletion of the superfluid density consequently differs from the traditional lore owing to our ‘proper’ handling (more precisely, bypassing) such non-standard statistics that would always be required for systems with steady internal relative flow.

References

- [1] Kapitza, P.: Viscosity of liquid helium below the λ -point. Nature **141**(3558), 74–74 (1938) <https://doi.org/10.1038/141074a0>
- [2] Allen, J.F., Misener, A.D.: Flow of liquid helium II. Nature **141**(3558), 75–75 (1938) <https://doi.org/10.1038/141075a0>
- [3] Bogoliubov, N.: On the theory of superfluidity. J. Phys **11**(1), 23 (1947)
- [4] Landau, L.D., Lifshitz, E.M.: vol. 5, pp. 88–92. Pergamon Press Ltd., London-Paris (1958)
- [5] Bardeen, J., Cooper, L.N., Schrieffer, J.R.: Theory of superconductivity. Phys. Rev. **108**, 1175–1204 (1957) <https://doi.org/10.1103/PhysRev.108.1175>
- [6] Ashcroft, N.W., Mermin, N.D. Holt-Saunders (1976)
- [7] Broun, D.M., Huttema, W.A., Turner, P.J., Özcan, S., Morgan, B., Liang, R., Hardy, W.N., Bonn, D.A.: Superfluid density in a highly underdoped $\text{YBa}_2\text{Cu}_3\text{O}_{6+y}$ superconductor. Phys. Rev. Lett. **99**, 237003 (2007)
- [8] Löhneysen, H.v., Pietrus, T., Portisch, G., Schlager, H.G., Schröder, A., Sieck, M., Trappmann, T.: Non-fermi-liquid behavior in a heavy-fermion alloy at a magnetic instability. Phys. Rev. Lett. **72**, 3262–3265 (1994)

- [9] Doiron-Leyraud, N., Auban-Senzier, P., Cotret, S., Bourbonnais, C., Jérôme, D., Bechgaard, K., Taillefer, L.: Correlation between linear resistivity and T_c in the bechgaard salts and the pnictide superconductor $\text{Ba}(\text{Fe}_{1-x}\text{Co}_x)_2\text{As}_2$. *Phys. Rev. B* **80**, 214531 (2009)
- [10] Moler, K.A., Sisson, D.L., Urbach, J.S., Beasley, M.R., Kapitulnik, A., Baar, D.J., Liang, R., Hardy, W.N.: Specific heat of $\text{YBa}_2\text{Cu}_3\text{O}_{7-\delta}$. *Phys. Rev. B* **55**, 3954–3965 (1997)
- [11] Kim, H., Cho, K., Tanatar, M.A., Taufour, V., Kim, S.K., Bud'ko, S.L., Canfield, P.C., Kogan, V.G., Prozorov, R.: Self-consistent two-gap description of MgB_2 superconductor. *Symmetry* **11**(8) (2019)
- [12] Kim, H., Tanatar, M.A., Song, Y.J., Kwon, Y.S., Prozorov, R.: Nodeless two-gap superconducting state in single crystals of the stoichiometric iron pnictide LiFeAs . *Phys. Rev. B* **83**, 100502 (2011) <https://doi.org/10.1103/PhysRevB.83.100502>
- [13] Zhang, J.L., Chen, Y., Jiao, L., Gumeniuk, R., Nicklas, M., Chen, Y.H., Yang, L., Fu, B.H., Schnelle, W., Rosner, H., Leithe-Jasper, A., Grin, Y., Steglich, F., Yuan, H.Q.: Multiband superconductivity in $\text{PrPt}_4\text{Ge}_{12}$ single crystals. *Phys. Rev. B* **87**, 064502 (2013) <https://doi.org/10.1103/PhysRevB.87.064502>
- [14] Karakozov, A., Zapf, S., Gorshunov, B., Ponomarev, Y., Magnitskaya, M., Zhukova, E., Prokhorov, A., Anzin, V., Haindl, S.: Temperature dependence of the superfluid density as a probe for multiple gaps in $\text{Ba}(\text{Fe}_{0.9}\text{Co}_{0.1})_2\text{As}_2$: Manifestation of three weakly interacting condensates. *Physical Review B* **90** (2014) <https://doi.org/10.1103/PhysRevB.90.014506>
- [15] Weng, Z.F., Zhang, J.L., Smidman, M., Shang, T., Quintanilla, J., Annett, J.F., Nicklas, M., Pang, G.M., Jiao, L., Jiang, W.B., Chen, Y., Steglich, F., Yuan, H.Q.: Two-gap superconductivity in LaNiGa_2 with nonunitary triplet pairing and even parity gap symmetry. *Phys. Rev. Lett.* **117**, 027001 (2016) <https://doi.org/10.1103/PhysRevLett.117.027001>
- [16] Shang, T., Xie, W., Gawryluk, D.J., Khasanov, R., Zhao, J.Z., Medarde, M., Shi, M., Yuan, H.Q., Pomjakushina, E., Shiroka, T.: Multigap superconductivity in the Mo_5PB_2 boron–phosphorus compound. *New Journal of Physics* **22**(9), 093016 (2020) <https://doi.org/10.1088/1367-2630/abac3b>
- [17] Duan, W., Nie, Z., Luo, S., Yu, F., Ortiz, B.R., Yin, L., Su, H., Du, F., Wang, A., Chen, Y., Lu, X., Ying, J., Wilson, S.D., Chen, X., Song, Y., Yuan, H.: Nodeless superconductivity in the kagome metal CsV_3Sb_5 . *Science China Physics, Mechanics & Astronomy* **64** (2021) <https://doi.org/10.1007/s11433-021-1747-7>
- [18] Uemura, Y.J., Le, L.P., Luke, G.M., Sternlieb, B.J., Wu, W.D., Brewer, J.H., Riseman, T.M., Seaman, C.L., Maple, M.B., Ishikawa, M., Hinks, D.G.,

- Jorgensen, J.D., Saito, G., Yamochi, H.: Basic similarities among cuprate, bismuthate, organic, chevrel-phase, and heavy-fermion superconductors shown by penetration-depth measurements. *Phys. Rev. Lett.* **66**, 2665–2668 (1991) <https://doi.org/10.1103/PhysRevLett.66.2665>
- [19] Uemura, Y.J., Keren, A., Le, L.P., Luke, G.M., Wu, W.D., Tsai, J.S., Tanigaki, K., Holczer, K., Donovan, S., Whetten, R.L.: System dependence of the magnetic-field penetration depth in C_{60} superconductors. *Physica C Superconductivity* **235**, 2501–2502 (1994) [https://doi.org/10.1016/0921-4534\(94\)92471-6](https://doi.org/10.1016/0921-4534(94)92471-6)
- [20] Kim, M.-S., Skinta, J.A., Lemberger, T.R., Tsukada, A., Naito, M.: Magnetic penetration depth measurements of $Pr_{2-x}Ce_xCuO_{4-\delta}$ films on buffered substrates: Evidence for a nodeless gap. *Phys. Rev. Lett.* **91**, 087001 (2003) <https://doi.org/10.1103/PhysRevLett.91.087001>
- [21] Fletcher, J.D., Carrington, A., Diener, P., Rodière, P., Brison, J.P., Prozorov, R., Olheiser, T., Giannetta, R.W.: Penetration depth study of superconducting gap structure of $2H-NbSe_2$. *Phys. Rev. Lett.* **98**, 057003 (2007) <https://doi.org/10.1103/PhysRevLett.98.057003>
- [22] Broun, D.M., Huttema, W.A., Turner, P.J., Özcan, S., Morgan, B., Liang, R., Hardy, W.N., Bonn, D.A.: Superfluid density in a highly underdoped $YBa_2Cu_3O_{6+y}$ superconductor. *Phys. Rev. Lett.* **99**, 237003 (2007) <https://doi.org/10.1103/PhysRevLett.99.237003>
- [23] Kim, H., Sung, N.H., Cho, B.K., Tanatar, M.A., Prozorov, R.: Magnetic penetration depth in single crystals of $SrPd_2Ge_2$ superconductor. *Phys. Rev. B* **87**, 094515 (2013) <https://doi.org/10.1103/PhysRevB.87.094515>
- [24] Ait Ahmed, Y., Tirbiyine, A., Soubane, D., Taoufik, A., El Ouaddi, H., El hamidi, H., Abou Alhassan, A., Hafid, A., Senoussi, S.: Magnetic penetration depth in the κ -(BEDT – TTF) $_2$ Cu[N(CN) $_2$]Br organic superconductor. *Materials Today: Proceedings* **24**, 100–103 (2020) <https://doi.org/10.1016/j.matpr.2019.07.688>. International Conference on Plasma and Energy Materials ICPEM2019
- [25] Salis, M.V., Rodière, P., Leng, H., Huang, Y.K., Visser, A.: Penetration depth study of the type-I superconductor $PdTe_2$. *Journal of Physics: Condensed Matter* **30**(50), 505602 (2018)
- [26] Khasanov, R., Ramires, A., Grinenko, V., Shipulin, I., Kikugawa, N., Sokolov, D.A., Krieger, J.A., Hicken, T.J., Maeno, Y., Luetkens, H., Guguchia, Z.: In-plane magnetic penetration depth in Sr_2RuO_4 : Muon-spin rotation and relaxation study. *Phys. Rev. Lett.* **131**, 236001 (2023) <https://doi.org/10.1103/PhysRevLett.131.236001>

- [27] Ishihara, K., Roppongi, M., Kobayashi, M., Imamura, K., Mizukami, Y., Sakai, H., Opletal, P., Tokiwa, Y., Haga, Y., Hashimoto, K., Shibauchi, T.: Chiral superconductivity in UTe_2 probed by anisotropic low-energy excitations. *Nature Communications* **14** (2023) <https://doi.org/10.1038/s41467-023-38688-y>
- [28] Thiemann, M., Beutel, M.H., Dressel, M., Lee-Hone, N.R., Broun, D.M., Fillis-Tsirakis, E., Boschker, H., Mannhart, J., Scheffler, M.: Single-gap superconductivity and dome of superfluid density in Nb-doped SrTiO_3 . *Phys. Rev. Lett.* **120**, 237002 (2018) <https://doi.org/10.1103/PhysRevLett.120.237002>
- [29] Emery, V.J., Kivelson, S.A.: Importance of phase fluctuations in superconductors with small superfluid density. *Nature* **374**(6521), 434–437 (1995) <https://doi.org/10.1038/374434a0>
- [30] Doniach, S.: Quantum fluctuations in two-dimensional superconductors. *Phys. Rev. B* **24**, 5063–5070 (1981)
- [31] Emery, V.J., Kivelson, S.A.: Superconductivity in bad metals. *Phys. Rev. Lett.* **74**, 3253–3256 (1995)
- [32] Higher powers can only result from specially fine-tuned pairing combinations with specific applied field directions[127].
- [33] Won, H.: BCS theory of nodal superconductors (2005) <https://doi.org/10.1063/1.2080347>
- [34] Tsuei, C.C., Kirtley, J.R., Chi, C.C., Yu-Jahnes, L.S., Gupta, A., Shaw, T., Sun, J.Z., Ketchen, M.B.: Pairing symmetry and flux quantization in a tricrystal superconducting ring of $\text{YBa}_2\text{Cu}_3\text{O}_{7-\delta}$. *Phys. Rev. Lett.* **73**, 593–596 (1994) <https://doi.org/10.1103/PhysRevLett.73.593>
- [35] Damascelli, A., Hussain, Z., Shen, Z.-X.: Angle-resolved photoemission studies of the cuprate superconductors. *Rev. Mod. Phys.* **75**, 473–541 (2003) <https://doi.org/10.1103/RevModPhys.75.473>
- [36] Miyagawa, K., Kawamoto, A., Kanoda, K.: Proximity of pseudogapped superconductor and commensurate antiferromagnet in a quasi-two-dimensional organic system. *Phys. Rev. Lett.* **89**, 017003 (2002) <https://doi.org/10.1103/PhysRevLett.89.017003>
- [37] Yildirim, Y., Ku, W.: Kinetics-driven superconducting gap in underdoped cuprate superconductors within the strong-coupling limit. *Phys. Rev. X* **1**, 011011 (2011)
- [38] Hegg, A., Hou, J., Ku, W.: Geometric frustration produces long-sought bose metal phase of quantum matter. *Proceedings of the National Academy of Sciences* **118**(46) (2021) <https://doi.org/10.1073/pnas.2100545118>

- [39] White, S.R.: Numerical canonical transformation approach to quantum many-body problems. The Journal of Chemical Physics **117**(16), 7472–7482 (2002) <https://doi.org/10.1063/1.1508370> https://pubs.aip.org/aip/jcp/article-pdf/117/16/7472/10843158/7472_1.online.pdf
- [40] Kanno, S.: A Method of a Quasi-Linear Canonical Transformation for the Many-Body Problem. I. Progress of Theoretical Physics **41**(4), 966–995 (1969) <https://doi.org/10.1143/PTP.41.966> <https://academic.oup.com/ptp/article-pdf/41/4/966/5338277/41-4-966.pdf>
- [41] Landau, L.: Theory of the superfluidity of helium ii. Physical Review **60**(356) (1941)
- [42] Lee, T.D., Huang, K., Yang, C.N.: Eigenvalues and eigenfunctions of a bose system of hard spheres and its low-temperature properties. Physical Review **106**(1135) (1957)
- [43] Pollock, E.L., Ceperley, D.M.: Path-integral computation of superfluid densities. Phys. Rev. B **36**, 8343–8352 (1987) <https://doi.org/10.1103/PhysRevB.36.8343>
- [44] Fisher, M.P.A., Weichman, P.B., Grinstein, G., Fisher, D.S.: Boson localization and the superfluid-insulator transition. Physical Review B **40**(1), 546–570 (1989) <https://doi.org/10.1103/PhysRevB.40.546> . PRB
- [45] Wang J. et al. in preparation.
- [46] Powell, B., McKenzie, R.H.: Quantum frustration in organic mott insulators: from spin liquids to unconventional superconductors. Reports on Progress in Physics **74**(5), 056501 (2011)
- [47] Borisenko, S., Kordyuk, A., Yaresko, A., Zabolotnyy, V., Inosov, D., Schuster, R., Büchner, B., Weber, R., Follath, R., Patthey, L., *et al.*: Pseudogap and charge density waves in two dimensions. Physical review letters **100**(19), 196402 (2008)
- [48] Chen, P., Pai, W.W., Chan, Y.-H., Takayama, A., Xu, C.-Z., Karn, A., Hasegawa, S., Chou, M.-Y., Mo, S.-K., Fedorov, A.-V., *et al.*: Emergence of charge density waves and a pseudogap in single-layer tite 2. Nature communications **8**(1), 1–6 (2017)
- [49] Umemoto, Y., Sugawara, K., Nakata, Y., Takahashi, T., Sato, T.: Pseudogap, fermi arc, and peierls-insulating phase induced by 3d–2d crossover in monolayer vse 2. Nano Research **12**(1), 165–169 (2019)
- [50] Iwaya, K., Satow, S., Hanaguri, T., Shannon, N., Yoshida, Y., Ikeda, S.I., He, J.P., Kaneko, Y., Tokura, Y., Yamada, T., Takagi, H.: Local tunneling spectroscopy across a metamagnetic critical point in the bilayer ruthenate $\text{Sr}_3\text{Ru}_2\text{O}_7$. Phys. Rev. Lett. **99**, 057208 (2007) <https://doi.org/10.1103/PhysRevLett.99>

- [51] Bruin, J., Sakai, H., Perry, R., Mackenzie, A.: Similarity of scattering rates in metals showing t-linear resistivity. *Science* **339**(6121), 804–807 (2013)
- [52] Löhneysen, H.v., Pietrus, T., Portisch, G., Schlager, H., Schröder, A., Sieck, M., Trappmann, T.: Non-fermi-liquid behavior in a heavy-fermion alloy at a magnetic instability. *Physical review letters* **72**(20), 3262 (1994)
- [53] Paglione, J., Sayles, T., Ho, P.-C., Jeffries, J., Maple, M.: Incoherent non-fermi-liquid scattering in a kondo lattice. *Nature Physics* **3**(10), 703–706 (2007)
- [54] Shimojima, T., Sonobe, T., Malaeb, W., Shinada, K., Chainani, A., Shin, S., Yoshida, T., Ideta, S., Fujimori, A., Kumigashira, H., Ono, K., Nakashima, Y., Anzai, H., Arita, M., Ino, A., Namatame, H., Taniguchi, M., Nakajima, M., Uchida, S., Tomioka, Y., Ito, T., Kihou, K., Lee, C.H., Iyo, A., Eisaki, H., Ohgushi, K., Kasahara, S., Terashima, T., Ikeda, H., Shibauchi, T., Matsuda, Y., Ishizaka, K.: Pseudogap formation above the superconducting dome in iron pnictides. *Phys. Rev. B* **89**, 045101 (2014) <https://doi.org/10.1103/PhysRevB.89.045101>
- [55] Sato, T., Souma, S., Nakayama, K., Terashima, K., Sugawara, K., Takahashi, T., Kamihara, Y., Hirano, M., Hosono, H.: Superconducting gap and pseudogap in iron-based layered superconductor $\text{La}(\text{O}_{1-x}\text{F}_x)\text{FeAs}$. *Journal of the Physical Society of Japan* **77**(6), 063708 (2008) <https://doi.org/10.1143/JPSJ.77.063708>
- [56] Fink, J., Charnukha, A., Rienks, E., Liu, Z., Thirupathaiah, S., Avigo, I., Roth, F., Jeevan, H.S., Gegenwart, P., Roslova, M., *et al.*: Non-fermi-liquid scattering rates and anomalous band dispersion in ferropnictides. *Physical Review B* **92**(20), 201106 (2015)
- [57] Dai, Y., Miao, H., Xing, L., Wang, X., Wang, P., Xiao, H., Qian, T., Richard, P., Qiu, X., Yu, W., *et al.*: Spin-fluctuation-induced non-fermi-liquid behavior with suppressed superconductivity in $\text{Li}_{1-x}\text{Co}_x\text{As}$. *Physical Review X* **5**(3), 031035 (2015)
- [58] Uchida, M., Ishizaka, K., Hansmann, P., Kaneko, Y., Ishida, Y., Yang, X., Kumai, R., Toschi, A., Onose, Y., Arita, R., Held, K., Andersen, O.K., Shin, S., Tokura, Y.: Pseudogap of metallic layered nickelate $\text{R}_{2-x}\text{Sr}_x\text{NiO}_4$ ($\text{R} = \text{Nd}, \text{Eu}$) crystals measured using angle-resolved photoemission spectroscopy. *Phys. Rev. Lett.* **106**, 027001 (2011) <https://doi.org/10.1103/PhysRevLett.106.027001>
- [59] Kim, Y.K., Krupin, O., Denlinger, J.D., Bostwick, A., Rotenberg, E., Zhao, Q., Mitchell, J.F., Allen, J.W., Kim, B.J.: Fermi arcs in a doped pseudospin-1/2 heisenberg antiferromagnet. *Science* (2014) <https://doi.org/10.1126/science.1251151>

- [60] Valla, T., Fedorov, A., Johnson, P., Wells, B., Hulbert, S., Li, Q., Gu, G., Koshizuka, N.: Evidence for quantum critical behavior in the optimally doped cuprate $\text{Bi}_2\text{Sr}_2\text{CaCu}_2\text{O}_{8+\delta}$. *Science* **285**(5436), 2110–2113 (1999)
- [61] Abdel-Jawad, M., Kennett, M., Balicas, L., Carrington, A., Mackenzie, A., McKenzie, R., Hussey, N.: Anisotropic scattering and anomalous normal-state transport in a high-temperature superconductor. *Nature Physics* **2**(12), 821–825 (2006)
- [62] Johnston, S., Vishik, I., Lee, W., Schmitt, F., Uchida, S., Fujita, K., Ishida, S., Nagaosa, N., Shen, Z., Devereaux, T.: Evidence for the importance of extended coulomb interactions and forward scattering in cuprate superconductors. *Physical review letters* **108**(16), 166404 (2012)
- [63] Kaminski, A., Fretwell, H., Norman, M.R., Randeria, M., Rosenkranz, S., Chatterjee, U., Campuzano, J., Mesot, J., Sato, T., Takahashi, T., *et al.*: Momentum anisotropy of the scattering rate in cuprate superconductors. *Physical review B* **71**(1), 014517 (2005)
- [64] Tao, H., Lu, F., Wolf, E.: Observation of pseudogap in $\text{Bi}_2\text{Sr}_2\text{CaCu}_2\text{O}_{8+\delta}$ single crystals with electron tunneling spectroscopy. *Physica C: Superconductivity* **282**, 1507–1508 (1997)
- [65] Renner, C., Revaz, B., Genoud, J.-Y., Kadowaki, K., Fischer, Ø.: Pseudogap precursor of the superconducting gap in under- and overdoped $\text{Bi}_2\text{Sr}_2\text{CaCu}_2\text{O}_{8+\delta}$. *Physical Review Letters* **80**(1), 149 (1998)
- [66] Timusk, T., Statt, B.: The pseudogap in high-temperature superconductors: an experimental survey. *Reports on Progress in Physics* **62**(1), 61 (1999)
- [67] Lang, K., Madhavan, V., Hoffman, J., Hudson, E.W., Eisaki, H., Uchida, S., Davis, J.: Imaging the granular structure of high- T_c superconductivity in underdoped $\text{Bi}_2\text{Sr}_2\text{CaCu}_2\text{O}_{8+\delta}$. *Nature* **415**(6870), 412–416 (2002)
- [68] Damascelli, A., Hussain, Z., Shen, Z.-X.: Angle-resolved photoemission studies of the cuprate superconductors. *Reviews of modern physics* **75**(2), 473 (2003)
- [69] Yang, H.-B., Rameau, J., Johnson, P., Valla, T., Tsvetlik, A., Gu, G.: Emergence of preformed cooper pairs from the doped mott insulating state in $\text{Bi}_2\text{Sr}_2\text{CaCu}_2\text{O}_{8+\delta}$. *Nature* **456**(7218), 77–80 (2008)
- [70] Hashimoto, M., He, R.-H., Tanaka, K., Testaud, J.-P., Meevasana, W., Moore, R.G., Lu, D., Yao, H., Yoshida, Y., Eisaki, H., *et al.*: Particle-hole symmetry breaking in the pseudogap state of $\text{Bi}_2\text{201}$. *Nature Physics* **6**(6), 414–418 (2010)
- [71] Kondo, T., Hamaya, Y., Palczewski, A.D., Takeuchi, T., Wen, J.S., Xu, Z.J., Gu, G., Schmalian, J., Kaminski, A.: Disentangling cooper-pair formation above

- the transition temperature from the pseudogap state in the cuprates. *Nature Physics* **7**(1), 21–25 (2011) <https://doi.org/10.1038/nphys1851>
- [72] He, R.-H., Hashimoto, M., Karapetyan, H., Koralek, J., Hinton, J., Testaud, J., Nathan, V., Yoshida, Y., Yao, H., Tanaka, K., *et al.*: From a single-band metal to a high-temperature superconductor via two thermal phase transitions. *Science* **331**(6024), 1579–1583 (2011)
 - [73] Vishik, I.M., Lee, W.S., He, R.-H., Hashimoto, M., Hussain, Z., Devereaux, T.P., Shen, Z.-X.: ARPES studies of cuprate fermiology: superconductivity, pseudogap and quasiparticle dynamics. *New Journal of Physics* **12**(10), 105008 (2010) <https://doi.org/10.1088/1367-2630/12/10/105008>
 - [74] Yoshida, T., Hashimoto, M., Vishik, I., Shen, Z.-X., Fujimori, A.: Pseudogap, superconducting gap, and fermi arc in high-*t_c* cuprates revealed by angle-resolved photoemission spectroscopy. *Journal of the Physical Society of Japan* **81**(1), 011006 (2012) <https://doi.org/10.1143/JPSJ.81.011006>
 - [75] Jiang, S., Zou, L., Ku, W.: Non-fermi-liquid scattering against an emergent bose liquid: Manifestations in the kink and other exotic quasiparticle behavior in the normal-state cuprate superconductors. *Phys. Rev. B* **99**, 104507 (2019) <https://doi.org/10.1103/PhysRevB.99.104507>
 - [76] Yue, X., Hegg, A., Li, X., Ku, W.: Probing a bose metal via electrons: inescapable non-fermi liquid scattering and pseudogap physics. *New Journal of Physics* **25**(5), 053007 (2023) <https://doi.org/10.1088/1367-2630/acce5b>
 - [77] Zeng, T., Hegg, A., Zou, L., Jiang, S., Ku, W.: Transport in the emergent bose liquid: Bad metal, strange metal, and weak insulator, all in one system. *arXiv e-prints* (2021)
 - [78] Yildirim, Y., Ku, W., *et al.*: Weak phase stiffness and nature of the quantum critical point in underdoped cuprates. *Physical Review B* **92**(18), 180501 (2015)
 - [79] Lang, Z.-J., Yang, F., Ku, W.: Mottness induced phase decoherence suggests bose-einstein condensation in overdoped cuprate high-temperature superconductors. *arXiv e-prints* (2019)
 - [80] Bishop, D.J., Reppy, J.D.: Study of the superfluid transition in two-dimensional ⁴He films. *Phys. Rev. Lett.* **40**, 1727–1730 (1978) <https://doi.org/10.1103/PhysRevLett.40.1727>
 - [81] Hohenberg, P.C.: Existence of long-range order in one and two dimensions. *Phys. Rev.* **158**, 383–386 (1967) <https://doi.org/10.1103/PhysRev.158.383>
 - [82] Pathria, R.K., 2nd edn., p. 190. Butterworth-Heinemann (1996). Chap. 7

- [83] Halperin, B.I.: On the hohenberg–mermin–wagner theorem and its limitations. *Journal of Statistical Physics* **175**(3–4), 521–529 (2018) <https://doi.org/10.1007/s10955-018-2202-y>
- [84] Gozar, A., Logvenov, G., Kourkoutis, L.F., Bollinger, A.T., Giannuzzi, L.A., Muller, D.A., Bozovic, I.: High-temperature interface superconductivity between metallic and insulating copper oxides. *Nature* **455**(7214), 782–785 (2008) <https://doi.org/10.1038/nature07293>
- [85] Wang, Q.-Y., Li, Z., Zhang, W.-H., Zhang, Z.-C., Zhang, J.-S., Li, W., Ding, H., Ou, Y.-B., Deng, P., Chang, K., Wen, J., Song, C.-L., He, K., Jia, J.-F., Ji, S.-H., Wang, Y.-Y., Wang, L.-L., Chen, X., Ma, X.-C., Xue, Q.-K.: Interface-induced high-temperature superconductivity in single unit-cell FeSe films on SrTiO₃. *Chinese Physics Letters* **29**(3), 037402 (2012) <https://doi.org/10.1088/0256-307x/29/3/037402>
- [86] Ge, J.-F., Liu, Z.-L., Liu, C., Gao, C.-L., Qian, D., Xue, Q.-K., Liu, Y., Jia, J.-F.: Superconductivity above 100 k in single-layer FeSe films on doped SrTiO₃. *Nature Materials* **14**(3), 285–289 (2014) <https://doi.org/10.1038/nmat4153>
- [87] Huang, Z.C., Pu, Y.J., Xu, H.C., Xu, D.F., Song, Q., Lou, X., Wen, C.H.P., Peng, R., Feng, D.L.: Electronic structure and superconductivity of single-layer FeSe on Nb : SrTiO₃/LaAlO₃ with varied tensile strain. *2D Materials* **3**(1), 014005 (2016) <https://doi.org/10.1088/2053-1583/3/1/014005>
- [88] Cao, Y., Fatemi, V., Fang, S., Watanabe, K., Taniguchi, T., Kaxiras, E., Jarillo-Herrero, P.: Unconventional superconductivity in magic-angle graphene superlattices. *Nature* **556**, 43–50 (2018) <https://doi.org/10.1038/nature26160>
- [89] Yankowitz, M., Chen, S., Polshyn, H., Zhang, Y., Watanabe, K., Taniguchi, T., Graf, D., Young, A., Dean, C.: Tuning superconductivity in twisted bilayer graphene. *Science* **363**, 1910 (2019) <https://doi.org/10.1126/science.aav1910>
- [90] Lu, X., Stepanov, P., Yang, W., Xie, M., Aamir, M.A., Das, I., Urgell, C., Watanabe, K., Taniguchi, T., Zhang, G., Bachtold, A., MacDonald, A.H., Efetov, D.K.: Superconductors, orbital magnets and correlated states in magic-angle bilayer graphene. *Nature* **574**(7780), 653–657 (2019)
- [91] Saito, Y., Ge, J., Watanabe, K., Taniguchi, T., Young, A.: Independent superconductors and correlated insulators in twisted bilayer graphene. *Nature Physics* **16** (2020)
- [92] Cao, Y., Chowdhury, D., Rodan-Legrain, D., Rubies-Bigorda, O., Watanabe, K., Taniguchi, T., Senthil, T., Jarillo-Herrero, P.: Strange metal in magic-angle graphene with near planckian dissipation. *Phys. Rev. Lett.* **124**, 076801 (2020) <https://doi.org/10.1103/PhysRevLett.124.076801>

- [93] Chen, G., Jiang, L., Wu, S., Lyu, B., Li, H., Chittari, B.L., Watanabe, K., Taniguchi, T., Shi, Z., Jung, J., Zhang, Y., Wang, F.: Evidence of a gate-tunable mott insulator in a trilayer graphene moiré superlattice. *Nature Physics* **15** (2019)
- [94] Chen, G., Sharpe, A., Gallagher, P., Rosen, I., Fox, E., Jiang, L., Lyu, B., Li, H., Watanabe, K., Taniguchi, T., Jung, J., Shi, Z., Goldhaber-Gordon, D., Zhang, Y., Wang, F.: Signatures of tunable superconductivity in a trilayer graphene moiré superlattice. *Nature* **572**, 1 (2019) <https://doi.org/10.1038/s41586-019-1393-y>
- [95] Park, J., Cao, Y., Watanabe, K., Taniguchi, T., Jarillo-Herrero, P.: Tunable strongly coupled superconductivity in magic-angle twisted trilayer graphene. *Nature* **590**, 1–7 (2021) <https://doi.org/10.1038/s41586-021-03192-0>
- [96] Zhang, X., Tsai, K.-T., Zhu, Z., Ren, W., Luo, Y., Carr, S., Luskin, M., Kaxiras, E., Wang, K.: Correlated insulating states and transport signature of superconductivity in twisted trilayer graphene superlattices. *Phys. Rev. Lett.* **127**, 166802 (2021) <https://doi.org/10.1103/PhysRevLett.127.166802>
- [97] Wang, L., Shih, E.-M., Ghiotto, A., Xian, L., Rhodes, D., Claassen, M., Kennes, D., Bai, Y., Kim, B., Watanabe, K., Taniguchi, T., Zhu, X., Hone, J., Rubio, A., Pasupathy, A., Dean, C.: Correlated electronic phases in twisted bilayer transition metal dichalcogenides. *Nature Materials* **19** (2020)
- [98] Sajadi, E., Palomaki, T., Fei, Z., Zhao, W., Bement, P., Olsen, C., Luescher, S., Xu, X., Folk, J.A., Cobden, D.H.: Gate-induced superconductivity in a monolayer topological insulator. *Science* **362**(6417) (2018)
- [99] Ichinokura, S., Nakata, Y., Sugawara, K., Endo, Y., Takayama, A., Takahashi, T., Hasegawa, S.: Vortex-induced quantum metallicity in the mono-unit-layer superconductor NbSe₂. *Phys. Rev. B* **99**, 220501 (2019) <https://doi.org/10.1103/PhysRevB.99.220501>
- [100] Fu, Y., Liu, E., Yuan, H., Tang, P., Lian, B., Xu, G., Zeng, J., Chen, Z., Wang, Y., Zhou, W., Xu, K., Gao, A., Pan, C., Wang, M., Wang, B., Zhang, S.-C., Cui, Y., Hwang, H., Miao, F.: Gated tuned superconductivity and phonon softening in monolayer and bilayer MoS₂. *npj Quantum Materials* **2** (2017)
- [101] Huang, K., Yang, C.N.: Quantum-mechanical many-body problem with hard-sphere interaction. *Physical Review* **105**(767) (1957)
- [102] Prix, R.: Variational description of multifluid hydrodynamics: Uncharged fluids. *Phys. Rev. D* **69**, 043001 (2004) <https://doi.org/10.1103/PhysRevD.69.043001>
- [103] Harling, O.K.: High-energy neutron scattering measurements on liquid helium and bose condensation in he ii. *Physical Review A* **3**(3), 1073–1087 (1971) <https://doi.org/10.1103/PhysRevA.3.1073>

[//doi.org/10.1103/PhysRevA.3.1073](https://doi.org/10.1103/PhysRevA.3.1073)

- [104] Yarnell, J.L., Arnold, G.P., Bendt, P.J., Kerr, E.C.: Excitations in liquid helium: Neutron scattering measurements. *Physical Review* **113**(6), 1379–1386 (1959) <https://doi.org/10.1103/PhysRev.113.1379>
- [105] Klerk, D., Hudson, R.P., Pellam, J.R.: Normal fluid concentration in liquid helium ii below 1°K. *Phys. Rev.* **89**, 662–663 (1953)
- [106] Klerk, D., Hudson, R.P., Pellam, J.R.: Second sound velocity measurements below 1°K. *Phys. Rev.* **89**, 326–327 (1953)
- [107] Ward, J.C., Wilks, J.: The velocity of second sound in liquid helium near the absolute zero. *The London, Edinburgh, and Dublin Philosophical Magazine and Journal of Science* **42**(326), 314–316 (1951) <https://doi.org/10.1080/14786445108561271> . doi: 10.1080/14786445108561271
- [108] Ward, J.C., Wilks, J.: Iii. second sound and the thermo-mechanical effect at very low temperatures. *The London, Edinburgh, and Dublin Philosophical Magazine and Journal of Science* **43**(336), 48–50 (1952) <https://doi.org/10.1080/14786440108520965> . doi: 10.1080/14786440108520965
- [109] Hardy, R.J.: Phonon boltzmann equation and second sound in solids. *Phys. Rev. B* **2**, 1193–1207 (1970) <https://doi.org/10.1103/PhysRevB.2.1193>
- [110] Rogers, S.J.: Transport of heat and approach to second sound in some isotopically pure alkali-halide crystals. *Physical Review B* **3**(4), 1440–1457 (1971) <https://doi.org/10.1103/PhysRevB.3.1440>
- [111] Narayanamurti, V., Dynes, R.C.: Observation of second sound in bismuth. *Physical Review Letters* **28**(22), 1461–1465 (1972) <https://doi.org/10.1103/PhysRevLett.28.1461>
- [112] Ackerman, C.C., Overton, W.C.: Second sound in solid helium-3. *Physical Review Letters* **22**(15), 764–766 (1969) <https://doi.org/10.1103/PhysRevLett.22.764>
- [113] Tough, J.T., McCormick, W.D., Dash, J.G.: Viscosity of liquid he ii. *Physical Review* **132**(6), 2373–2378 (1963) <https://doi.org/10.1103/PhysRev.132.2373>
- [114] Romer, R.H., Duffy, R.J.: Normal-fluid densities in liquid helium ii under pressure. *Physical Review* **186**(1), 255–262 (1969) <https://doi.org/10.1103/PhysRev.186.255>
- [115] Hardy, W.N., Bonn, D.A., Morgan, D.C., Liang, R., Zhang, K.: Precision measurements of the temperature dependence of λ in $\text{YBa}_2\text{Cu}_3\text{O}_{6.95}$: Strong evidence for nodes in the gap function. *Phys. Rev. Lett.* **70**, 3999–4002 (1993)

<https://doi.org/10.1103/PhysRevLett.70.3999>

- [116] Throughout this manuscript, discrete position and momentum are employed to facilitate careful counting of the Hilbert space and states.
- [117] Nozieres, P., Pines, D. Perseus Books, LLC (1999)
- [118] Svistunov, B.V., Babaev, E.S., Prokof'ev, N.V. Crc Press (2015)
- [119] Hohenberg, P.C., Martin, P.C.: Microscopic theory of superfluid helium. *Ann. Phys.* **34**, 291–359 (1965)
- [120] Landau, L.D.: 46 - the theory of superfluidity of helium ii, 301–330 (1965)
- [121] Prokof'ev, N.V., Svistunov, B.V., Tupitsyn, I.S.: Exact, complete, and universal continuous-time worldline monte carlo approach to the statistics of discrete quantum systems. *Journal of Experimental and Theoretical Physics* **87**(2), 310–321 (1998) <https://doi.org/10.1134/1.558661>
- [122] Ambegaokar, V., Troyer, M.: Estimating errors reliably in monte carlo simulations of the ehrenfest model. *American Journal of Physics* **78**(2), 150–157 (2010)
- [123] Anderson, P.W.: An approximate quantum theory of the antiferromagnetic ground state. *Phys. rev.* **86**(5) (1952)
- [124] Negele, J.W., Orland, H., p. 48. Westview Press (1998)
- [125] Fujiwara, I., Haar, D., Wergeland, H.: Fluctuations in the population of the ground state of bose systems. *Journal of Statistical Physics* **2**(4), 329–346 (1970)
- [126] Ku, W., Hegg, A.: Showcasing the necessity of the principle of relative motion in physical statistics: Inconsistency of the 'segmented fermi surface'. *arXiv e-prints* (2024)
- [127] Annett, J., Goldenfeld, N., Renn, S.R.: Interpretation of the temperature dependence of the electromagnetic penetration depth in $\text{YBa}_2\text{Cu}_3\text{O}_{7-\delta}$. *Phys. Rev. B* **43**, 2778–2782 (1991)